Fall 1-3-2014

Towards Improving Drought Forecasts Across Different Spatial and Temporal Scales

Shahrbanou Madadgar
Portland State University

Towards Improving Drought Forecasts Across Different Spatial and Temporal Scales

by

Shahrbanou Madadgar

A dissertation submitted in partial fulfillment of the
requirements for the degree of

Doctor of Philosophy
in
Civil and Environmental Engineering

Dissertation Committee:
Hamid Moradkhani, Chair
Scott Wells
Stefan Talke
Aslam Khalil

Portland State University
2013

Abstract

Recent water scarcities across the southwestern U.S. with severe effects on the living environment inspire the development of new methodologies to achieve reliable drought forecasting in seasonal scale. Reliable forecast of hydrologic variables, in general, is a preliminary requirement for appropriate planning of water resources and developing effective allocation policies. This study aims at developing new techniques with specific probabilistic features to improve the reliability of hydrologic forecasts, particularly the drought forecasts. The drought status in the future is determined by certain hydrologic variables that are basically estimated by the hydrologic models with rather simple to complex structures. Since the predictions of hydrologic models are prone to different sources of uncertainties, there have been several techniques examined during past several years which generally attempt to combine the predictions of single (multiple) hydrologic models to generate an ensemble of hydrologic forecasts addressing the inherent uncertainties. However, the imperfect structure of hydrologic models usually lead to systematic bias of hydrologic predictions that further appears in the forecast ensembles. This study proposes a post-processing method that is applied to the raw forecast of hydrologic variables and can develop the entire distribution of forecast around the initial single-value prediction. To establish the probability density function (PDF) of the forecast, a group of multivariate distribution functions, the so-called copula functions, are incorporated in the post-processing procedure. The performance of the new post-processing technique is tested on 2500 hypothetical case studies and the streamflow forecast of Sprague River Basin in southern Oregon. Verified by some deterministic and

probabilistic verification measures, the method of Quantile Mapping as a traditional post-processing technique cannot generate the qualified forecasts as comparing with the copula-based method.

The post-processing technique is then expanded to exclusively study the drought forecasts across the different spatial and temporal scales. In the proposed drought forecasting model, the drought status in the future is evaluated based on the drought status of the past seasons while the correlations between the drought variables of consecutive seasons are preserved by copula functions. The main benefit of the new forecast model is its probabilistic features in analyzing future droughts. It develops conditional probability of drought status in the forecast season and generates the PDF and cumulative distribution function (CDF) of future droughts given the past status. The conditional PDF can return the highest probable drought in the future along with an assessment of the uncertainty around that value. Using the conditional CDF for forecast season, the model can generate the maps of drought status across the basin with particular chance of occurrence in the future. In a different analysis of the conditional CDF developed for the forecast season, the chance of a particular drought in the forecast period can be approximated given the drought status of earlier seasons.

The forecast methodology developed in this study shows promising results in hydrologic forecasts and its particular probabilistic features are inspiring for future studies.

Dedication

To:

Mom and Dad

Acknowledgements

I would like to express my sincere gratitude to my advisor, Dr. Hamid Moradkhani for his support and patience throughout the years of my study at Portland State University. I am honored to have had the opportunity to be a student in his classes and a member of his research team for the past few years. Without his helps, it was not possible for me to implement this research. I also would like to thank my thesis committee, Dr. Wells, Dr. Talke, and Dr. Khalil, for their support and for their timely review of my dissertation. I greatly appreciate their willingness to serve in my thesis committee and their constructive and valuable suggestions as to further improve the products of my research. I also would like to thank my research group for their support during these years and providing a wonderful atmosphere to keep up the hard work and improve my research.

My special thanks go for my parents and family for their patience and heartwarming supports throughout my studies. Without their encouragements, I could not bear the hardships of living far away from home to implement my research and dissertation. I am also grateful to all my friends who made my time in Portland a pleasant and memorable experience. I always felt their moral supports in my hard times.

Table of Contents

List of Tables

List of Figures

1. Introduction

1.1 Uncertainties in Hydrologic Forecasts

Estimating the future status of random variables such as hydrological and hydro-meteorological variables is prone to various uncertainties. There are three main sources of uncertainties in hydrologic forecasts; climatology, model structure and parameters, and initial conditions at the forecast date (Fig. 1). Several techniques have been studied during the past decades to address different sources of uncertainties in estimating the hydrologic variables in the forecast period.

An ensemble of forecast trajectories is generally generated to capture total forecast uncertainty due to several sources of uncertainties (Olsson and Lindstrom, 2008; Wood and Lettenmaier, 2008; Moradkhani and Sorooshian, 2008; DeChant and Moradkhani, 2011; Parrish et al., 2012; Moradkhani et al., 2012). In generating the ensemble of forecasts, different methodologies may be employed. In hydrologic applications with the lack of knowledge about future climate conditions, the sampling of historical meteorological data can provide a range of possible future climate condition used for generating the ensemble hydrologic forecasts (McEnery et al., 2005; Wood and Lettenmaier, 2008). The so-called Ensemble Streamflow Prediction (ESP; Twedt et al., 1977; and Day, 1985) model has been used by the National

Weather Service River Forecast Centers (NWS-RFC) for more than 30 years to address the uncertainties of climate data in the future river flows. Briefly, an ESP incorporates the observed meteorology of a historical time period in the forecast period to reflect the unseen future climate in estimated streamflow. The hydrologic model is driven

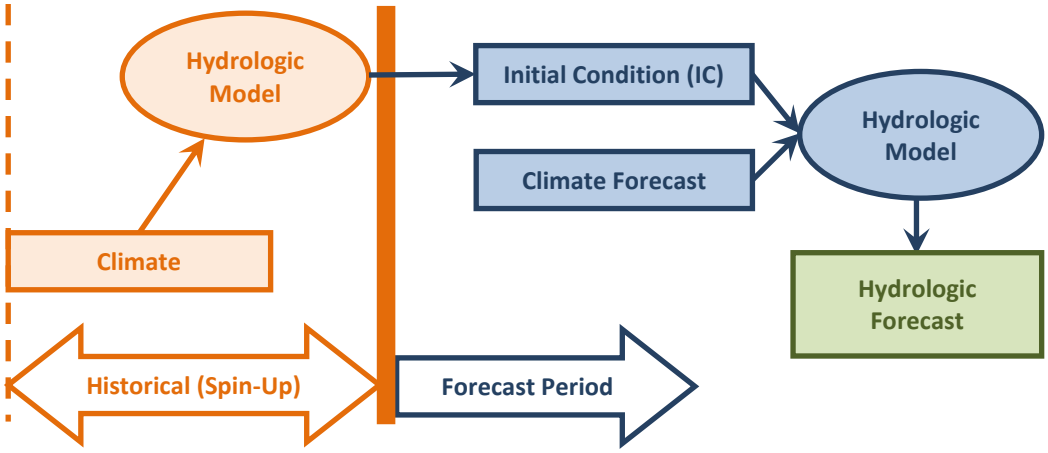

Figure 1: Diagram of hydrologic forecast procedure along with the three different sources of uncertainties including IC, climatology, and the structure and parameter of hydrologic model.

by the historical climatology during a spinup period before the forecast date. Beginning from the forecast date, the model is forced by the resampled historical meteorology to produce an ensemble of hydrologic forecasts. Since the resampled climate data reasonably reflects the uncertainty of the unseen future meteorology, the generated ESP is assumed to properly model the uncertainty of future hydrology caused by unknown climatology. To improve forecast skills, some studies generate ESPs from meteorological forecast ensembles made by numerical weather prediction models (Clark and Hay, 2004; Roulin and Vannitsem, 2005; Thirel et al., 2008; Li et al., 2009). In some recent studies, forecast reliability was increased by combining the ESP with data assimilation (DeChant and Moradkhani, 2011) or weighting ESP traces according to climate signals (Najafi et al., 2012).

Forecast uncertainty is partially referred to the structure and parameterization of the prediction model (Fig. 1). A hydrologic model is a simplified representation of the complicated physical process within a hydrologic system. Obviously, the assumptions in

model conceptualization and numerical structure make it difficult to accurately and precisely simulate every single process in a hydrologic model. Hence, a part of uncertainties in hydrologic predictions stems from the model structure, parameterization, and spatial discretization of physical processes. To overcome the overconfidence of relying on the predictions of a single model, there has been developed different techniques to average several model predictions and take the most advantage of different models. Model-averaging techniques vary in mathematical complexities; however, they are all similarly supported by the concept of linear combination of different models. Some model-averaging techniques such as equal weights, Granger-Ramanathan averaging (Granger and Ramanathan, 1984), Bates-Granger averaging (Bates and Granger, 1969), AIC and BIC-based model averaging (Buckland et al. 1997; Burnham and Anderson 2002; Hansen, 2008) take the linear average of the deterministic outputs and produce a combined single-value forecast (Diks and Vrugt, 2010). Despite the satisfactory performance of these model-averaging techniques, Hoeting et al. (1999) argued that the weights would not properly reflect the strength of single models and recommended the use of Bayesian Model Averaging (BMA) to calculate the model weights. In BMA technique, the weights are calculated upon the model performance and likelihood of predicting the observation in the past. The BMA output is a probabilistic forecast instead of a deterministic forecast; i.e. it transforms the single-value forecasts to probabilistic forecast. Raftery et al. (2005) applied BMA in developing the predictive pdf of an ensemble of meteorological forecasts. Since then, there has been extensive application of BMA in hydrologic forecasts (Duan et al., 2007; Vrugt and Robinson,

2007; Ajami et al., 2007; Rojas et al, 2008). In a climate change impact study, Najafi et al. (2011) used the BMA framework to incorporate the outputs of different hydrologic models forced by a group of Global Circulation Models (GCMs). Parrish et al. (2012) integrated the sequential data assimilation and BMA technique to relax the fix distribution assumption in developing the predictive pdf.

To address the uncertainty of initial conditions (ICs) at the forecast date, Wood and Lettenmaier (2008) proposed Reverse-ESP approach vs the regular ESP method. In the RevESP method, the resampled historical climatology is applied to the spinup period up to the forecast date to generate an ensemble of ICs that are each paired with assumingly perfect observations of the future climate. Their results indicated that the impact of uncertain ICs on the forecast quality is related to the forecast date, lead time, and the area of study. In a recent study, DeChant and Moradkhani (2011) employed the data assimilation method as a flexible and statistically defensible procedure to quantify the initial condition uncertainty by obtaining the probability distribution function (PDF) of state variables at the time of forecast and then used those for generating ESPs.

1.2 Post-processing of Hydrologic Forecasts

Incorporating different sources of uncertainty into the hydrologic forecasts would be appealing when the deterministic forecasts from hydrologic models are primarily reliable and unbiased. In spite of the significant efforts on the calibration of hydrologic models during the past decades, they are still subject to errors and systematic biases that affect the forecast quality in small to large extents. Hence, the post-processing of model forecasts is necessary to ensure that forecasts are unbiased and fairly reliable and have the

proper dispersion. Several techniques have been tried to accomplish this, which are reviewed below. In an initial study, Smith et al. (1992) assumed constant errors multiplied by the monthly simulations generated from a particular forcing regardless of the initial conditions at the forecast date. The multiplied error was estimated by historical simulations and observations. Among several post-processing methods, the conventional Quantile Mapping (QM) technique has been frequently applied in different studies (Hashino et al., 2006; Wood and Lettenmaier, 2006; Biagorria et al., 2007; Piani et al., 2010; among others). With this method, a transfer function is used to map the quantiles of simulated forecasts to the corresponding quantiles of the observations based on the cumulative distribution functions (CDFs) of simulations and observations developed for a historical period. The observation and simulation CDFs may be estimated by either empirical CDFs or parametric distributions fitted to historical data (Ines and Hansen, 2006; Piani et al., 2010). A major drawback of this method, however, is that it does not maintain the pairing of corresponding simulated and observed flows. To restrict the shortcoming of QM technique, Madadgar and Moradkhani (2011) generated several ESPs for various analysis periods prior to the forecast period. Several simulation CDFs were produced for the simulations associated with each historical forcing implemented on the analysis periods; which are then used for bias correction of the forecast trajectory corresponding to that particular forcing. Bias correction of forecasts with particular CDFs produced specifically for each forcing data reduces the forcing uncertainty of QM method. Despite the extensive applications of QM, several other techniques have been developed and tested to overcome the limitations of QM technique. Candille et al. (2010)

applied a bias correction method with the so called “on the fly” scheme (Cui et al, 2008) updating and correcting the ensemble bias over time. In their study, the multi ensemble, from the so called North American Ensemble Forecast System (NAEFS) comprising National Centers for Environmental Prediction (NCEP) and Meteorological Service of Canada (MSC) ensembles, is bias corrected through individual on-the-fly analysis scheme for each model of ESP. Their method is only applied to the variables with normally distributed errors like temperature and wind vector components. In another study, Djalalova et al. (2010) used the Kalman-Filter (KF; Kalman, 1960) method (Brookner, 1998) to estimate the bias from air quality forecasts. KF is a sequential data assimilation method that integrates the observed variables characterizing the state of a system into the model. Observations are assimilated as they become available over time.

A perfect post-processing method would estimate the observed variable given the forecast at any time. In stochastic context, this is equivalent to find the most likely value of the probability distribution of the observed variable. Post-processing is mathematically indicated by approximating the conditional probability distribution of the observed variable given the forecast generated by hydrologic model. To do so, the joint probability of the observations and simulations should first be estimated. The bivariate normal distribution is usually applied to develop the join distributions (Schaake et al., 2007; Zhao et al., 2011; Todini, 2008). Assigning bivariate normal distribution for the joint distribution requires the normally distributed observations and simulations. Since the marginal distributions of hydrologic variables such as streamflow are hardly found to be normal, a transformation of non-normal variables (X and Y) to the standard normal

variables (U and V) would be required. Brown and Seo (2010), however, argued that back and forth transformation from the Gaussian space can invalidate the optimality of estimated parameters of the conditional probability distribution. They discussed the drawbacks of fitting parametric distributions to the observations and simulations and proposed a non-parametric post-processor analogous to indicator co-Kriging in geostatistics (Isaaks and Srivastava, 1989). They also discussed that, according to the aggregate effect of various physical processes on meteorological and hydrological variables, the joint behavior of their observations and simulations is not usually well-fitted to any parametric distributions. Instead, they proposed a non-parametric method based on Bayesian optimal linear estimation of indicator variables as described by Schweppe (1973). The proposed conditional probability is estimated as the non-exceedance probability of a discrete threshold of the observed variable ($x \le c_a ; e.g. c_a = flood\ stage$) given the forecast of the jth ensemble member (zj). To capture the accurate shape of conditional probability, a large number of thresholds should be defined for the observed variable. A shortcoming of this technique, however, is its inability to specify the conditional probability of a certain observed value given the forecast. In fact, using the non-parametric probability does not allow the conditional probability to be estimated at a particular threshold but rather enables the approximation of the conditional probability of either exceeding or non-exceeding the thresholds. Furthermore, the size of the forecast ensemble is an effective factor in the accurate estimation of the non-parametric conditional probability. Thus, for an accurate estimation of the expectation operator, a relatively large number of forecast members is required.

An alternative approach for the post-processing of hydrologic forecasts is to apply a group of multivariable probability functions, the so-called copula functions, to develop the conditional probabilities of observed variable given forecast value. Unlike the most of multivariate functions, copulas do not make any restriction on the type of marginal distributions. Moreover, using copula functions make it possible to estimate the conditional probability of the observed variable at any particular forecast value. Furthermore, as discussed later, the copula functions bind the marginal CDFs; thus, the unknown and complicated relationships in hydrological processes do not hinder fitting the multivariable joint distribution to the observed and forecast variables.

1.3 Hydrologic Drought Forecast

Reliable forecast of the hydrologic extreme events plays a significant role in developing appropriate policies to allocate the available water resources among the different users. Although several studies have proposed promising methods to improve hydrologic forecasts, the observed effects of climate change on floods and droughts across different regions of the globe highlights the needs for more sophisticated methods in predicting extreme events (Mishra and Singh, 2010; Moradkhani et al., 2010; Halmstad et al., 2012; Risley et al., 2011; Madadgar and Moradkhani, 2013; Najafi et al., 2012).

Drought is a recurrent extreme event that roots in the shortage of precipitation over an extended period of time, resulting in water scarcity. Droughts events have strong impacts on the water supply and water quality; society and public health; crop production and agriculture; plants, wild fires, and living environments. Compared to other natural

disasters, droughts are “creeping disasters” with small to severe damages. As reported by Federal Emergency Management Agency (1995), the annual drought losses for the United States are estimated at $6–8 billion. Only in 2002, the western U.S. drought costs exceeded $10B (National climate Data Center, 2003). Several recent efforts have attempted to enhance forecast accuracy, mitigation policies, and damage estimate of drought events in the globe, specifically in the United States. The Drought Impact Reporter (DIR), launched by National Drought Mitigation Center (NDMC), is a comprehensive database reporting damages caused by recent droughts within the United States. Reported by North America Drought Monitor of National Oceanic and Atmospheric Administration’s (NOAA) National Climate Data Center (NCDC), droughts with an estimated damage of over 100 billion dollars (Lott and Ross, 2000) have been among the costliest natural disasters in the U.S. since 1980. Lott and Ross (2006) estimated drought and heat wave induced damages to the U.S. economy at $174 billion, between 1980 and 2005. In 2012, more than 70% of the United States was under drought conditions ranging from abnormally dry to exceptional droughts (Showstack, 2012). Besides the U.S., almost all the continents throughout the globe have been affected by various drought phenomena during the recent decades (Mishra and Singh, 2010). Large areas in South, Central, and North America, Europe, Asia, Africa, and Australia have been affected by large scale droughts in recent years (Mishra and Singh, 2010).

Although there is not a universal definition of drought, in the most general sense, drought can be defined with different disciplinary perspectives, namely, meteorological, agricultural, hydrological, and socioeconomic droughts (National Drought Mitigation

Center; http://www.drought.unl.edu/whatis/concept.htm). Different types of drought are closely related and they interact with each other (Dingman 1994). The cycle of different droughts usually starts with meteorological drought when the amount of precipitation received over a time period falls below the associated average amount. Below-average precipitation causes insufficient soil moisture, runoff, and water supply which leads to agricultural and hydrological droughts. Hydrological droughts and streamflow shortage would decrease the inflow to hydropower reservoirs causing small energy production and socioeconomic droughts.

Drought events are detected by particular indices in each category. Among several indices, the following ones are frequently used in the literature: Palmer Drought Severity Index (PDSI; Palmer 1965), Crop Moisture Index (CMI; Palmer, 1968), Soil Moisture Drought Index (SMDI; Hollinger et al., 1993), Vegetation Condition Index (VCI; Liu and Kogan, 1996), Surface Water Supply Index (SWSI; Shafer and Dezman, 1982), Standardized Precipitation Index (SPI; McKee et al., 1993 and 1995), and Reclamation Drought Index (RDI; Weghorst, 1996). Based on the concept behind SPI formulation, Nalbantis (2008) introduced Streamflow Drought Index (SDI) to evaluate hydrological droughts using cumulative streamflow volumes of a basin. Shukla and Wood (2008) developed the Standardized Runoff Index (SRI) by replacing the observed streamflow volumes in SDI with the simulated runoff obtained from a hydrological model. Fleig et al. (2010) introduced Regional Drought Area Index (RDSI) based on daily streamflow to represent the drought affected area in north-western Europe. To capture the correlation of

hydrological variables, Kao and Govindaraju (2010) developed Joint Deficit Index (JDI) to address the joint behavior of precipitation and streamflow in a same index.

According to the limited sources of manageable water and the population growth rate, the quality and quantity of supplied water are highly affected by ongoing droughts across different regions over the globe. The NOAA-NCDC reported year 2012 as the warmest year on record for the United States where the average temperatures of the contiguous United States were $3.2^{\circ}F$ above that of the 20^{th} century. According to the U.S. Drought Monitor, more than 70% of the contiguous United States experienced some level of dry spells which extended to the next year and approximately 58% of the contiguous United States was under drought conditions as of January 29, 2013. Streamflow forecast of the spring and summer of 2013 predicts below normal conditions for many major rivers in the Western U.S., including the Colorado and the Rio Grande. Where the ongoing droughts in the North America and many other regions across the globe are referred to the climate change and global warming effects (Trenberth, 2011; Peterson et al., 2012), the frequency of droughts in the future is likely to increase, rather than decrease (Sheffield and Wood, 2008; Dai, 2011). However, since drought is a slowly developed phenomenon, there might be a chance to mitigate drought impacts if the events are forecasted within an appropriate timeframe. The reliable forecast of the hydrologic status of a region in the future has a significant role in efficient planning of available water resources, and helps water supply systems to survive in enduring droughts.

Among different issues that have been examined in drought studies during the past decades, drought forecasting and accurate estimation of onset and likelihood of future

droughts have been focused in recent years. In an earlier study, Karl et al. (1987) evaluated the probability of receiving sufficient amount of precipitation to recover from an ongoing drought over a particular period of time. They rewrote the PDSI formula and utilized the unconditional gamma distribution to obtain the probabilities of future droughts. The limitation, however, was using an unconditional distribution- ignoring the dependency and auto-correlation of precipitation in time- to obtain the probabilities. Lohani and Laganathan (1997) used a non-homogeneous Markov chain model to generate the transition probability matrix of drought states. In another study, the Markov chain model was employed to evaluate drought transition probabilities, persistence, duration, and frequency within six categories of different severities (Steinemann, 2003). Some other studies used the stochastic renewal models, stochastic autoregressive models, and Artificial Neural Networks (ANN) to estimate different characteristics of future droughts and low-flow periods (Kendall and Dracup, 1992; Loaiciga and Leipnik, 1996; Mishra and Desai, 2005 and 2006; Barros and Bowden, 2008). However, the autoregressive and neural network models were later questioned by Hwang and Carbone (2009) due to limiting the forecasts into the deterministic estimate of the mean drought status. Recently, Özger et al. (2012) developed a wavelet and fuzzy logic combination model for long-lead drought forecasting. The technique was found to outperform fuzzy logic, ANN, or coupled wavelet and fuzzy logic models, yet prior to an application it needs a significant work to find the appropriate independent predictors, which strongly affect the forecast. Without using any frequency-analysis methods, Cancelliere et al. (2007) derived the transition probabilities matrix by revising the statistics underlying the

SPI series. They also questioned the validity of Markov chain model in forming the transition probability matrix for forecasting SPI values. However, two major limitations of their study are: (a) there are promising approaches like copula functions, as discussed later, for frequency analyses of drought status that look promising and avoid overwhelming procedures to analytically derive the transition probability matrix from the index formulas; (b) to reduce the computational burden, they assumed that aggregated monthly precipitations are uncorrelated and normally distributed variables whereas this is not a valid assumption specifically when the method is expanded to other hydrologic variables like streamflow. Some other studies took advantage of seasonal climate forecasts to predict the future droughts. Carbone and Dow (2005) and Hwang and Carbone (2009) incorporated the seasonal forecast products of NOAA Climate Prediction Center (CPC) with historical climate records to address the uncertainties of future droughts. However, Steinemann (2006) argued the poor interpretation of forecast probability and uncertainty information supported by CPC seasonal precipitation outlooks by the water managers despite the potential of CPC products in drought forecasting.

While a number of studies have focused on the accurate forecast of future droughts, it is still required to work on the forecast methods and develop the probabilistic features of future droughts. The current methods lack to fully support the probabilistic distribution of future droughts while the dependencies of correlated variables are also preserved. The conditional probabilities of future droughts given the past drought status of a region needs further analysis of the joint behavior of dependent variables. For this purpose, the

powerful mathematical functions such as copulas are potential tools in establishing the forecast models with conditional probabilistic features. Such forecast models would be able to reflect the water availability of the past in the future status of droughts.

2. Copulas

2.1 Mathematical Background

Copulas are joint cumulative distribution functions of n univariate marginal distributions being uniform on the interval [0, 1], i.e. $C:[0,1]^n \to [0,1]$ (Joe, 1997; Nelsen, 1999). Supported by Sklar's Theorem (Sklar, 1959), copula functions can express a multivariate distribution, $F(x_1, x_2, ..., x_n)$, as follows:

$$F(x_1, x_2, ..., x_n) = C\left[F_{X_1}(x_1), F_{X_2}(x_2), ..., F_{X_n}(x_n)\right] = C(u_1, u_2, ..., u_n)$$
$$C(u_1, ..., u_n) = \Pr\{U_1 \le u_1, ..., U_n \le u_n\} \quad (1)$$

where, C refers to the Cumulative Distribution Function (CDF) of copula; and $F_{X_i}(x_i)$ is the marginal distribution of the i^{th} variable, which is denoted by variable u_i in the cdf of copula. According to the 2nd line of Eq. 1, copulas return the multivariate joint probability of random variables.

A copula should satisfy the "boundary" and "increasing" conditions defined as follows:

- *Boundary conditions*

  1) $C(\mathbf{u}) = 0 \quad if \ \{u_i = 0, i \notin \phi\}$; i.e. there is at least one component of **u** where $u_i = 0$, ϕ is the null set.

  2) $C(\mathbf{u}) = u \quad if \ \{u_i = u, u_j = 1 \ \ \forall j \neq i\}$; i.e. all components of **u** are equal to 1 except u_i.

- *Increasing condition*

The probability of any n-dimensional hypercube in the unit hypercube is non-negative:

$$\sum_{k_1=1}^{2}\cdots\sum_{k_n=1}^{2}(-1)^{\sum_{i=1}^{n}k_i}C(u_{1k_1},\ldots,u_{ik_i},\ldots,u_{nk_n})\geq 0 \quad for \;\; all \;\; 0\leq u_{i1}\leq u_{i2}\leq 1$$

where in 2D copula, the conditions are simplified to:

- *Boundary conditions*

3) $C(u_1,0)=C(0,u_2)=0$

4) $C(u_1,1)=u_1 \;\;,\;\; C(1,u_2)=u_2$

- *Increasing condition*

$$C(u_{12},u_{22})+C(u_{11},u_{21})\geq C(u_{12},u_{21})+C(u_{11},u_{22}) \; for \; u_{11}\leq u_{12} \;\; and \;\; u_{21}\leq u_{22}$$

The derivative of an absolutely continuous cdf of copula returns the pdf of copula, $c(u_1,\ldots,u_n)$, as follows:

$$c(u_1,\ldots,u_n)=\frac{\partial^n C(u_1,\ldots,u_n)}{\partial u_1\ldots\partial u_n} \tag{2}$$

The pdf of copula can be used to determine the joint probability density function of a set of random variables, $(x_1,x_2,\ldots,x_n)$. The product of the pdf of copula and the marginal density function of each variable returns the joint probability density function of the entire group of variables:

$$f(x_1,...,x_n)=c(u_1,...,u_n)\prod_{i=1}^{n} f_{X_i}(x_i) \quad (3)$$

The main advantage of copula application is to use separate marginal distributions of random variables while at the same time their inherent correlations are reflected. Except for the correlations, no other unknown relations and complications among the dependent variables are used in the process of developing the joint distribution function via the copula functions (Eq. 3).

2.2 Elliptical and Archimedean Copulas

Copulas are categorized into several families. The Elliptical and Archimedean copulas (Embrechts et al., 2003; Nelsen, 1999) are the two most applied copulas in different fields of science and engineering.

Elliptical copulas can reflect all pair-wise correlations among the variables with any level of correlation; however, they are only able to model the group of variables with a positive-definite correlation matrix (Johnson, 1970). It is statistically proved that a covariance matrix is positive-definite matrix unless one variable is an exact linear combination of the others. Therefore, to ensure the application of the Elliptical family of copulas in real applications, correlation matrix is defined in forms of the covariance matrix. Moreover, this family of copulas does not have a closed form expression.

Unlike Elliptical copulas, the Archimedean copulas have closed form expressions but do not preserve all pair-wise correlations for problems with more than two variables. Archimedean copulas are divided into symmetric and asymmetric functions; Gumbel and Clayton copulas are from the asymmetric group, and the Frank copula is from the

symmetric group. The Gumbel copula in asymmetric division has been shown to properly fit to hydrological variables (Dupuis, 2007; Zhang and Singh, 2007; Serinaldi and Grimaldi, 2007; Wong et al., 2010; Madadgar and Moradkhani, 2013). Table 1 summarizes the different Elliptical and Archimedean copula functions with the dimension of $n = 2$.

Extension of Archimedean copulas to high dimensional problems with more than two variables has the serious limitation of preserving all pair-wise dependencies running among the variables. Nested copulas are usually attempted to build the multivariate Archimedean copulas; however, they still lack to model all dependency levels among variables. Moreover, nested copulas are only valid for positively correlated variables. To overcome such drawbacks of Archimedean copulas, Kao and Govindaraju (2008) applied Plackett family of copulas to trivariate analysis of extreme rainfall events. However, the sensitivity of Plackett family of copulas to the parameter estimation methods and the analytical approaches to verify the presumed conditions to use this family of copula needs further studies and evaluations (Kao and Govindaraju, 2008).

Table 1: Summary of Elliptical and Archimedean copula functions with n=2

Copula	Function	Support
Gaussian	$C(u_1,u_2)=\int_{-\infty}^{\Phi^{-1}(u_2)}\int_{-\infty}^{\Phi^{-1}(u_1)}\frac{1}{2\pi\left(1-\rho^2\right)^{\frac{1}{2}}}\exp\left\{-\frac{x_1^{\,2}+x_2^{\,2}-2\rho x_1 x_2}{2\left(1-\rho^2\right)}\right\}dx_1\,dx_2$ $u_1=\Phi(x_1)\ ,\quad u_2=\Phi(x_2)$ ρ : Linear correlation coefficient Φ : Standard normal cumulative distribution function	$x_1,x_2\in R$
t	$C(u_1,u_2)=\int_{-\infty}^{t_\nu^{-1}(u_2)}\int_{-\infty}^{t_\nu^{-1}(u_1)}\frac{1}{2\pi\left(1-\rho^2\right)^{\frac{1}{2}}}\exp\left\{1+\frac{x_1^{\,2}+x_2^{\,2}-2\rho x_1 x_2}{\nu\left(1-\rho^2\right)}\right\}^{-(\nu+2)/2}dx_1\,dx_2$ $u_1=t_\nu(x_1)\ ,\quad u_2=t_\nu(x_2)$ ρ : Linear correlation coefficient t_ν : Cumulative distribution function of t distribution with ν degree of freedom.	$x_1,x_2\in R$
Gumbel	$C(u_1,u_2)=\exp\left\{-\left[(-\ln u_1)^\theta+(-\ln u_2)^\theta\right]^{1/\theta}\right\}$ θ : Measure of dependency between u_1 and u_2. Either Pearson's correlation coefficient or Kendal's tau correlation are usually used to estimate θ.	$\theta\in[1,\infty)$
Clayton	$C(u_1,u_2)=\left(u_1^{-\theta}+u_2^{-\theta}-1\right)^{-1/\theta}$ θ : Similar to Gumbel copula.	$\theta\in(0,\theta)$
Frank	$C(u_1,u_2)=-\frac{1}{\theta}\ln\left[1+\frac{\left(e^{-\theta u_1}-1\right)\left(e^{-\theta u_2}-1\right)}{e^{-\theta}-1}\right]$ θ : Similar to Gumbel copula.	$\theta\in R$

2.3 Goodness of Fit Tests

Copula applications start with finding a copula function that appropriately fit the marginal distribution of random variables. To select a copula function fitting a particular dataset better than other alternatives, various methods may be applied as the goodness-of-fit (GOF) tests. The simplest method is a visual comparison between the empirical copula and the theoretical copula. The scatterplot would follow the line 1:1 if the theoretical copula perfectly fit the empirical copula. Nevertheless, to compare different copulas fitted to the same set of data, it is more reliable to use the GOF test statistics instead of a mere visual inspection. A mathematical GOF test for copula functions may be based on the distance between the empirical copula and the parametric copula under the null hypothesis (H0). Genest and Rémillard (2008) implemented a bootstrapping process to obtain the Cramér-von Mises (Eq. 4) and Kolmogorov-Smirnov statistics as the measures of distance between the empirical and parametric copulas. There are some other test statistics analogues to the Cramér-von Mises and Kolmogorov-Smirnov statistics which are based on Kendall's transform (Genest et al., 2006; Savu and Trede, 2008) and Rosenblatt's transform (Rosenblatt, 1952). Recently, the extended version of the Kullback-Leibler Information Criterion (KLIC) developed by Diks et al. (2010) has been applied in copula selection (Weiß, 2011), but the results showed that the criterion does not perform better than GOF test statistics in detecting the best copula fitted to the data. On the other hand, some studies show that the GOF test statistics based on the empirical copula outperform the others (Genest et al., 2009; Berg, 2009). Therefore, this study

proceeds with the GOF test statistic based upon the empirical process with the following definition for Cramér-von Mises statistic:

$$S_n = \int_{\mathbf{u}} \Delta C_n(\mathbf{u})^2 \, dC_n(\mathbf{u}) \tag{4}$$

where, Sn is Cramér-von Mises statistic and ΔC_n is expressed as:

$$\Delta C_n = \sqrt{n}\left(C_n - C_{\theta_n}\right) \tag{5}$$

where C_n is the empirical copula with a sample size of n, and C_{θ_n} is the parametric copula estimated for a sample size of n. Genest et al. (2009) elaborated on a parametric bootstrap procedure to find the p-value of the test via Monte Carlo sampling. Since the null hypothesis of the test is that the parametric copula fits the data ($H_0 : C_n \in C_{\theta_n}$), p-values greater than the significance level (α) means the null hypothesis is accepted, otherwise, it is rejected. Therefore, among a group of copulas, the one with the greatest p-value (and the smallest S_n) is preferred.

Several methods have been applied to estimate the parameters of copula functions; Exact Maximum Likelihood (EML) (Dupuis, 2007), Inference Functions for Margins (IFM) (Joe, 1997, Dupuis, 2007; Wong et. al, 2010), and Canonical Maximum Likelihood (CML) (Genest et al., 1995; Cherubini et al., 2004; Serinaldi and Grimaldi, 2007). This study uses IFM to estimate the parameters of both copula functions. IFM is a two-step approach: in the first step the Maximum Likelihood Estimation (MLE) is applied to estimate the parameters of univariate marginal distributions $\left(\hat{\beta}_i\right)$ and in the

second step the copula parameters (θ) are found using MLE and $\hat{\beta}_i$ obtained in the first step:

$$L(\theta) = \sum_{i=1}^{n} \ln C_\theta \left[F_1\left(x_1|\hat{\beta}_1\right), F_2\left(x_2|\hat{\beta}_2\right), \ldots, F_n\left(x_n|\hat{\beta}_n\right) \right] \tag{6}$$

where $L(.)$ is the log-likelihood function to be maximized.

The method of Maximum Likelihood Estimation (MLE) is used to estimate the parameters of the marginal distributions. Then, the best marginal distribution is found upon the results of Kolmogorov-Smirnov (K-S; Kolmogorov, 1933; Massey, 1951) test and the Akaike Information Criterion (AIC; Akaike, 1974) test. The K-S test statistic (D) measures the maximum distance of the empirical CDF to the CDF of the reference distribution:

$$D = Max\left\{ \left| F(x) - G(x) \right| \right\} \tag{7}$$

where F(x) and G(x) are the empirical and reference CDFs respectively. The null hypothesis (H0) of the K-S test states that the data set belongs to the reference distribution.

The AIC test statistic is defined as follows:

$$AIC = 2K - 2\ln(L) \tag{8}$$

where; K is the number of parameters of the marginal distribution, and L is the maximized value of the likelihood function of the candidate distribution.

While the K-S test evaluates the appropriateness of a particular distribution fitting a given dataset, the AIC test can find the best alternative in a group of distributions. Hence, neither one is conclusive by itself to find the best choice in the group. The

appropriateness of a distribution should be first accepted by the K-S test. The K-S test returns the p-value, which should be greater than the significance level of α to accept the null hypothesis. Under the null hypothesis, the dataset is assumed to come from the reference distribution. If the goodness of a particular distribution is approved by the K-S test, then its superiority to other alternative distributions is evaluated by the AIC test, where the distribution with the smallest AIC value is assumed to be the best choice among others.

3. Post-processing of Hydrologic Forecasts[1]

Different sources of uncertainties are included in the hydrological and hydro-meteorological forecasts. Lack of knowledge about the future climatology, model structure and parameters, and initial conditions at the forecast date are three sources of uncertainties in hydrological forecasts. Several techniques such as Ensemble Streamflow Prediction (ESP; Twedt et al., 1977; and Day, 1985) and model averaging (e.g. Bayesian Model Averaging (BMA); Raftery et al., 2005) techniques have been practiced during the past several years to address the uncertainties in hydrologic forecasts. To successfully incorporate different sources of uncertainty into the hydrologic forecasts, the deterministic forecasts from hydrologic models should be post-processed to become reliable and unbiased. Despite qualified calibration methods in estimating the parameters of hydrologic models, there are still different errors and systematic bias in hydrologic forecasts that influence the forecast reliability and appropriate dispersion of forecast ensemble.

3.1 Ensemble Streamflow Prediction (ESP)

A number of methods are available for quantification of uncertainty in land surface modeling. Each method takes one of two forms: Ensemble based products based on Monte Carlo experiments (Wood and Lettenmaier, 2006) or fitted probability functions to a set of data (Moradkhani and Meier, 2010). Both methods provide a means for generating probabilistic estimates of desired land surface variables, and have both been

[1] The scientific content of this chapter has been published in J. Hydrological Processes:
Madadgar, S., Moradkhani, H., and D. Garen (2012), Towards Improved Post-processing of Hydrologic Forecast Ensembles, *J. Hydrol. Process.*, doi: 10.1002/hyp.9562.

widely used in hydrologic forecasting. To address the uncertainties of climate data in the future river flows, the National Weather Service River Forecast Centers (NWS-RFC) has been used the ESP technique for more than 30 years. An ESP reflects the uncertainty of unseen future climate by incorporating the historical meteorology in the forecast period. The observed historical climate drives the hydrologic model during a spin-up period before the forecast date and the hydrological state at the forecast date is determined. Beginning from the forecast date, the hydrologic model is forced by the resampled historical meteorology and an ensemble of hydrologic forecasts is generated accordingly. The assumption behind the resampling approach is that the resampled climate of the historical period can reflect the uncertainty of unseen future climate; and hence, the ESP produced for a hydrologic variable (e.g. streamflow) can represent the uncertainty associated with the climatology. Figure 2 shows the application of ESP technique to represent the uncertainty in river flow forecast. Each ensemble member is corresponding to a climate realization resampled from the historical period. The resampled climate of the historical time should be from the same duration as the forecast period. The uncertainty bound around the hydrologic forecast at any time is determined from the upper and lower limit of the ESP.

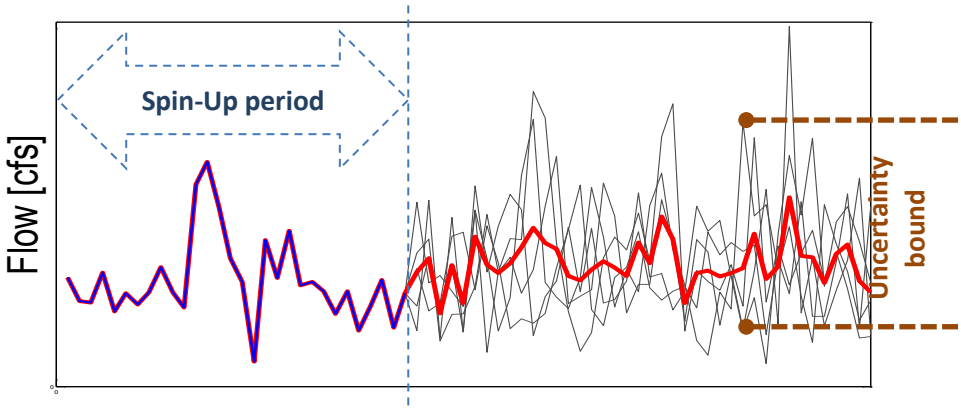

Figure 2: Schematic of ESP reflecting the climate uncertainty by resampling the historical climate.

In a recent study, Najafi et al. (2012) assigned a particular weight to each ESP member according to the climate signals and improved the forecast reliability. The weighted ESP members performed better than the raw ESP. Some other studies have replaced the resampling process from the historical meteorology with the meteorological forecast ensembles made by numerical weather prediction models and improved forecast skills (Clark and Hay, 2004; Roulin and Vannitsem, 2005; Thirel et al., 2008; Li et al., 2009).

3.2 Conventional Quantile Mapping (QM)

Quantile Mapping is a statistical technique and most popular post-processing method in hydrologic forecasting that adjusts model forecasts based upon the cumulative distribution functions (CDFs) of historical observations and model simulations. In the QM approach, the forecast quantile at a given time is found from the simulation CDF, and the corresponding observed quantile is taken from the observation CDF to adjust the forecast (Fig. 3). So, if the model simulations and observations are ranked, the ranks of the post-processed forecasts and raw forecasts are the same. The approach was primarily

designed to remove bias from forecasts; however, its outcome is not always appropriate and may degrade rather than improve the raw forecast under some circumstances. A major drawback of this approach is that the pairing associations between individual simulated and observed values is not preserved, the two CDFs being constructed independently from each other, so this connection is not constantly represented (Madadgar et al., 2012).

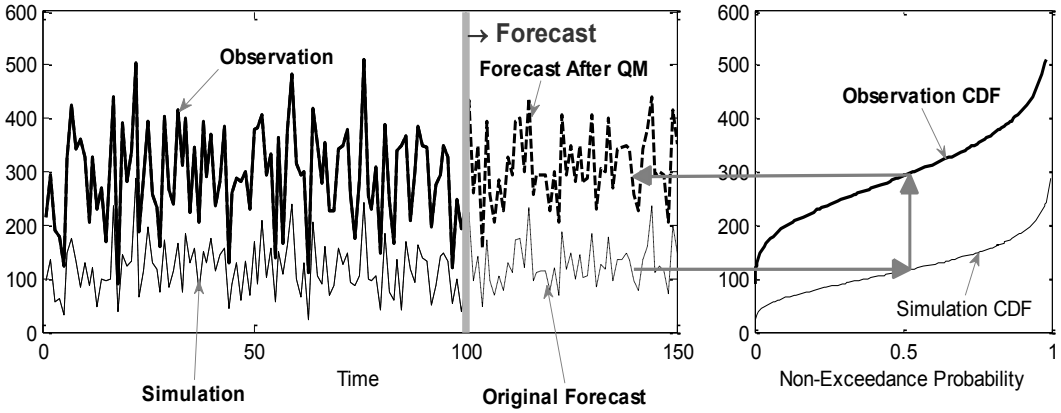

Figure 3: Schematic of Quantile Mapping technique in post-processing (bias correction) of original forecasts

Therefore, QM may be also called a "blind-matching" approach (Madadgar et al., 2012) that sometimes degrades the results; and in some circumstances, as shown in Figure 4, the adjusted simulated values may deviate even further from the observations than the unadjusted simulated values. As seen in Figure 4, at t = 3, the bias corrected simulation after QM does not get closer to the corresponding observation but rather moves further away from the observation, creating an even larger error. In other words, the direction of the desired move (towards the observation) is opposite from the adjustment move (by QM application). However, unlike the improper adjustment at t=3, the original forecast at t = 7 moves towards the observed value, and then QM at this point

has a positive effect. A large number of points with adjustments in the opposite direction of what is desired may lead to the overall deficiency of the QM method.

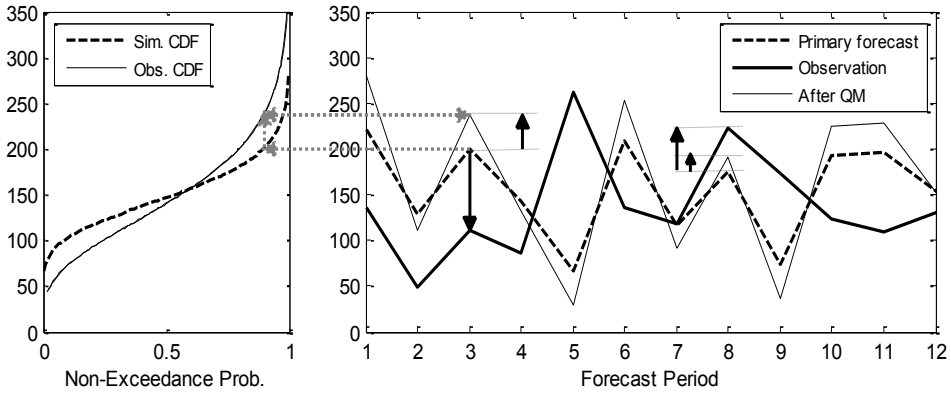

Figure 4: Failure or success of QM method caused by blind-matching procedure.

3.3 New Index for Analyzing the Post-processing Methods; Failure Ratio

Using the historical observations and model simulations, a new measure (γ), called Failure Ratio, is proposed to predict the overall performance of the post-processing methods like QM technique (Madadgar et al., 2012):

$$\gamma = \frac{1}{T}\sum_{t=1}^{T} I\left\{\left(\beta_t < 0\right) or \left(\beta_t > 2\right)\right\} \tag{9}$$

$$\beta_t = \frac{x_t - y_t}{o_t - y_t} \tag{10}$$

$$x_t = F_O^{-1}\left\{F_Y\left(y_t\right)\right\} \tag{11}$$

where, o_t and y_t are the observation and simulation, respectively, at time t; x_t is the QM-adjusted simulation at time t; F_O and F_Y are the CDF of observations and simulations, respectively; T is the number of time steps in the analysis (historical) period; and I(.) is the Indicator function defined as follows:

$$I\{(\beta_t < 0)\ or\ (\beta_t > 2)\} = \begin{cases} 1 & if\ (\beta_t < 0)\ or\ (\beta_t > 2) \quad \forall t \in [1,T] \\ 0 & Otherwise \end{cases} \tag{12}$$

The proposed index, γ, hereinafter called failure ratio of quantile mapping, is the fraction of time steps during the analysis period when βt is negative or greater than 2. Indeed, γ represents the frequency of simulated values being degraded after QM application, varying between 0 and 1. The term β calculates the ratio of the difference between the simulated and adjusted values to the difference between the simulated and observed values (elaborated later) and it can take any real number in $\Re$. Since observations are not available for the forecast time period, the QM technique is employed for the analysis period to adjust the simulations and derive γ to predict the performance of QM in forecast mode. It is noted that in the QM technique, the behavior of the entire system is assumed to be similar in both the analysis and forecast periods, which is equivalent to having identical CDFs in these two periods.

In case of a river flow forecast, β maps the non-negative values of y_t, o_t, and x_t to a real number $\Re$; $\beta:[0,\infty)^3 \rightarrow (-\infty,\infty)$. In perfect adjustments, β_t is equal to 1, meaning that the adjusted forecast exactly equals the observation. Any time that the simulation change is not towards the observation, i.e. the movements are not in the same direction, β_t would be negative (Fig. 5). Additionally, if both changes have the same direction whereas $(x_t - y_t) >> (o_t - y_t)$, β_t may become greater than 2. Data point b in Fig. 5 shows the situation where both moves are in the same direction but the $(x_t - y_t)$ is more than twice the $(o_t - y_t)$. As can be seen, the absolute error after such an adjustment

would be greater than the absolute error before the adjustment. Furthermore, as seen in data point a, the opposite direction of movement causes a larger error regardless of the amount of move. Therefore, β_t values smaller than zero or greater than 2 are associated with the data points where the QM method does not perform effectively. And, according to Eq. 9, γ (failure index) reflects the frequency of such data points in the analysis period in which the QM technique would have a negative impact on them.

Hence, small values of γ states that the QM technique has been ineffective at only a small number of data points, and as the value of γ increases, more and more data points are negatively affected by the QM method. Therefore, efficient performance of the QM should be accompanied by a small value of γ in Eq. 9.

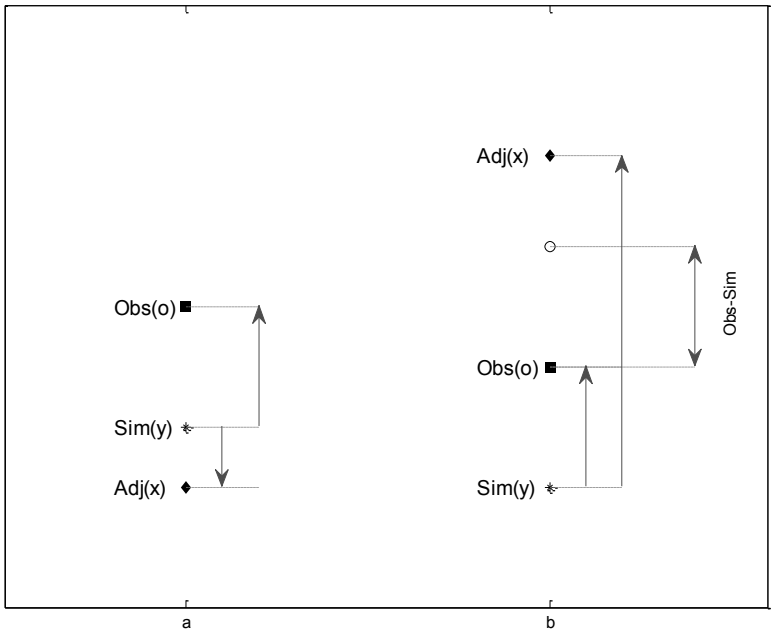

Figure 5: Schematic of data points with a) β < 0, and b) β > 2

For more clarification on β as the main component of the failure index, two different cases are shown in Fig. 6 (Madadgar et al., 2012). Simulation and observation time series

are fitted to lognormal distributions in each case with different parameter values. The first row of the plots shows associated CDFs, and the second row shows their PDFs. Case A represents a situation where simulated values are very different from the observed values, that is, there is little to no overlap between the simulation and observation ranges as seen in the PDF plots. In such circumstances, moving from the simulated value to the adjusted value is in the same direction as moving from the simulated value to the observed value regardless of where it is located in the range of observations. β is therefore always positive, and QM is an effective approach unless β exceeds 2 in too many points. Cases with CDFs located close to each other probably have more frequent points with $\beta > 2$. Case B shows a situation where an overlap of simulated and observed values occurs. As depicted in the CDF plot, depending on where a simulated value is located, the direction of movement to the adjusted value differs; it may be either towards the corresponding observation or in the opposite direction. Therefore, both positive and negative signs are possible for β. Moreover, $\beta > 2$ may also occur frequently in such cases. Hence, QM usually functions effectively in cases with distant CDFs and very small or no overlapped PDFs. However, it is more likely that the QM fails where the CDFs are close or the PDFs are largely overlapped. This makes intuitive sense. Despite the deficiency in the QM technique by not accounting for the pairing between individual simulated and observed values, it can still be helpful in correcting gross differences between simulated and observed values. However, when the two distributions are relatively close, as would be the case for a well-calibrated hydrologic model, this deficiency in the QM technique becomes more significant and the technique may fail.

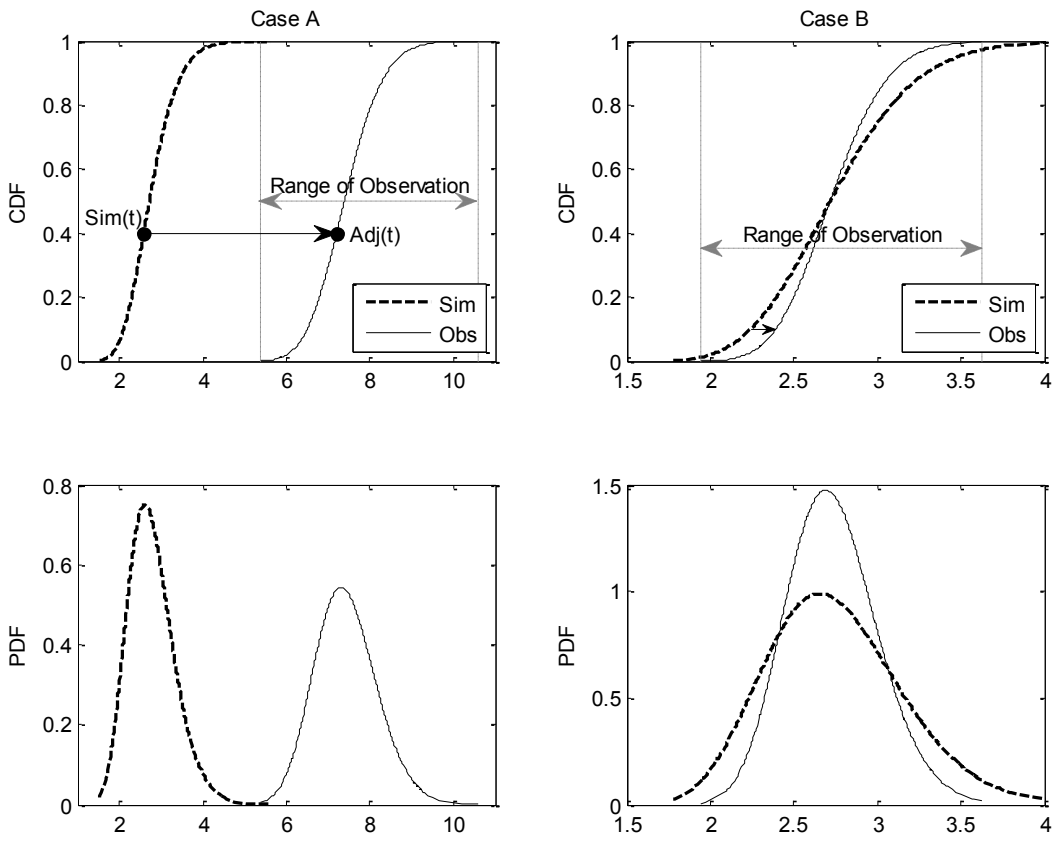

Figure 6: Impact of relative position of simulation and observation CDFs on the performance of the QM adjustments: Case A with distant CDFs is more likely to be well-adjusted by QM method comparing to Case B with close CDFs

3.4 Post-processing by Copula Functions

Post-processing of forecasts is mathematically equivalent to estimate the most likely observation given the raw forecast. Such value would be found from the conditional probability distribution of the observed variable given forecast. Since the observed and forecast variables form a Direct Acyclic Graph (DAG), their probabilistic queries can be represented within a Bayesian network. Briefly, a DAG represents a set of variables in a direct ordering without any direct circuits and the hydrologic forecasts and observations can be fitted in a DAG. Interested readers are encouraged to study Thulasiraman and Swamy (1992) for more detailed descriptions about DAG.

In a Bayesian network, the joint probability density function of the set of random variables in vector $\mathbf{x}$ is written as the product of individual density functions conditional on their parent variables (Russell and Peter, 2009):

$$f(\mathbf{x}) = f(x_1, \ldots, x_n) = \prod_{\forall i} f(x_i \mid \mathbf{x}_{pa(i)}) \tag{13}$$

where $\mathbf{x}_{pa(i)}$ is the subset of $\mathbf{x}$ representing the parent variables of x_i. If $\mathbf{x}$ consists two variables (let's say the observed and forecast variables), Eq. 13 is simplified to:

$$f(\mathbf{x}) = f(x_1, x_2) = f(x_1).f(x_2 \mid x_1) \tag{14}$$

From Eq. 14, the conditional probabilities can be written as:

$$f(x_2 \mid x_1) = \frac{f(x_2, x_1)}{f(x_1)} \tag{15}$$

An intense analytical effort is required to directly model the joint behavior of the variables in Eq. 15 and obtain the joint probability density function in the right-hand side of the equation, specifically if the variables are more than only two variables. By the help of copula functions in estimating the joint pdf (Eq. 3), the conditional pdf (Eq. 15) can be decomposed to a simpler form as:

$$f(x_2 \mid x_1) = \frac{f(x_2, x_1)}{f(x_1)} = \frac{c(u_2, u_1).f(x_2).f(x_1)}{f(x_1)} = c(u_2, u_1).f(x_2) \tag{16}$$

For the forecast post-processing, x_2 and x_1 are referred to the observed and forecast variables, respectively; and u_2 and u_1 are the corresponding marginal distributions. The copula density function - $c(.,.)$- is obtained from an analysis period before the forecast date.

Conditional pdf from Eq. 16 is an estimation of the uncertainty around the forecast value; while, its highest probable value (mode of pdf) can be taken as the single-value post-processed value. Given the forecast at any time step, a particular conditional probability can be estimated with the mode value (x) found as follows (Madadgar et al., 2012):

$$\arg\max_x \left[f(o_t \mid y_t) \right] \;\; ; \;\; where \;\; f(o_t \mid y_t) = c(u_{o_t}, u_{y_t}) f(o_t) \tag{17}$$

where; argmax returns the value of x that maximizes the argument in the brackets- $f(o_t \mid y_t)$, y_t and o_t are the forecast and observation at time t.

To obtain the conditional PDF of Eq. 17 and extract its mode, we suggest Monte Carlo sampling from the copula density function- $c(u_{o_t}, u_{y_t})$, where u_{y_t} is computed for the forecast at time t. Then, u_{y_t} is fixed at time t and u_{o_t} varies for different samples. Proceeding the Monte Carlo sampling leads to form the conditional PDF- $f(o_t \mid y_t)$ whose mode is the most probable observation given the forecast at time t. Figure 7 visualizes the PDF of a copula and the marginal distribution at $u_1 = 0.8$, $c(u_2, u_1 = 0.8)$.

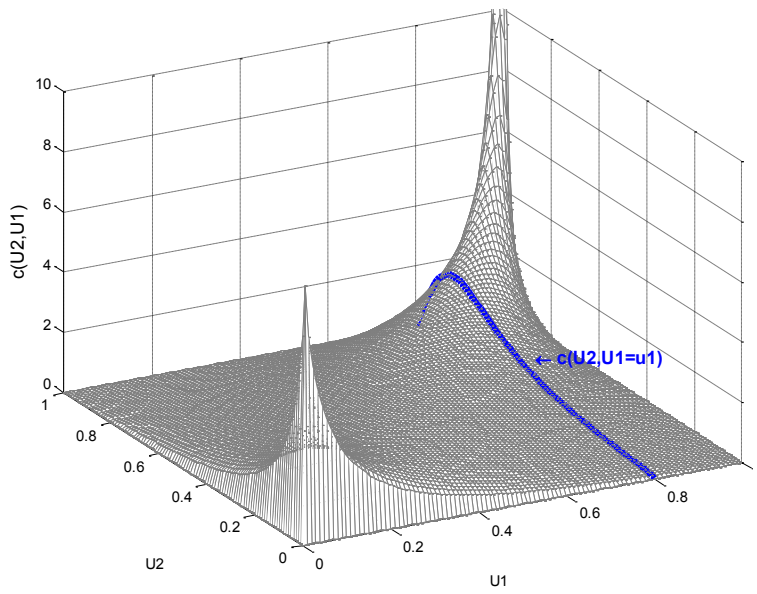

Figure 7: Schematic of a copula pdf with marginal distribution of U2 shown by the solid line.

3.5 Application of Post-processing Methods

The QM and copula-based post-processing methods described in earlier sections are evaluated by hypothetical and real case studies. In the hypothetical case study, forecasts and observations are sampled from separate parametric distributions, and then each post-processing method is applied to adjust the raw ESPs. In the real case study, the streamflow forecasts for a river basin in southern Oregon, USA are post-processed to obtain the adjusted ESPs.

3.5.1 Hypothetical Case Studies

To evaluate the performance of each post-processing method and explore the relation of γ values (Eq. 9) with the effectiveness of each method, 2500 sets of simulation and observation data series are tested in this section. Test cases are generated independently from each other. Each case is to join the marginal distributions of the

simulation and observations by an appropriate t-copula. Simulations and observations of each case have a level of dependency and correlation with each other; nevertheless, the simulations and observations in a single case are produced totally independent from those of another case. Gamma and Lognormal distributions with 30 different parameter sets are used to randomly sample the forecasts and observations of 2500 cases. Following steps are taken to form the hypothetical case studies:

1. N=1, case number
2. Form the data series for the analysis period
    a. Sample from a parametric distribution (D_1) for 1000 times to build the simulation timeseries. D_1 is either Gamma or Lognormal distribution.
    b. Sample from either Gamma or Lognormal distribution (D_2) for 1000 times to build the observation timeseries.
3. Find a bivariate t-copula to join the marginal distributions fitted to the simulations and observations generated in steps (2-a) and (2-b).
4. Generate datasets for the forecast period
    a. Sample from a D_1 (step 2-a) for 12 times to build the forecast timeseries. Forecast lead-time is set as 12.
    b. Repeat step (4-a) for 50 times to make a forecast ensemble with 50 traces.
    c. Sample from a D_2 (step 2-b) for 12 times to build the observation timeseries.
5. Post-process the forecast ensemble obtained in step (4-a) by either copula-based or QM method.
6. N=N+1

7. If N≤2500, then go to 2. Else, terminate!

In step (4-c), the real-time observations in forecast period are sampled from the observation distribution function used at step (2-b). The observations of the forecast period enable a performance evaluation of the post-processing methods. Table 2 summarizes the list of verification measures to evaluate the performance of each method. Point-wise performance measures are utilized in evaluating the deterministic forecast (ensemble mean), while the probabilistic measures are used to assess the performance of the forecast ensembles. Figure 8 shows the results of the QM technique against the copula-based post-processor (Madadgar et al., 2012). Probability of success in Figure 8 is the probability that the post-processing method performs successfully with respect to the associated metric for different values of the failure index (γ). γ is computed for the analysis period of each case, and then cases with a given value of γ are taken out from the pool of 2500 cases. Therefore, for each metric of interest, cases with successful performance are counted to compute the probability of success. Success is defined upon the metric value, that is, if implementation of the post-processing method improves the metric score towards its perfect value as noted in Table 2, then the method is considered as successful for that metric. Figure 8 shows that as γ increases, the probability of success strictly declines in the first three metrics (MAE, NSE, and RPSS) when QM is in use. Given the definition of γ in Eq. 9, if the post-processing method constantly degrades the forecasts, γ becomes greater and approaches 1. In such circumstances, the QM method may not be able to improve the forecasts owing to its inherent blind-matching nature where the adjustments are merely dependent on the quantile values. Evidently, the

probability of success in the QM method is dependent on the γ value, whereas this is not the case for the copula-based post-processing method. The main reason of insensitivity of copula-based method to the failure index value is its ability to model the joint behavior of the simulations and observations unlike the QM method with inherent blind-matching approach. In other words, the copula approach is able to perform effectively even in cases with a large failure index. Generally, the copula approach is more likely to succeed than the QM method in the first three metrics. Other metrics in Figure 8 (α, ε, and π) are the supportive quantitative scores derived from the predictive quantile-quantile (QQ) plot (Laio and Tamea, 2007; Thyer et al., 2009), which compares the empirical CDF of the probability of observations ($P_t(o_t)$ in Table 2) using the forecast ensemble at each time t (CDF of the probabilities) against the CDF of a uniform distribution. For a perfect forecast ensemble, the empirical CDF of the p values is consistent with the CDF of the uniform distribution on the interval [0,1]. The metrics α and ε assess the reliability of forecasts, and π indicates the resolution (precision, sharpness) of the forecast ensemble. According to Thyer et al. (2009), as the area between the empirical CDF of the observations's p values and the CDF of the uniform distribution in the predictive QQ plot becomes larger, the value of α decreases towards zero. Results indicate that for $\gamma \leq 0.7$, the post-processing methods perform closely, while for large γ values, the QM method is more successful than the copula-based method for the α measure. The subplot of the ε metric illustrates that the copula method is more effective than the QM method (regardless of γ value) to envelop observations after post-processing of the forecasts. In other words, fewer observations fall outside the range of the forecast ensemble after post-

processing by the copula approach. The resolution (π), also called sharpness, states that adjustment by QM leads to greater resolution (precision). However, comparison of sharpness may not be a meaningful approach when the employed methods do not primarily perform equally in the α and ε metrics. Assuming that precision has lower priority than reliability, given similar forecast reliabilities, the method with greater resolution (lower uncertainty) is preferred; otherwise, the method with higher resolution does not reveal any superiority.

As a brief summary of the hypothetical-case results, the multivariate copula-based post-processor performs considerably better than the QM method in the point-wise measures. For the RPSS metric among the probabilistic measures, the copula procedure is again evaluated as a much better method than QM. The predictive uncertainty is also more reliable in encompassing observations when the multivariate copula-based post-processor is in use. Moreover, unlike the QM method, performance of the multivariate post-processor is generally insensitive to the failure index of the analysis period. Using the QM method, the predictability of the forecast ensemble is not effectively improved in cases with large γ values, illustrating the drawback of the blind-matching procedure that corresponds to the same quantiles of simulation and observation CDFs.

3.5.2 Hydrological Forecast Case Study

The Sprague River basin, with a drainage area of approximately $4100\ km^2$, is a sub-basin of the Upper Klamath River basin located in southern Oregon and northern California, USA (Fig. 9). The Sprague River valley is enclosed by forested mountain ridges and includes large marshes, meadows, and irrigated pastures. A large proportion of

irrigation water demand is supplied by river flow, and the rest is pumped from local wells. A major environmental concern in the Sprague River basin is the water quality, which directly impacts fish and wildlife habitat throughout the Upper Klamath basin as reported by Klamath Basin Ecosystem Foundation (2007). Some flow conditions interrupt fish passage through the Sprague River, which necessitates accurate forecast for better understanding of flow conditions in coming seasons. The Sprague River is also a major tributary to Upper Klamath Lake, an important and highly contested water body used for irrigation water supply, hydropower generation, and fish habitat.

The U.S. Geological Survey (USGS) Precipitation-Runoff Modeling System (PRMS; Leavesley et al., 1983), a distributed parameter hydrologic model, is applied to streamflow forecast of the Sprague River basin. Daily temperature and precipitation observations drive PRMS to predict the daily flow of the basin. Two different sources provide the climate records: the NWS Cooperative Network (COOP), and the NRCS Snow Telemetry (SNOTEL) network of weather stations.

Table 2: Performance metrics to evaluate the employed bias correction methods

Performance Measure	Mathematical Representation	Terminology	Description
Mean Absolute Error (MAE)	$MAE = \frac{1}{T}\sum_{t=1}^{T}\left\|\overline{y_t} - o_t\right\|$ $\overline{y_t} = \frac{1}{N_{ens}}\sum_{i=1}^{ens} y_{t,i}$	$\overline{y_t}$: Average over ensemble predictions at time t o_t : Observation at time t	Deterministic metric, varies $[0,\infty)$, with perfect score of 0.
Nash-Sutcliffe Efficiency[a] (NSE)	$NSE = 1 - \frac{1}{\sigma_o^2}\left[\frac{1}{T}\sum_{t=1}^{T}\left(\overline{y_t} - o_t\right)^2\right]$	σ_o^2 : Variance of observations	Deterministic metric, varies $(-\infty,1]$, with perfect score of 1.
Rank Probability Skill Score[b] (RPSS)	$RPSS = 1 - \frac{\overline{RPS}}{RPS_{ref}}$ $RPS_t = \sum_{k=1}^{K}\left[P_k(y_t) - P_k(o_t)\right]$ $P_k(y_t) = \frac{1}{N_{ens}}\sum_{i=1}^{N_{ens}} I(y_{t,i} < Q_k)$ $P_k(o_t) = I(o_t < Q_k)$ $RPS_{ref} = \frac{1}{T}\sum_{t=1}^{T}\sum_{k=1}^{K}\left[P_k(o_t) - \overline{P(o)}\right]$	I : Indicator function Q_k : k^{th} threshold of Q $\overline{P(o)}$: Average probability of all observations over all thresholds. $\overline{P(o)} = \frac{1}{T}\sum_{t=1}^{T}\sum_{k=1}^{K} P_k(o_t)$	Probabilistic metric, varies $(-\infty,1]$, with perfect score of 1. Negative values mean predictions perform worse than the average observation.
Reliability[c] (α)	$\alpha = 1 - 2\left[\frac{1}{T}\sum_{t=1}^{T}\left\|P_t(o_t) - U(o_t)\right\|\right]$ $P_t(o_t) = \frac{I(y_{t,i} < o_t)}{N_{ens}}$	$P_t(o_t)$: Non-exceedance probability of o_t using the ensemble predictions at time t. $U(o_t)$: Non-exceedance probability of o_t using the uniform distribution $U[0,1]$	Probabilistic metric, measuring the closeness of quantile plot of the observations to the corresponding uniform quantiles. It varies $[0,1]$, while 0 is the worst and 1 is the best score.
Reliability[c] (ε)	$\varepsilon = 1 - \varepsilon'$ $\varepsilon' = \frac{1}{T}\sum_{t=1}^{T} I\left[P_t(o_t) = 1 \text{ or } P_t(o_t) = 0\right]$	Similar to α	Probabilistic metric. It varies $[0,1]$, while 0 is the worst and 1 is the best score.
Resolution[c] (π)	$\pi = \frac{1}{T}\sum_{t=1}^{T}\frac{E[y_{t,i}]}{\sigma[y_{t,i}]}$	$E[y_{t,i}]$: Expected value of ensemble predictions at time t $\sigma[y_{t,i}]$: Standard deviation of ensemble predictions at time t	Probabilistic metric, a measure of precision of ensemble predictions. Greater values indicate less precision (larger uncertainty) of forecasts.

[a] Nash and Sutcliffe (1970)
[b] Wilks (1995)
[c] Renard et al. (2010)

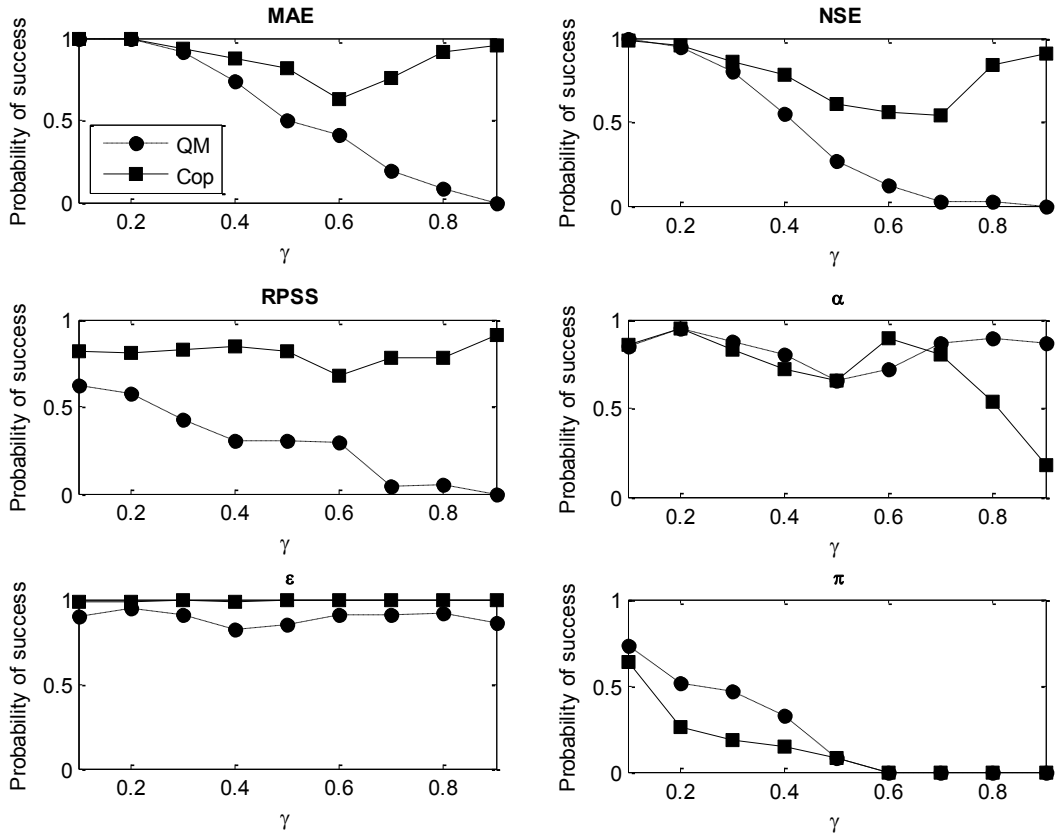

Figure 8: Probability of success against γ for point-wise (MAE and NSE) and probabilistic performance measures (RPSS, α, ε, π) in QM and copula-based post-processing methods. Probability of success is obtained with respect to the associated metric for different values of the failure index.

PRMS is a modular deterministic, distributed-parameter, physical-process watershed model that simulates the hydrologic response of a watershed to the combined effect of precipitation, climate, and land use. The inherent algorithms can represent each physical process or empirical relation among different hydrologic components. The model can simulate the response to normal and extreme climate events including sudden storms and extreme dry conditions. The model setup evaluates the changes in water-balance relations, streamflow regimes, soil-water relations, and ground-water recharge. PRMS simulates the hydrologic processes of a watershed using a series of reservoirs with

different capacities that are interconnected to each other (Fig. 10). Each reservoir passes and/or stores the in- and out- fluxes to simulate the flow, evapotranspiration, and sublimation. Parameters of the model can be calibrated manually by an expert or the optimization algorithms. This study uses the Shuffled Complex Evolution (SCE) global search algorithm (Duan et al., 1994) within the multiple-objective stepwise calibration (LUCA) (Hay and Umemoto, 2006) framework. Interested readers are encouraged to study the relevant references for more details about the calibration algorithms.

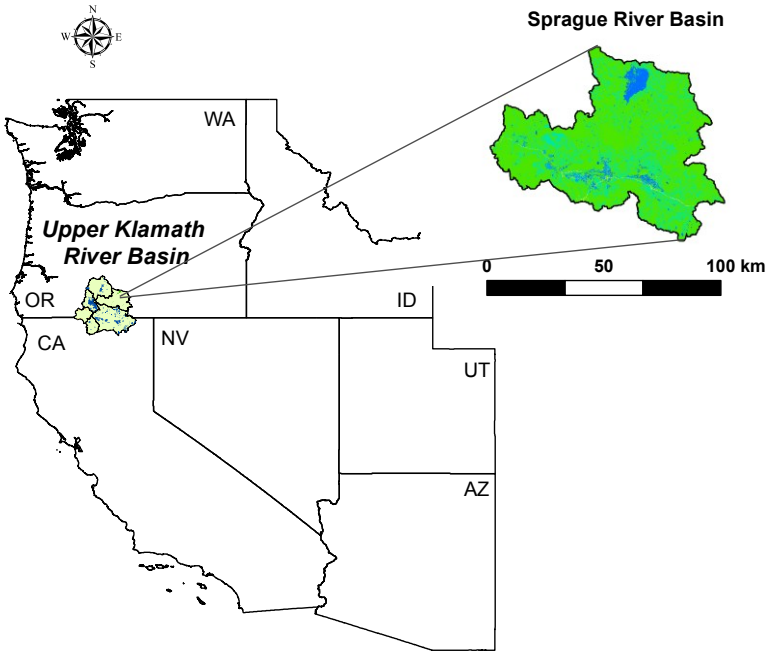

Figure 9: Sprague River Basin, a sub-basin of Upper Klamath River Basin in southern OR and northern CA

Copula application starts with fitting appropriate marginal distributions to the variables to be post-processed. Monthly flow observations and model simulations of Sprague River basin outflow are each fitted to eight distributions, including Gamma, Generalized Extreme Value (GEV), Lognormal, Gaussian, Generalized Pareto (GP), Weibull, Gumbel, and Exponential distributions. Several forecast periods starting from

different months (Jan, Feb, Mar) of 2001-2003 are analyzed for the post-processing application. The forecast lead time is fixed at 6 months and the total of 9 forecast periods are chosen as Jan-Jun, Feb-Jul, and Mar-Aug for each of the three years from 2001 to 2003. The marginal distributions are separately fitted to historical observations and model simulations in the analysis periods. The historical period from 1980 to 2000 is used to set the analysis periods associated with each forecast period. The analysis periods are then taken as Jan-Jul, Feb-Jul, and Mar-Aug of 1980-2000. The histograms of monthly averaged PRMS simulations and river flow observations for the analysis period of Feb-Jul in 1980-2000 and the fitted distributions are shown in Figures 11 and 12 (Madadgar et al., 2012). The parameters of the marginal distributions are estimated by the Maximum Likelihood Estimation (MLE) method. From visual inspection, most theoretical distributions except Gaussian and Gumbel are well-fitted to PRMS simulations. It seems hard, however, to find a suitable distribution to fit flow observations properly, with only the GEV and Lognormal distributions looking suitable. Table 3 lists the statistics used for evaluation of the theoretical marginal distributions. The K-S test (Eq. 7) is used to verify the appropriateness of the marginal distributions.

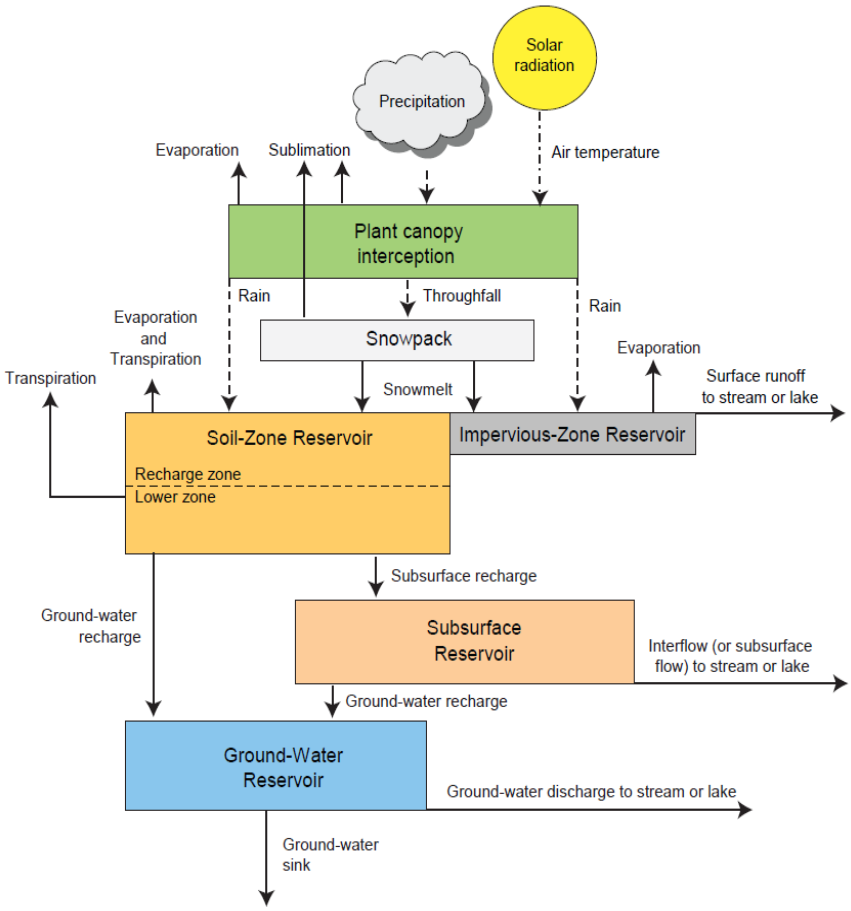

Figure 10: Schematic of the reservoirs and their connections in PRMS.

In Table 3, the acceptable marginal distributions with the significance level of $\alpha = 0.05$ are shown in bold fonts. Gaussian and Gumbel distributions are not suitable choices for simulated flows for any of the three analysis periods, while the other distributions fit more or less well. On the contrary, almost none of the distributions except GEV properly fit the observed flows. These results have been visually verified in Figures 8 and 9 for the analysis period of Feb-Jul, 1980-2000. Furthermore, for the Jan-Jun analysis period, the Lognormal distribution is the second-most suitable choice for the observed flow. However, the GEV distribution is the best candidate for the observations

of any analysis period; hence, for the copula application, the GEV distribution is hereinafter coupled with the marginal distributions of the simulated flows.

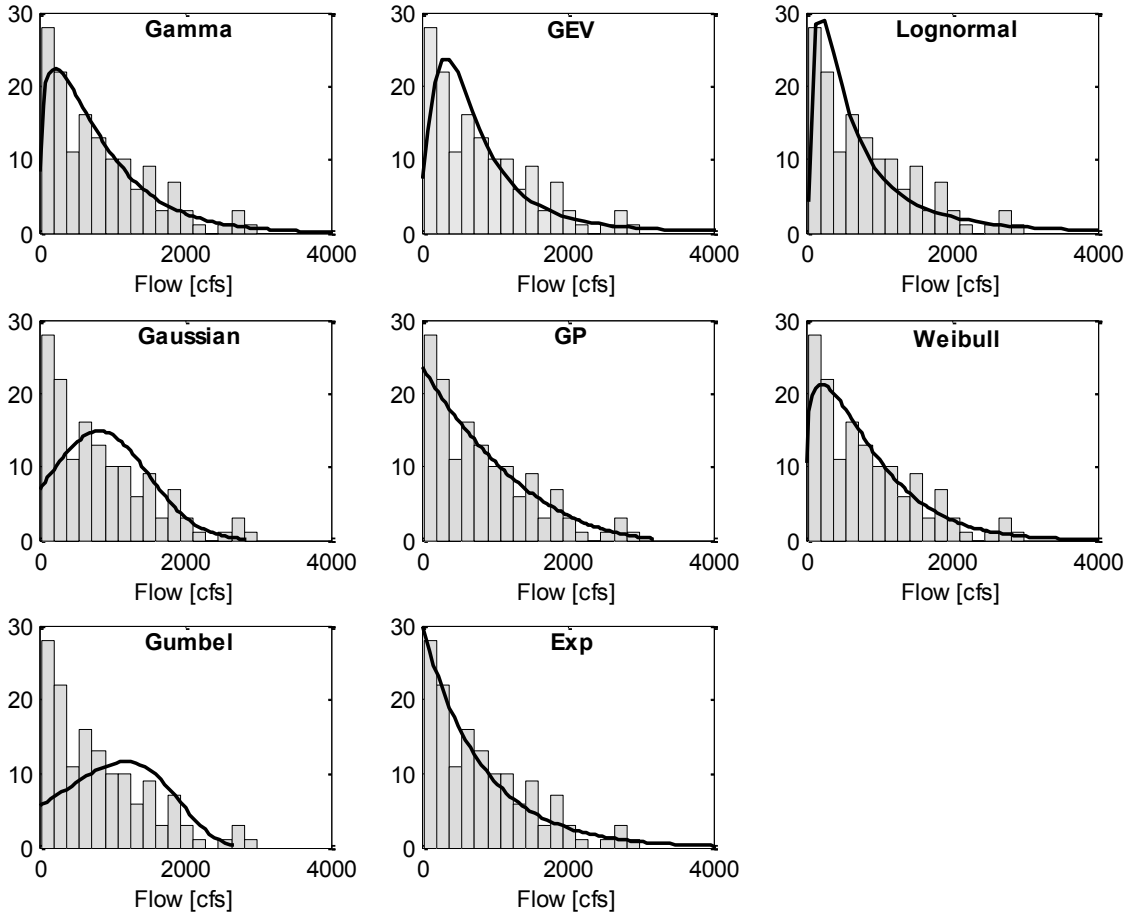

Figure 11: Flow histogram against marginal distribution fitted to monthly averaged PRMS simulations in the analysis period of Feb-Jul, 1980-2000.

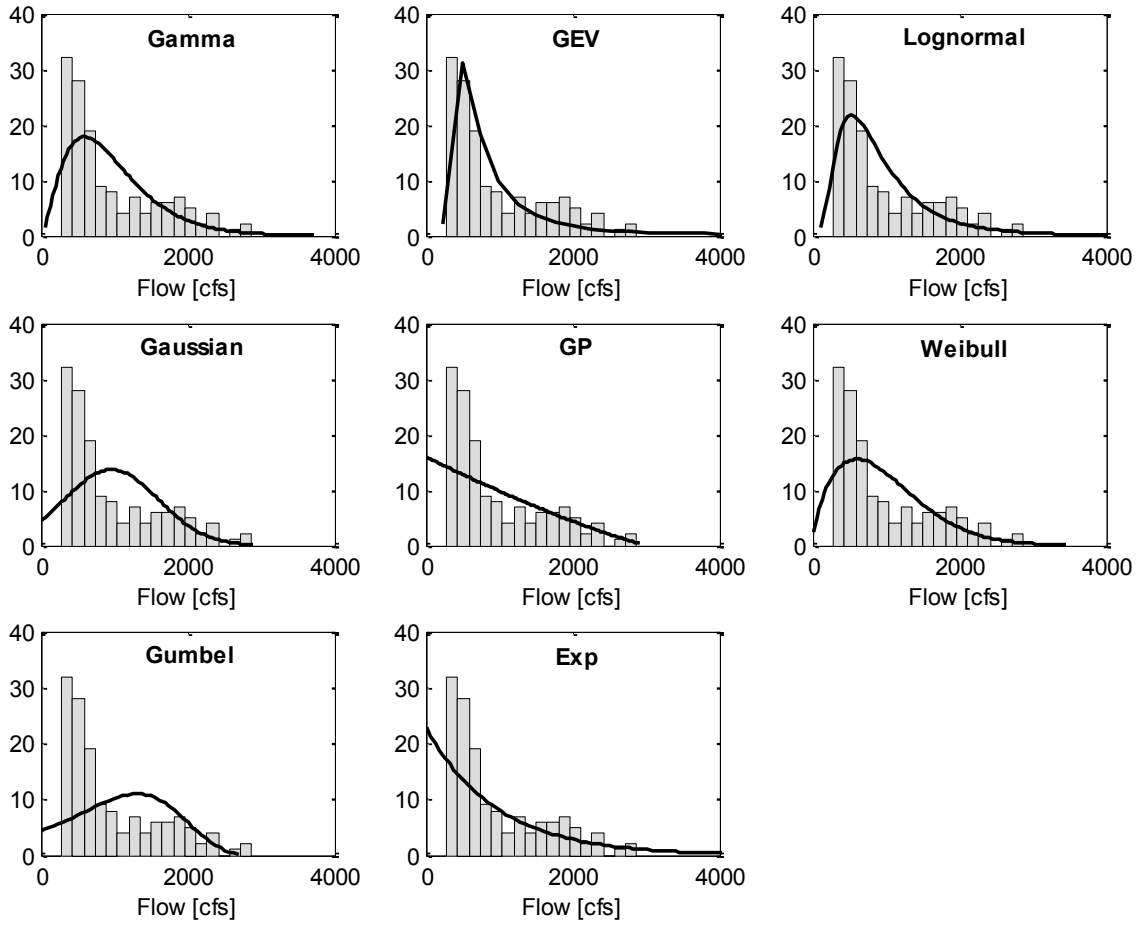

Figure 12: Flow histogram against marginal distribution fitted to monthly averaged river flow observations during the analysis period of Feb-Jul, 1980-2000.

The Elliptical and Archimedean families of copulas (Table 1) are applied to join the marginal distributions of historical monthly observations and model simulations during each analysis period (Jan-Jun, Feb-Jul, and Mar-Aug of 1980-2000). The Cramér-von Mises statistic (Eq. 4) is applied to verify which copula joins the marginal distributions better than others. In a group of copulas, the one with the greatest p-value (and smallest S_n) is a better choice to join the marginal distributions.

Table 3: K-S test statistics of fitting different distributions to the simulated and observed flows during different analysis periods in 1980-2000

	Jan-Jun			**Feb-Jul**			**Mar-Aug**		
	D	P-value	Hypothesis Test	D	P-value	Hypothesis Test	D	P-value	Hypothesis Test
Simulated flow									
Gamma	0.08	**0.25**	Accept	0.07	**0.39**	Accept	0.07	**0.44**	Accept
GEV	0.08	**0.25**	Accept	0.09	**0.22**	Accept	0.07	**0.40**	Accept
Logn	0.11	**0.07**	Accept	0.10	**0.10**	Accept	0.08	**0.27**	Accept
Gaus	0.13	0.01	Reject	0.18	0.03	Reject	0.12	0.03	Reject
GP	0.08	**0.22**	Accept	0.06	**0.64**	Accept	0.06	**0.64**	Accept
Wbl	0.08	**0.20**	Accept	0.08	**0.31**	Accept	0.07	**0.40**	Accept
Gumbel	0.22	2.2E-6	Reject	0.21	5.8E-6	Reject	0.21	3.2E-6	Reject
Exp	0.07	**0.47**	Accept	0.08	**0.29**	Accept	0.08	**0.25**	Accept
Observed flow									
Gamma	0.13	0.01	Reject	0.15	0.01	Reject	0.16	0.002	Reject
GEV	0.08	**0.32**	Accept	0.06	**0.24**	Accept	0.08	**0.25**	Accept
Logn	0.10	**0.13**	Accept	0.14	0.03	Reject	0.13	0.01	Reject
Gaus	0.18	1.3E-3	Reject	0.22	5.2E-5	Reject	0.21	3.4E-6	Reject
GP	0.18	1.6E-4	Reject	0.24	3.2E-5	Reject	0.21	7.1E-6	Reject
Wbl	0.14	9E-3	Reject	0.18	0.006	Reject	0.16	0.001	Reject
Gumbel	0.21	4.4E-6	Reject	0.29	1.4E-6	Reject	0.23	3.7E-7	Reject
Exp	0.24	1.3E-7	Reject	0.27	9.6E-9	Reject	0.28	3.7E-10	Reject

As described earlier, three analysis periods having their specific marginal distributions are tested in this study. Elliptical and Archimedean copulas are fitted to the simulations and observations of each analysis period; the S_n statistic and corresponding p-values of testing the null hypothesis ($H_0 : C_n \in C_{\theta_n}$) are summarized in Table 4. Results are the mean value of Cramér-von Mises statistic (S_n) and corresponding p-value when a

given copula is applied to different combinations of marginal distributions. As discussed earlier, GEV is selected for observed flows and Gamma, GEV, Lognormal, GP, Weibull, and Exponential distributions are selected for simulated flows. The p-values are computed using a parametric bootstrap procedure with N=1000 replications and a significance level of α=0.01. In each case, the copula function with the smallest S_n (Eq. 4) and the largest p-value is preferred; hence among the copula functions, the Frank copula is the best choice for the Jan-Jun and Feb-Jul periods, whereas the Gumbel copula is the best for the Mar-Aug period. However, the Clayton copula function is the worst choice for any analysis period.

Table 4: Results of GOF test for copula selection in each analysis period. Values of Cramér-von Mises statistic (Sn) are presented along with the corresponding p-value in parentheses. Statistics of the best fitted copuls are bolded.

Analysis Period / Copula Function	Jan-Jun	Feb-Jul	Mar-Aug
Gaussian	0.0232 (0.0664)	0.0292 (0.0255)	0.0550 (0.0005)
t	0.0330 (0.0055)	0.0406 (0.0025)	0.0653 (0.0005)
Gumbel	0.0242 (0.0644)	0.0299 (0.0315)	**0.0383 (0.0135)**
Clayton	0.2173 (0.0005)	0.2316 (0.0005)	0.3239 (0.0005)
Frank	**0.0217 (0.0794)**	**0.0257 (0.0415)**	0.0521 (0.0025)

After fitting the appropriate copula to the univariate marginal distributions of the associated analysis period, the conditional pdf of observation given the forecast is estimated to implement the post-processing of each forecast ensemble (Eq. 17). To

evaluate the performance of the post-processing methods, several 6-month hindcast periods within three target years (2001, 2002, and 2003) are tested. As explained earlier, three hindcast periods are chosen in each target year: Jan-Jun, Feb-Jul, and Mar-Aug. Note that post-processing is applied to monthly averaged flows of each forecast period. Using the same performance metrics applied to the hypothetical case studies (Table 2), the performance of post-processing methods on the streamflow forecasts of the Sprague River basin are shown in Figures 13-15 (Madadgar et al., 2012). The QM and copula post-processing techniques are both used to adjust the hind-casts predicted by PRMS. The initial hydrologic states of the basin at the hindcast date are obtained by running the PRMS model in the spinup period. To implement the multivariate copula-based post-processor, the selected copula function (see Table 4) is applied to all (six) possible combinations of marginal distributions that are best fitted to the simulated and observed flows in the analysis period (see Table 3). The results of copula application in Figures 13-15 are associated with the average metric value over all the combinations of marginal distributions. Prior to the QM application, the ability of QM to improve forecasts would be predicted from the value of γ estimated for the analysis period. The failure index for Jan-Jun, Feb-Jul, and Mar-Aug analysis periods through 1980-2000 is respectively found as 0.32, 0.29, and 0.28. Thus, according to Figure 8, it is not expected that QM would produce encouraging results for any of the analysis periods.

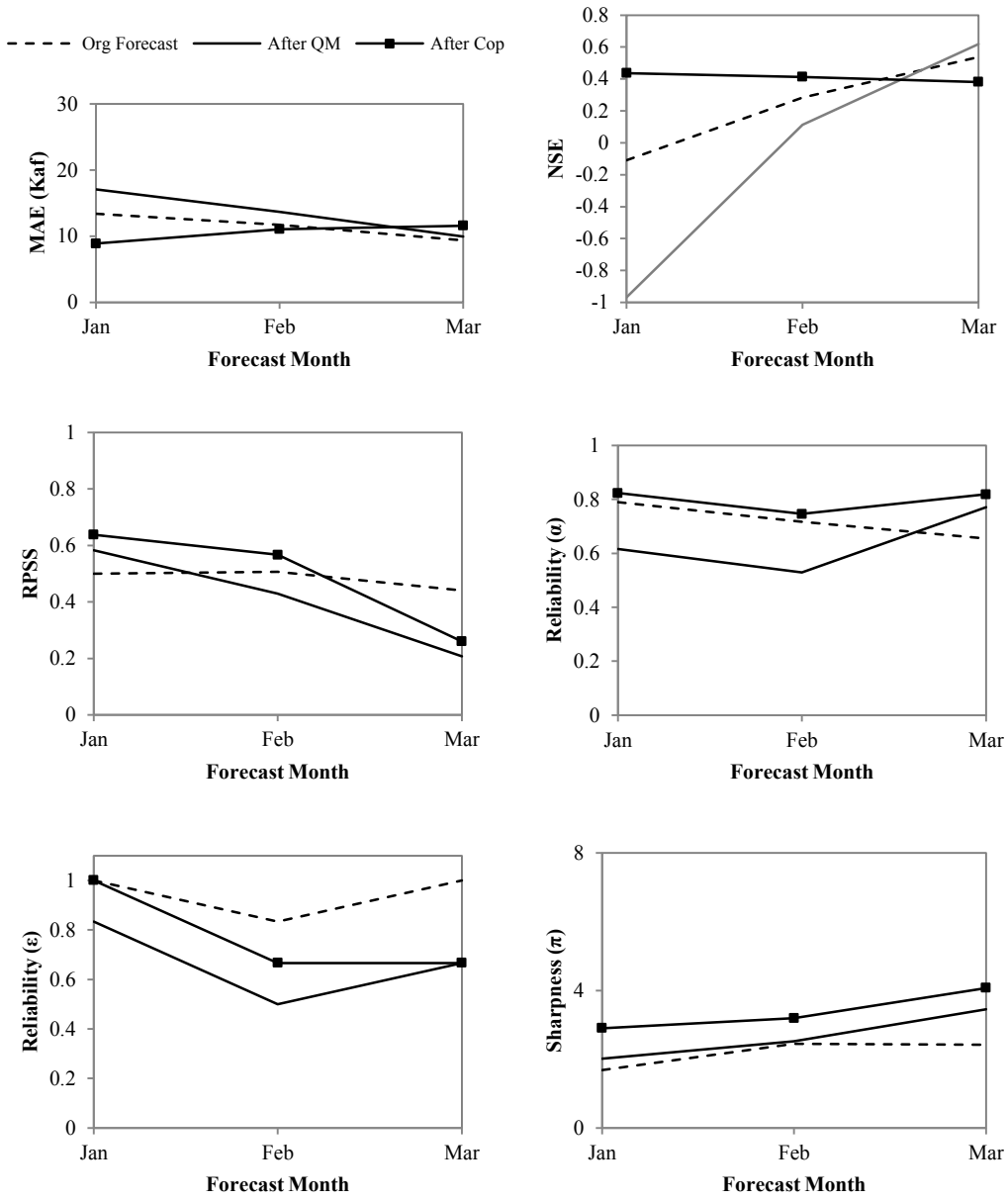

Figure 13: Comparing the performance of post-processing methods in adjusting the monthly streamflow hindcast starting from different forecast dates in 2003. The forecast period of each forecast ensemble is 6 months.

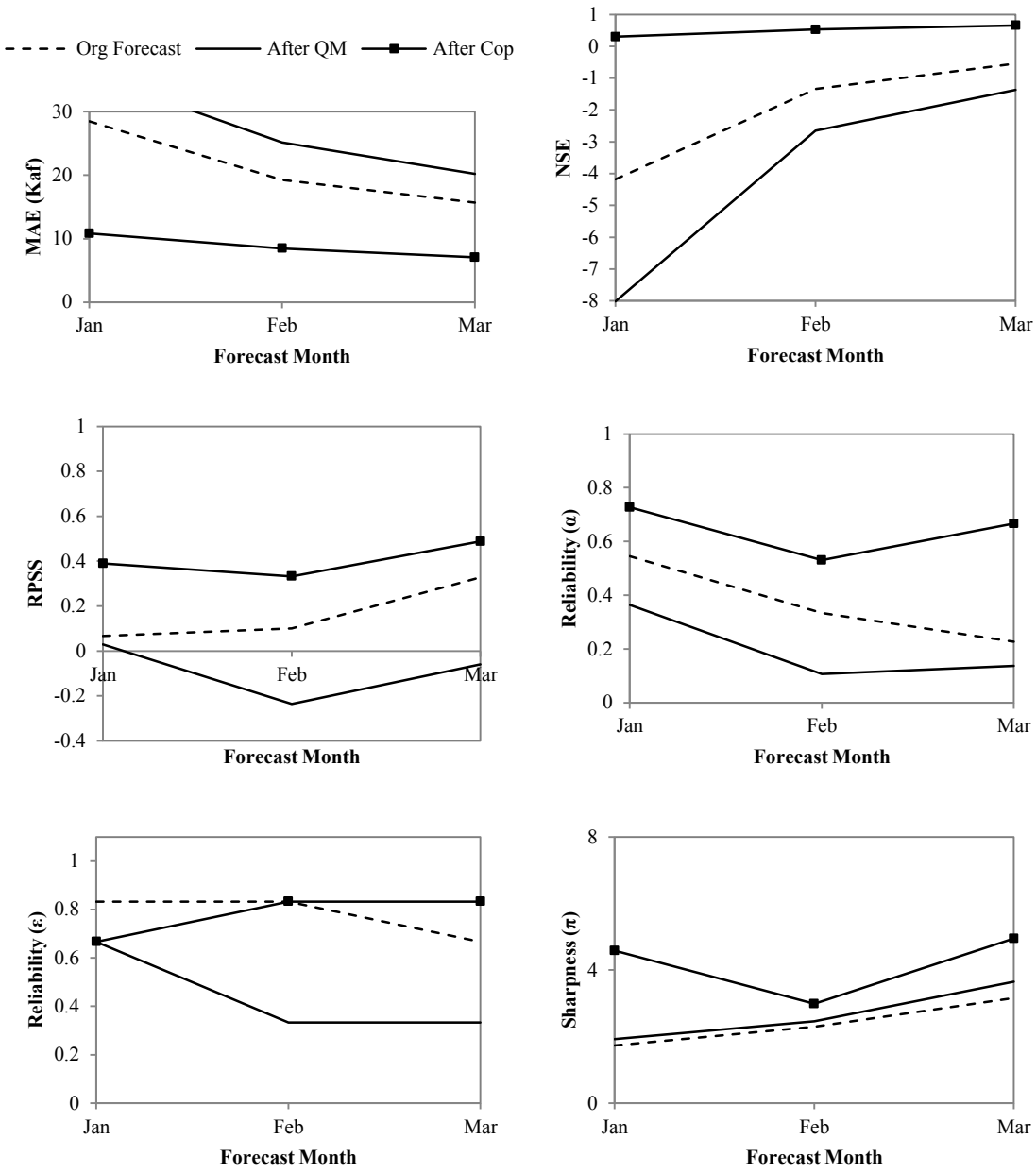

Figure 14: Comparing the performance of post-processing methods in adjusting the monthly streamflow hindcast starting from different forecast dates in 2002. The forecast period of each forecast ensemble is 6 months.

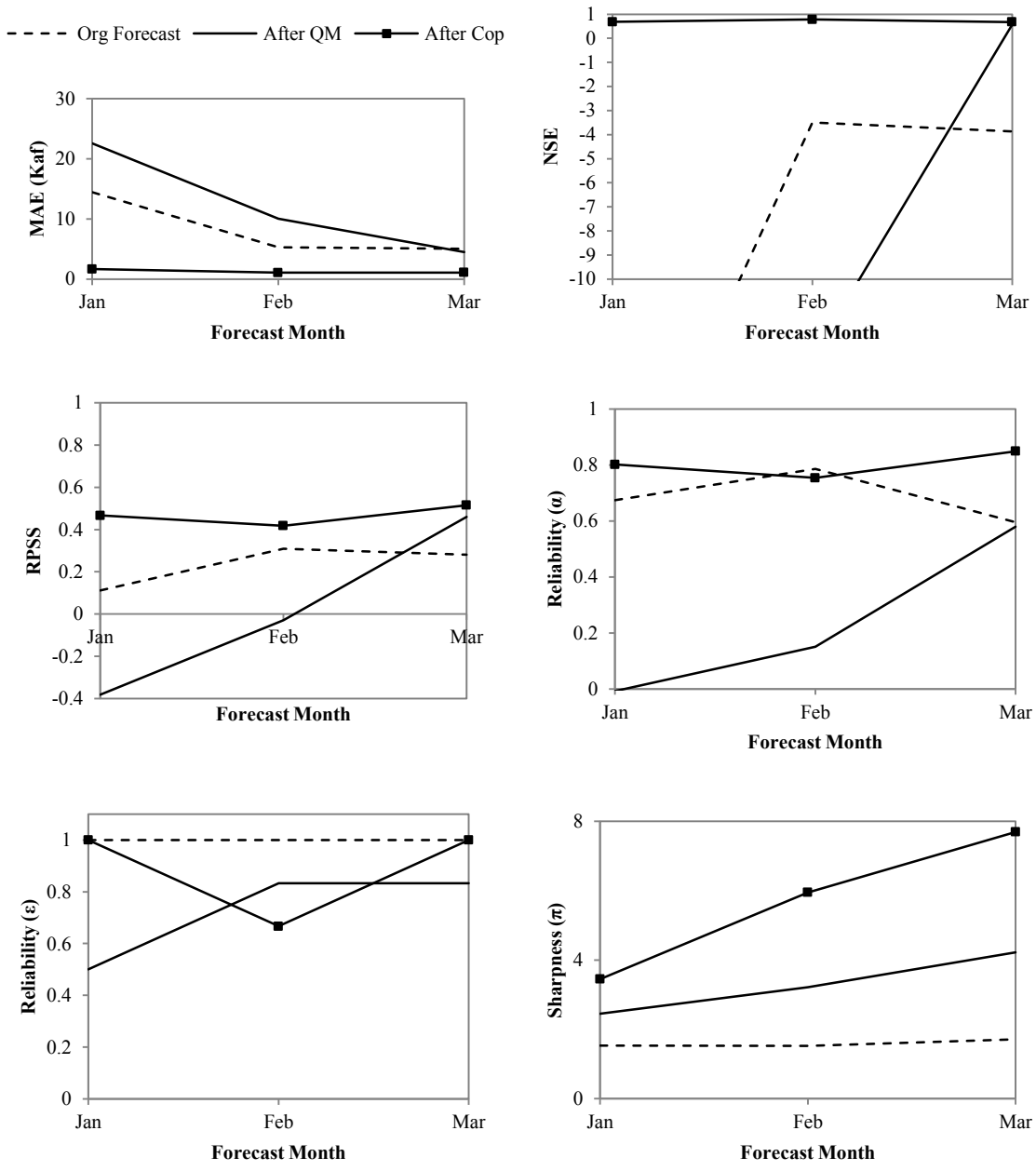

Figure 15: Comparing the performance of post-processing methods in adjusting the monthly streamflow hindcast starting from different forecast dates in 2001. The forecast period of each forecast ensemble is 6 months.

As shown in Figures 13-15, the QM method is not effective in improving the forecast ensemble with respect to the point-wise measures; MAE and NSE show the general failure of QM in reducing the error of the mean forecast. The copula post-processor, however, performs better than the QM method, and it adjusts the forecast ensemble closer to the observations except for the Mar-Aug forecast period of 2003. For the Jan-Jun and Feb-Jul forecast periods in any of the target years, the copula function performs significantly better than the original forecast and the QM method. Regarding the RPSS metric, QM generally fails to improve forecast traces, and it even worsens the quality of original forecasts in almost all forecast periods. Failure of the QM method is also predictable according to the γ values found for different analysis periods. Copula application, on the other hand, is consistently the prominent method for the Jan-Jun and Feb-Jul forecast periods. As the forecast starting date moves towards spring, the performance of multivariate post-processing gets closer to that of the original forecast; however, it is still better than the QM results. The reliability metric derived from a QQ-plot, α, shows that QM adjustments are not reliable compared to original forecasts, while the proposed copula method performs better than the original forecasts. Regarding the reliability metric ε, none of the employed methods is constantly effective in improving forecasts. The value of ε reflects the adequacy of the ensemble spread to encompass all the observations during the forecast period. Generally, neither QM nor copula-based methods are able to adjust the original forecasts so as to embrace all the observations within the ensemble range. The next metric (π) measures the precision (sharpness) of the ensemble. The sharpness of the adjusted ensemble after QM application is higher than the

original forecast ensemble; however, the reliability of QM corrections is less than the others. The subplots of ε and π indicate that a large sharpness of the forecast ensemble after copula application is at the expense of missing some observations to be inside the ensemble spread, implying overconfidence of the ensemble prediction. The QM method, on the other hand, results in better ensemble sharpness (precision) than that of the original forecast; however, as long as a specific method is steadily proved to be unreliable, comparing its precision with other methods is rather trivial and misleading. In other words, if an "inaccurate" forecast ensemble has high "precision", it cannot be accredited as a preferred forecast. Therefore, the evaluation of methods with respect to the sharpness metric should be done by first ensuring a satisfactory reliability of the methods.

For better understanding of the performance of the post-processing methods proposed in this study, the ensemble range and mean forecasts of monthly flow volumes for the forecast periods in 2002 are shown in Figure 16. As can be seen, the mean forecast after copula post-processor is close to the observation for all three observation periods while after QM application, the mean forecasts go even further away from the observed volumes. The MAE and NSE results shown in Figure 14 verify the close distance between the observations and the mean forecast after copula-based post-processing. Moreover, reliable and precise forecast after copula post-processor as expected from the probabilistic measures in Figure 14 are reflected in the ensemble ranges. Also from Figure 16, it can be seen that the error spread reduces significantly by the application of copula post-processor with the exception of few occasions where the observed volume

falls outside the ensemble range after copula post-processing. The overall conclusion from Figure 16 is that the QM method is not an effective method to adjust the original forecasts while the multivariate copula-based post-processor is a more effective method that can be used operationally.

In general, a well-fitted copula function to the marginal distribution is a better choice than the QM method (especially in cases with large γ). The results shown in Figures 13-16 also illustrate that the evaluation of different methods should not be merely based on the probabilistic metrics; they may be misleading if not being compared along with the point-wise measures.

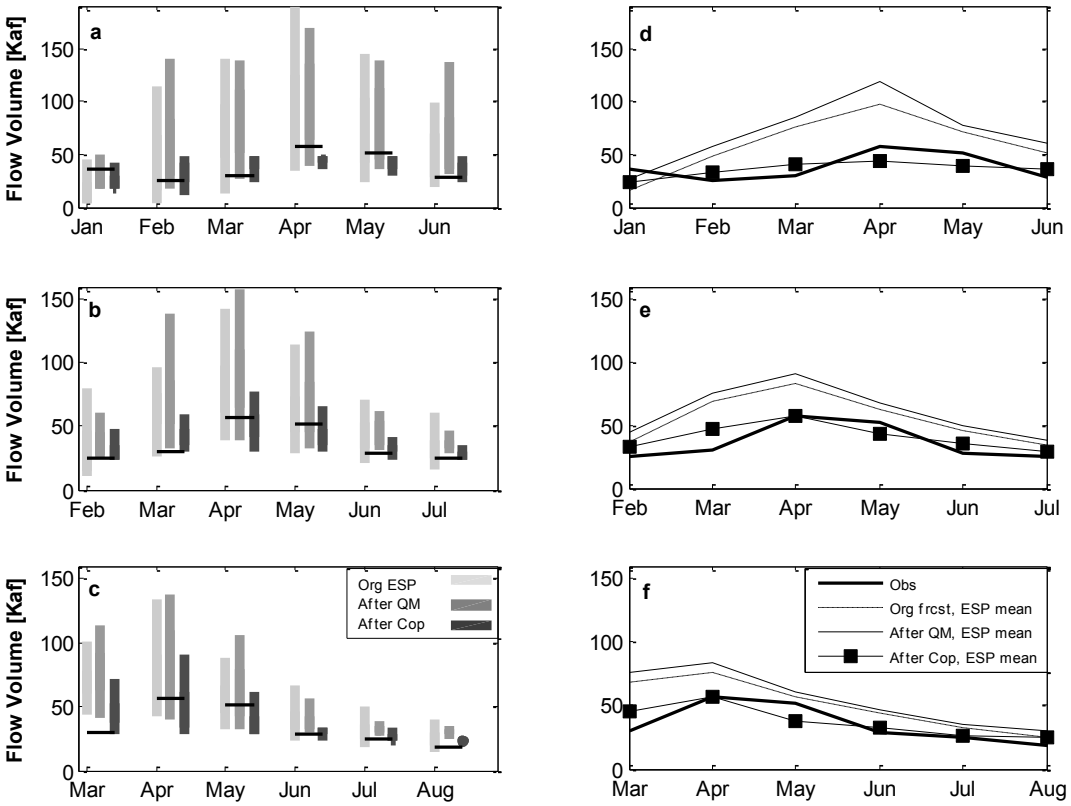

Figure 16: Comparison of the ensemble range before and after post-processing for three forecast periods in 2002 starting from a) Jan, b) Feb, and c) Mar, with the solid lines representing the monthly observations. Corresponding ESP mean are shown in subplots d-f.

4. Probabilistic Forecast of Seasonal Droughts[2]

Appropriate planning of water resources needs accurate knowledge about the accessible water in the future. Drought is a water-stress phenomenon that slowly develops across a region and affects the living environments from different aspects. The evident impacts of global warming and climate change on hydrologic extreme events make the accurate hydrologic forecast as a serious demand for the management and operation sectors. The reliable forecasts of hydrologic variables by the multivariate copula-based technique as discussed in the previous chapter inspires the extension of the proposed methodology to the drought forecasting problems with a new probabilistic outlook.

4.1 Methodology

Copula functions are proposed for drought forecasting. Despite the admiration of copulas in probability theory and statistics, they have yet to be effectively applied in probabilistic forecast of drought events, except few studies in determining drought characteristic. As discussed earlier, copulas can model the joint behavior of correlated and dependent variables such as hydrologic variables.

Similar to many other hydrologic states, the drought status of a location at a particular time is affected by its earlier status with rather short or long gap. Since streamflow is the

[2] The scientific content of this chapter has been published or is under peer review:

Madadgar, S., and H. Moradkhani (2013), A Bayesian Framework for Probabilistic Seasonal Drought Forecasting, *J. Hydrometeorology*, doi:10.1175/JHM-D-13-010.1, in press.

Madadgar, S., and H. Moradkhani, Spatio-Temporal Drought Forecast within Bayesian Networks, J. *Hydrology*, in review.

main factor in hydrologic droughts, the accurate modeling of future streamflow is essential to predict the future droughts. Upon the correlation of streamflow at a given time with a limited extent of its past observations, the Bayesian framework as discussed earlier can be utilized to reflect the sequential behavior of drought conditions within a probabilistic analysis on streamflow variable (Madadgar and Moradkhani, 2013). If it is assumed that the forecast variable is correlated to the variables with a lag-time equal to $n-1$, Eq. 16 would give us the conditional density function of the forecast variable at time t_n given all the past observations:

$$f\left(x_{t_n} \mid x_{t_{n-1}},...,x_{t_1}\right)=\frac{c\left(u_{t_n},...,u_{t_1}\right)\prod_{i=t_1}^{t_n} f_{X_i}(x_i)}{c\left(u_{t_{n-1}},...,u_{t_1}\right)\prod_{i=t_1}^{t_{n-1}} f_{X_i}(x_i)} \tag{18}$$

If $n=2$, streamflow at any time would be only conditional on its previous value; and the conditional density function (Eq. 18) would be simplified as follows (Madadgar and Moradkhani, 2013):

$$f\left(x_{t_2} \mid x_{t_1}\right)=\frac{c\left(u_{t_2},u_{t_1}\right).f_{X_{t_2}}(x_{t_2}).f_{X_{t_1}}(x_{t_1})}{f_{X_{t_1}}(x_{t_1})}=c\left(u_{t_2},u_{t_1}\right).f_{X_{t_2}}(x_{t_2}) \tag{19}$$

If streamflow dependency is reasonably extended to its two previous time steps, the conditional pdf turns to the following form (Madadgar and Moradkhani, 2013):

$$f\left(x_{t_3} \mid x_{t_2},x_{t_1}\right)=\frac{c\left(u_{t_3},\,u_{t_2},\,u_{t_1}\right).f_{X_{t3}}(x_{t_3}).f_{X_{t2}}(x_{t_2}).f_{X_{t1}}(x_{t_1})}{c\left(u_{t_2},u_{t_1}\right).f_{X_{t2}}(x_{t_2}).f_{X_{t1}}(x_{t_1})}=\frac{c\left(u_{t_3},\,u_{t_2},\,u_{t_1}\right).f_{X_{t3}}(x_{t_3})}{c\left(u_{t_2},u_{t_1}\right)} \tag{20}$$

This study aims at forecasting seasonal droughts conditional on the drought status of the past seasons with highest correlations. As shown later for the study basin; the target season is correlated the most to its previous season; however, its correlation to the second

earlier season (two prior seasons) is not insignificant to ignore. Thus, Eq. 19 and 20 are applied to practice the probabilistic drought analysis of the target season given the drought status of either one or two past seasons.

4.2 Case Study and Data

The Gunnison River Basin is one of the headwater sub-basins of the Colorado River Basin, located in the southwestern United States (Fig. 17). The Colorado River Basin, with an approximate drainage area of 640,000 km^2, is divided into upper and lower portions, and encompasses parts of seven States: WY, CO, UT, NV, CA, NM, and AZ. The Gunnison River Basin includes seven sub-basins with a total drainage area of 5,400 km^2 at the conjunction of two upstream reaches: the Tomichi Creek and the Gunnison. Streamflow observations of the upstream reaches immediately before the basin outlet at USGS 09119000 (Tomichi Creek River) and USGS 09114500 (Gunnison River) are accumulated to use as the basin's total outflow at any time.

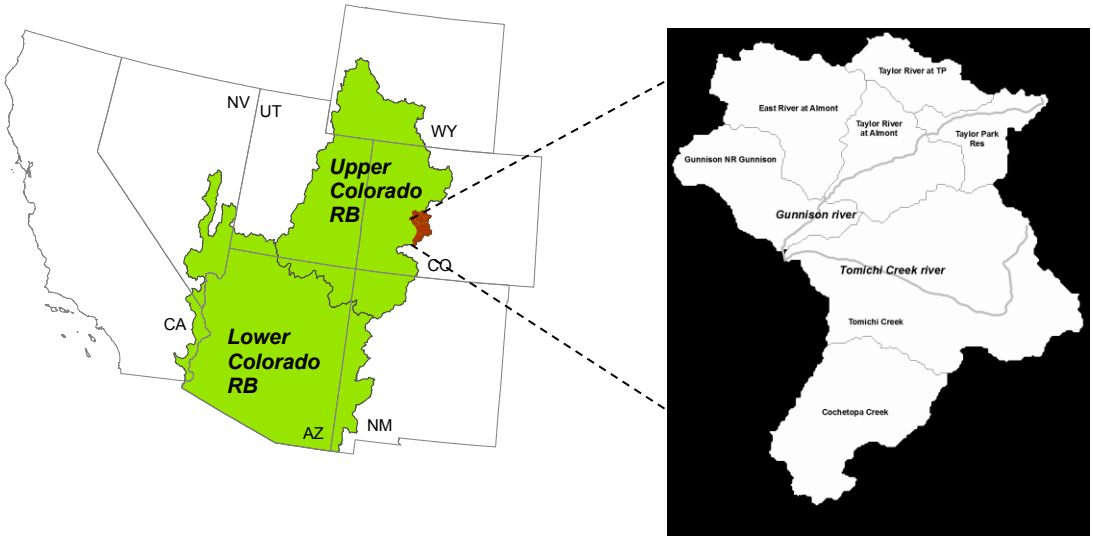

Figure 17: Gunnison River Basin, a sub-basin of the Colorado River Basin in southwestern United States.

The Gunnison river basin is a snowmelt dominated watershed. According to the drought summary by Western Water Assessment (WWA) and NIDIS released in July 2012 (WWA and NIDIS, 2012), depletion of the snowpack and the early meltout in the spring of 2012 caused the below-average flow in April-July of 2012. During the past 118 years, 2012 was 2nd warmest year on record in the state of Colorado. Regarding the inflows to Lake Powell, which reflects the runoff of the entire Upper Colorado River Basin, the water year 2012 was the 4th driest year in the past century. The intense drought of 2012 (comparable with the drought of 2002 across the region) in the states of Colorado, Utah, and Wyoming caused insufficient water supply, poor pasture and crop conditions, and region-wide wildfires. However, in general, the region has been undergoing various droughts since 2000, with the most intense drought occurring in 2002. Thus, accurate forecast of future droughts is significant for reliable planning and management of available water resources across this area.

4.3 Drought Indices

Droughts may occur in different phases of hydrologic cycle. Water movement through the hydrologic cycle is generally slow phenomenon, except for quick mass-transfer events like sudden storms. It happens that in a specific time window some hydrologic variables (e.g., soil moisture) experience a level of drought while some others (e.g., streamflow or water availability) do not undergo any identifiable drought categories. Therefore, drought status would appear differently upon the target hydrologic variable. To assess the drought status of a region, many drought indicators have been developed each using different hydrologic variables. The Palmer Drought Severity Index

(PDSI; Palmer, 1965), Standardized Precipitation Index (SPI; McKee et al., 1993), Crop Moisture Index (CMI; Palmer, 1968), Surface Water Supply Index (SWSI; Shafer and Dezman, 1982), and Vegetation Condition Index (VCI; Liu and Kogan, 1996) are among the most applied indices to characterize different drought types. Though all of these indices are widely used, each one focuses on particular hydrologic variables and has its own specific strengths and weaknesses.

This study adopts the definition of the meteorological drought index, SPI, for streamflow variable (Standardized Streamflow Index; SSI) to characterize the hydrological droughts at a particular river section. In drought studies, the indicators defined similar to SPI are generally called Standardized Indices (SI), which are able to capture the anomalies from the average moisture status of a region regarding the drought variable in use. An SI may utilize hydrologic variables other than precipitation (as in SPI) such as streamflow, snowpack, soil moisture, etc (McKee et al., 1993). The severity of droughts characterized by SI is usually identified by the U.S. Drought Monitor classification scheme as summarized in Table 5. The five drought categories (D0-D4) in dry periods are defined upon certain probability thresholds. The more severe droughts are associated with less probable categories (e.g. D4). Indeed, the SI drought indicators are normal variates; and hence, the smaller values of drought indicator are in accordance with more severe and less probable droughts. The SSI=-0.5 is a threshold to separate the dry periods from the wet (normal) periods; however, the variation in water availability during a time horizon results in a dynamic transition either between dry and wet spells, or among various drought categories. To calculate the SSI as defined in this study, the monthly

flow at a particular river section ($y_{yr,i}$) are aggregated starting from month m of the year yr for the time-window of length k ($X_{yr,m,k}$). Then, the marginal CDF of the aggregated flows is obtained as $u_{yr,m,k}$ to transform the aggregated flow to the standardized normal variable. Hence, the SSI is the inverse normal variate of $u_{yr,m,k}$ (Madadgar and Moradkhani, 2013):

$$\begin{aligned} SSI_{yr,m,k} &= \phi^{-1}(u_{yr,m,k}) \\ u_{yr,m,k} &= F_{X_{yr,m,k}}(X_{yr,m,k}) \\ X_{yr,m,k} &= \sum_{i=m}^{m+k-1} y_{yr,i} \end{aligned} \tag{21}$$

According to Eq. 21, separate distributions fit the aggregated flows with different starting months. This definition of SSI preserves the seasonality effect; otherwise, if the marginal distribution fitted to the entire series of the aggregated flows, the seasonal flow pattern would be disregarded.

Table 5: Drought classification used by the U.S. Drought Monitor.

The U.S. Drought Monitor Category	Drought severity	SI value
D0	Abnormally Dry	-0.5 to -0.7
D1	Moderate Drought	-0.8 to -1.2
D2	Severe Drought	-1.3 to -1.5
D3	Extreme Drought	-1.6 to -1.9
D4	Exceptional Drought	-2.0 or less

To study the spatial variation of hydrologic droughts, streamflow should be replaced by generated runoff across the basin. Note that streamflow at a particular river section is the accumulated flow generated across the entire area of the basin and have been routed

to that section. This study uses the Standardized Runoff Index (SRI; Shukla and Wood, 2008) to evaluate the spatial variation of hydrologic droughts. The basin should be divided to some hypothetical spatial units, each of which responses similarly to hydrologic excitements throughout their area. SRI is the SSI defined for each unit; hence, streamflow in Eq. 21 should be replaced by runoff to reflect the anomalies of surface runoff generated at each unit (s) from its corresponding average value:

$$\begin{aligned} SRI^{s}_{yr,m,k} &= \phi^{-1}(u^{s}_{yr,m,k}) \\ u^{s}_{yr,m,k} &= F_{X^{s}_{yr,m,k}}(X^{s}_{yr,m,k}) \\ X^{s}_{yr,m,k} &= \sum_{i=m}^{m+k-1} y^{s}_{yr,i} \end{aligned} \tag{22}$$

where, $u^{s}_{yr,m,k}$ is the probability of accumulated surface runoff of the spatial unit s in year yr over k months starting from month m; $F_{(.)}$ is the marginal distribution of aggregated runoff ($X^{s}_{yr,m,k}$); and $y^{s}_{(.)}$ is the monthly runoff of the spatial unit s. Therefore, SRI calculation starts with fitting an appropriate marginal distribution to the aggregated surface runoff over k months and computing the standardized normal variable for each aggregated runoff volume. Separate marginal distributions should fit the accumulated runoff beginning from different months to obtain the SRI variation over time for each spatial unit. Once the SRI is estimated for each spatial unit, the drought status of each unit can be determined similar to SSI from Table 5.

4.4 Analysis of Historical Droughts

Water supply in GRB is highly dependent on the snowmelt generated from the higher elevation areas. Decreased high elevation snowpack has caused droughts with of varying

intensities in Upper CRB during recent decades, while the most severe one occurred in 2002. Recently, snowpack depletion and early meltout in spring 2012 caused a widespread drought in the states of Colorado, Utah, and Wyoming (reported by Western Water Assessment (WWA) and National Integrated Drought Information System (NIDIS), July 2012). The below-average flow in April-July of 2012 triggered poor pasture and crop conditions, and region-wide wildfires. Despite the low inflow in 2012, the carryover of local reservoirs from the past couple of wet years (2010-2011) could mitigate the drought impact on the water supply throughout the region. Spring of 2012 was the 2^{nd} warmest spring on record in the state of Colorado and the 4^{th} driest spring in Upper CRB since 1900. Continued warm and dry climate increases the probability of contiguous droughts over the region, thus affecting the irrigation and crop production. As reported by NOAA's National Climate Data Center (NOAA, March 2013), the regions across the Central Plains and Mountain West have already received the below-average precipitation during winter 2013, and are likely to have another dry summer for the second year in a row. While the recent droughts might be the signature of global warming impacts on extreme events across the world, the reliable drought forecast across the CRB seems to be essential for planning and managing the available water in future.

4.4.1 Streamflow Record

To study the historical droughts of the Gunnison River Basin (GRB), the gage observations of the upstream reaches immediately before the basin outlet at USGS 09119000 (Tomichi Creek River) and USGS 09114500 (Gunnison River) are accumulated to use as the basin's total outflow at any time. SSI as defined by Eq. 21 is

applied to the basin outflow to detect and analyze the drought status of the basin in respect with stremaflow. As described earlier, $X_{yr,m,k}$ in Eq. 21 is the accumulated monthly flow over k months starting from month m of the year yr. For the seasonal drought forecast, monthly flow volumes are aggregated over a sequence of 3 months ($k = 3$), and then a set of distributions is tested to find the best marginal distribution fitted to the aggregated flows. Streamflow record during 1950-1990 is contributed to find the marginal distributions and establish the forecast model and the rest (1990-2011) is used for verification purposes. The following seven distributions are tested as the marginal distributions: Gamma, Generalized Extreme Value (GEV), Lognormal, Gaussian, Weibull, Gumbel, and Exponential distributions. The method of MLE is used to estimate the parameters of each distribution, and the best distribution fitted the seasonal flows is found by the K-S test (Eq. 7) and the AIC statistics (Eq. 8). Table 6 summarizes the AIC and the p-value associated with the K-S test for different distributions fitted to the seasonal flow volumes in the training period of 1950 to 1990. The best distributions, with the smallest AIC and the p-values greater than the significance level, $\alpha = 0.05$, are shown in bold. Either gamma or lognormal distribution is found to be the best fit to the seasonal flow volumes. Fig. 18 illustrates the marginal distributions against the histogram of the seasonal flow volumes ($X_{yr,m,3}$, $m = 1,...,12$).

Using the marginal distributions found upon the aggregated flow during the training period (1950-1990), the SSI with k=3 is calculated for the entire analysis period (1950-2011) as plotted in Fig.19 (Madadgar and Moradkhani, 2013). Using the U.S. Drought Monitor categories (Table 5), $SSI = -0.5$ is taken as a threshold to separate the dry and

wet conditions, and the shaded areas in Fig. 19 illustrate the dry periods with $SSI \leq -0.5$. As seen, that the Gunnison River Basin has been exposed to various droughts since 1950. During sixty-one years of the analysis period, the drought of 2002 was the most sever "exceptional" drought (D4; $SSI \leq -2.0$). Drought persistency is also obvious in Fig. 19. Evidently, several droughts frequently occurred in 1950s and 1960s; and the drought of 2000 continued for five years in spite of the earlier long wet period from 1995 to 2000. To easily follow the temporal sequence of seasonal droughts in Fig. 19, the matrix plot in Fig. 20 shows the status of dry spells for each season. Each cell of the matrix represents the drought status of a particular season in the year, and as shown, several dry periods occurred during the 1950s and 1960s, especially in the falls and winters (Oct-Nov-Dec and Jan-Feb-Mar). General evidence of the matrix plot is that the droughts have been more evenly distributed in the springs and summers than in the falls and winters of the analysis period (Madadgar and Moradkhani, 2013).

A backward calculation in the SSI formula would give us the range of seasonal flow within each drought category used by the U.S. Drought Monitor (Table 5). The bar chart in Fig. 21 shows the range of flow volume within each drought category D0-D4. From this figure, the seasonal pattern is evidently captured as expected from the SSI definition (Eq. 21). The high-flow season shows more variability in the required amount of water to transition to a different category. In other words, the same class of drought is likely to persist within a high-flow season (e.g. the spring) if the seasonal flow does not change significantly. Moreover, while a particular seasonal flow (e.g. 90 KAF) is defined as an absolutely wet condition in winter (Jan-Feb-Mar or Feb-Mar-Apr periods), the same

amount of flow might lead to an exceptional drought condition (D4) in spring (e.g. Apr-May-Jun and May-Jun-Jul periods). This is the seasonality issue reflected in drought definition which identifies the high dependency of drought status on the time of the year (Madadgar and Moradkhani, 2013).

Table 6: The AIC and the p-value of the K-S test found for different distributions fitted to the seasonal flow volumes starting from different months over a sequence of 3 months. The numbers in the parentheses are the p-values. The statistics of the best distributions are presented in bold.

Dist.	Jan	Feb	Mar	Apr	May	Jun	Jul	Aug	Sep	Oct	Nov	Dec
Gamma	495 (.85)	579 (.96)	**716 (.34)**	**789 (.70)**	**810 (.79)**	781 (.65)	705 (.41)	**621 (.96)**	562 (.52)	531 (.79)	498 (.82)	476 (.78)
GEV	496 (.85)	580 (.93)	718 (.47)	791 (.60)	812 (.84)	780 (.78)	701 (.91)	623 (.96)	563 (.68)	532 (.75)	499 (.95)	477 (.87)
Logn	**494 (.91)**	**578 (.95)**	717 (.64)	792 (.61)	812 (.87)	**779 (.64)**	**701 (.77)**	623 (.97)	**561 (.73)**	**530 (.80)**	**497 (.94)**	**475 (.90)**
Gaus	501 (.45)	585 (.51)	725 (.04)	794 (.13)	821 (.22)	799 (.14)	727 (.09)	625 (.57)	566 (.25)	536 (.39)	502 (.44)	481 (.42)
Weibull	506 (.28)	586 (.49)	720 (.10)	790 (.30)	813 (.56)	788 (.26)	718 (.19)	627 (.51)	568 (.29)	538 (.34)	506 (.26)	486 (.22)
Gumbel	526 (.06)	607 (.09)	746 (.01)	813 (.04)	845 (.06)	834 (.01)	769 (.00)	644 (.09)	583 (.15)	552 (.15)	521 (.06)	503 (.05)
Exp	623 (2E-11)	680 (2E-10)	779 (3E-07)	843 (3E-06)	856 (1E-06)	831 (3E-07)	768 (3E-08)	723 (4E-10)	675 (2E-11)	648 (2E-11)	625 (2E-11)	607 (7E-12)

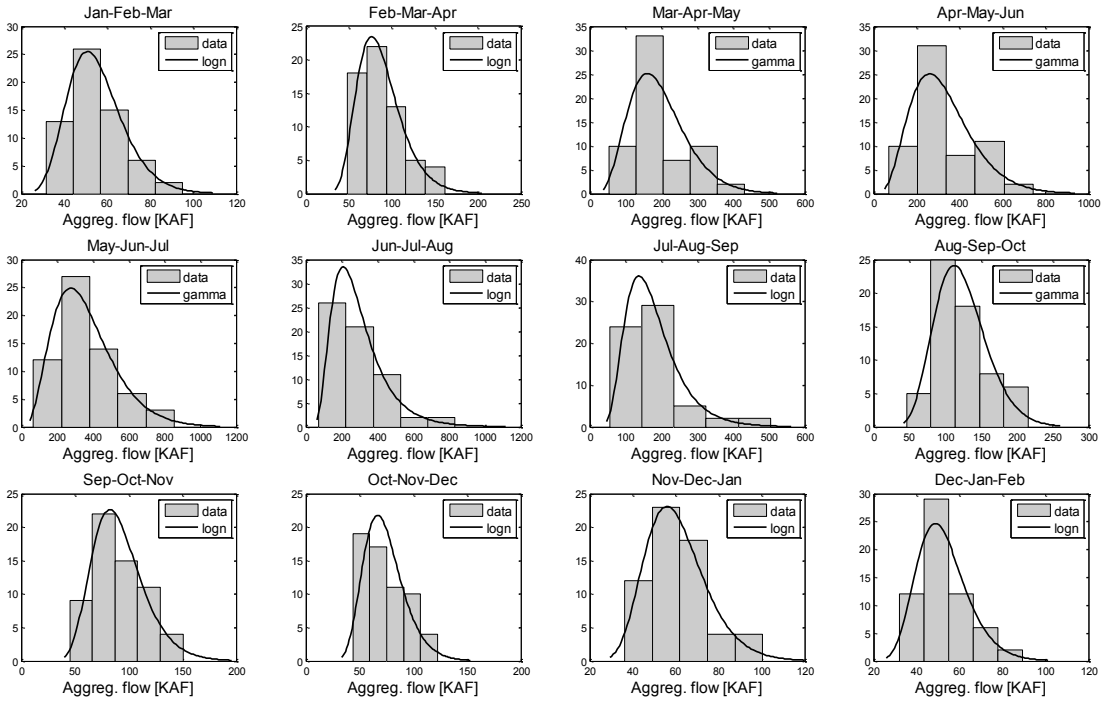

Figure 18: Histogram against the best fitted distribution of the aggregated flow volumes over a sequence of 3 months during the training period of 1950-1990.

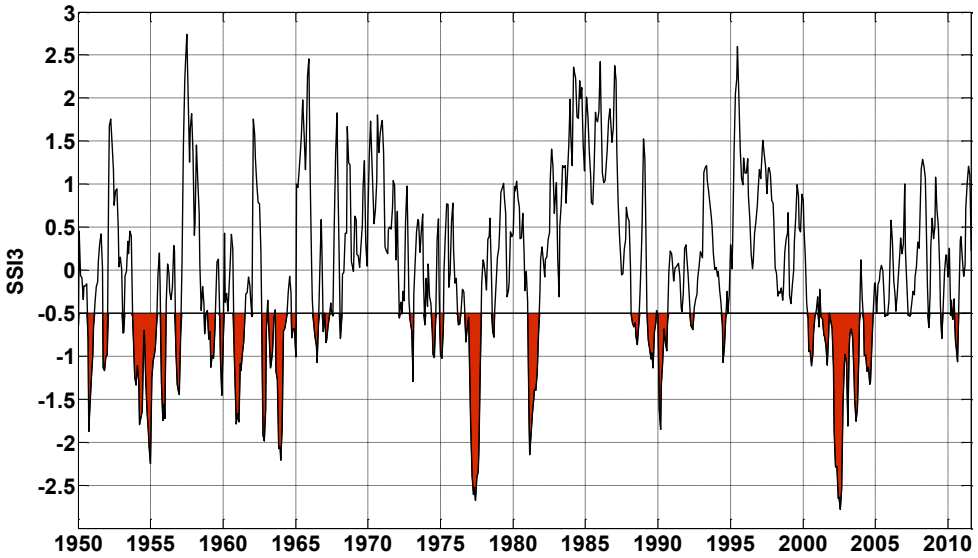

Figure 19: The SSI3 (SSI with k=3 in Eq. 11) timeseries during the analysis period. The line separates the dry and wet periods.

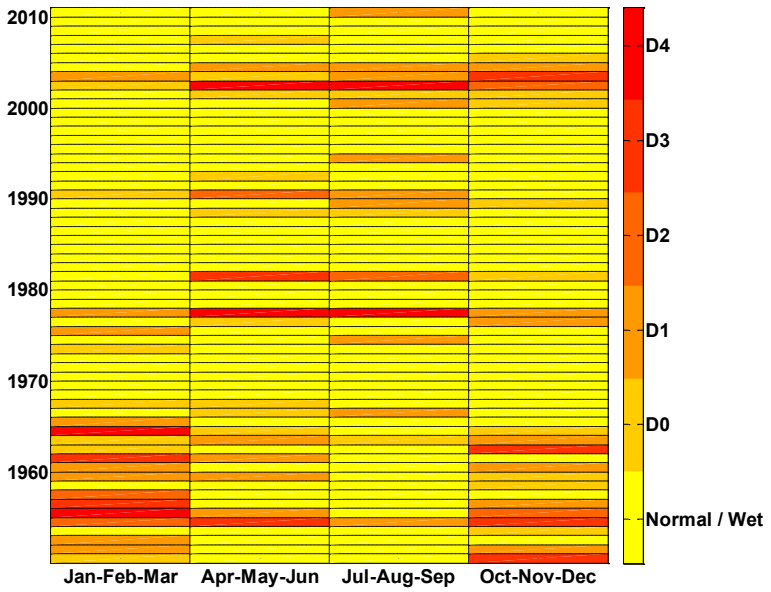

Figure 20: Matrix plot of seasonal droughts indicating the sequence of droughts during the analysis period.

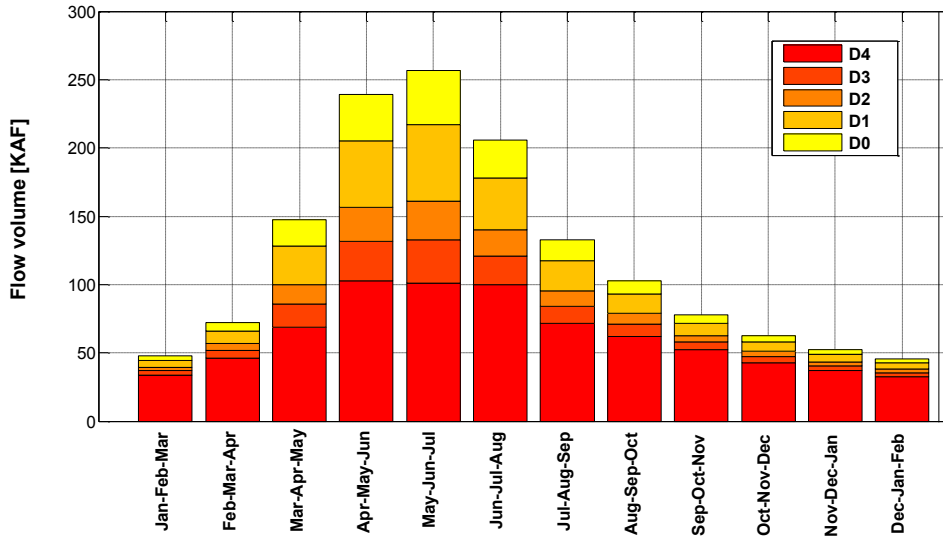

Figure 21: Seasonal flow volumes classified into different drought categories.

4.4.2 Estimated Runoff

The streamflow record measured at a certain section of the river is used to evaluate the whole picture of drought status of the entire basin; while evaluating the spatial

variation of hydrologic droughts across the basin needs the basin to be divided into some spatial units, each studied separately for hydrologic responses and drought variables.

PRMS is used to estimate the runoff volume generated across the study area of GRB. To apply PRMS, the basin should be partitioned into several Hydrologic Response Units (HRUs) each with various parameters to be calibrated. The predicted runoff in each HRU is the output of a series of conceptual reservoirs including impervious zone, soil zone, subsurface, and groundwater reservoirs. The final outflow of the basin is the total routed runoffs of all the HRUs that reach the basin outlet at the same time. The HRUs for GRB are set as the grid cells shown in Fig. 22. There are 37 grid cells across the basin with 12 by 12 km^2 resolution ($1/8^{th}$ degree).

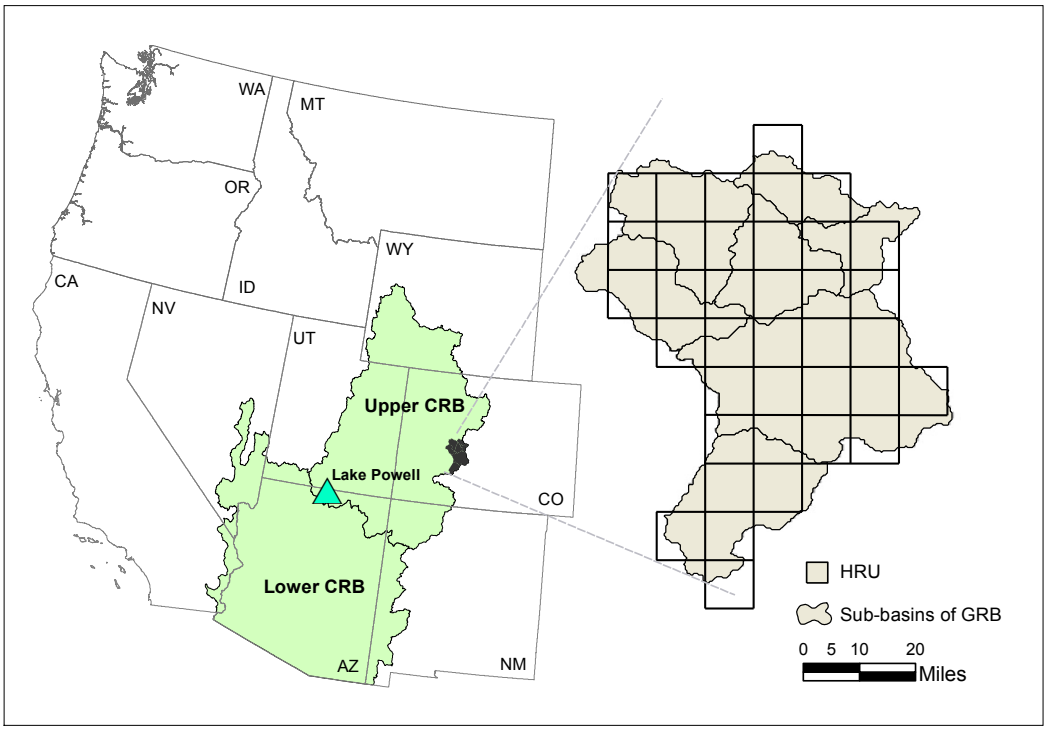

Figure 22: Gunnison River Basin located in southwestern United States with 37 spatial units with the size of $1/8^{th}$ degree (~12 km resolution).

Therefore, the total 37 HRUs are contributed to model the basin outflow during the modeling period from 1979 to 2011. For the hydrologic modeling of the basin, PRMS requires the daily maximum and minimum temperature, and precipitation for each HRU. The Inverse Distance Squared Weighting (IDSW) method is used to spatially distribute the daily records of a group of SNOTEL and COOP stations among the HRUs. In IDSW, the interpolation weights are calculated proportional to the squared inverse distance of the HRUs to the measuring sites. Hence, the measurement sites share more information with the nearby HRUs. Parameters of the hydrologic model are calibrated by Shuffled Complex Evolution (SCE) global search algorithm (Duan et al., 1994) with the objective function of maximizing the Nash Sutcliffe Efficiency (NSE) over the daily record of the basin outflow:

$$NSE = 1 - \frac{1}{\sigma_{y_{obs}}^2}\left[\frac{1}{T}\sum_{t=1}^{T}\left(y_{sim}^t - y_{obs}^t\right)^2\right] \tag{23}$$

where, y_{sim}^t and y_{obs}^t are the modeled and observed streamflow at time t, respectively; $\sigma_{y_{obs}}^2$ is the variance of observations; and T is the length of observation record.

Model parameters are calibrated and validated over the periods of 1979-1989 and 1989-2011 respectively with the associated NSEs equal to 0.7 and 0.72. According to these measures, the model performance seems reliable where the runoff at different HRUs can be assumed acceptable. Since the actual runoff is not measurable, this study relies on the simulated runoff by PRMS for sake of drought assessment.

To show the PRMS performance, Fig. 23a plots the modeled against the measured daily outflow of the basin for the entire period of 1979 to 2011. As seen, the estimated flow is similar to observed flow specifically in low-flow seasons. The interquartile range of monthly mean streamflow during 1979-2011 is shown in Fig. 23b. Generally, the peak flows occur in June and the low-flow season begins in July when the hydrograph starts descending. Furthermore, the model can capture the low flows better than the high flows. The main reason can be attributed to the elevation of the highest available station whose measurements are used as climate input to PRMS. The highest station is located at the elevation of 3523m while the highest elevation of the basin is 4221m. For a snow-dominated basin like GRB, where the snowmelt plays a significant role in the basin outflow, missing the climate data of elevated areas can cause under-estimating the high flows (Fig. 23a-b). In this regard, a recent study by Jung et al., (2012) showed the high sensitivity of the hydrologic models' performance to their parameters in snow-dominated basins.

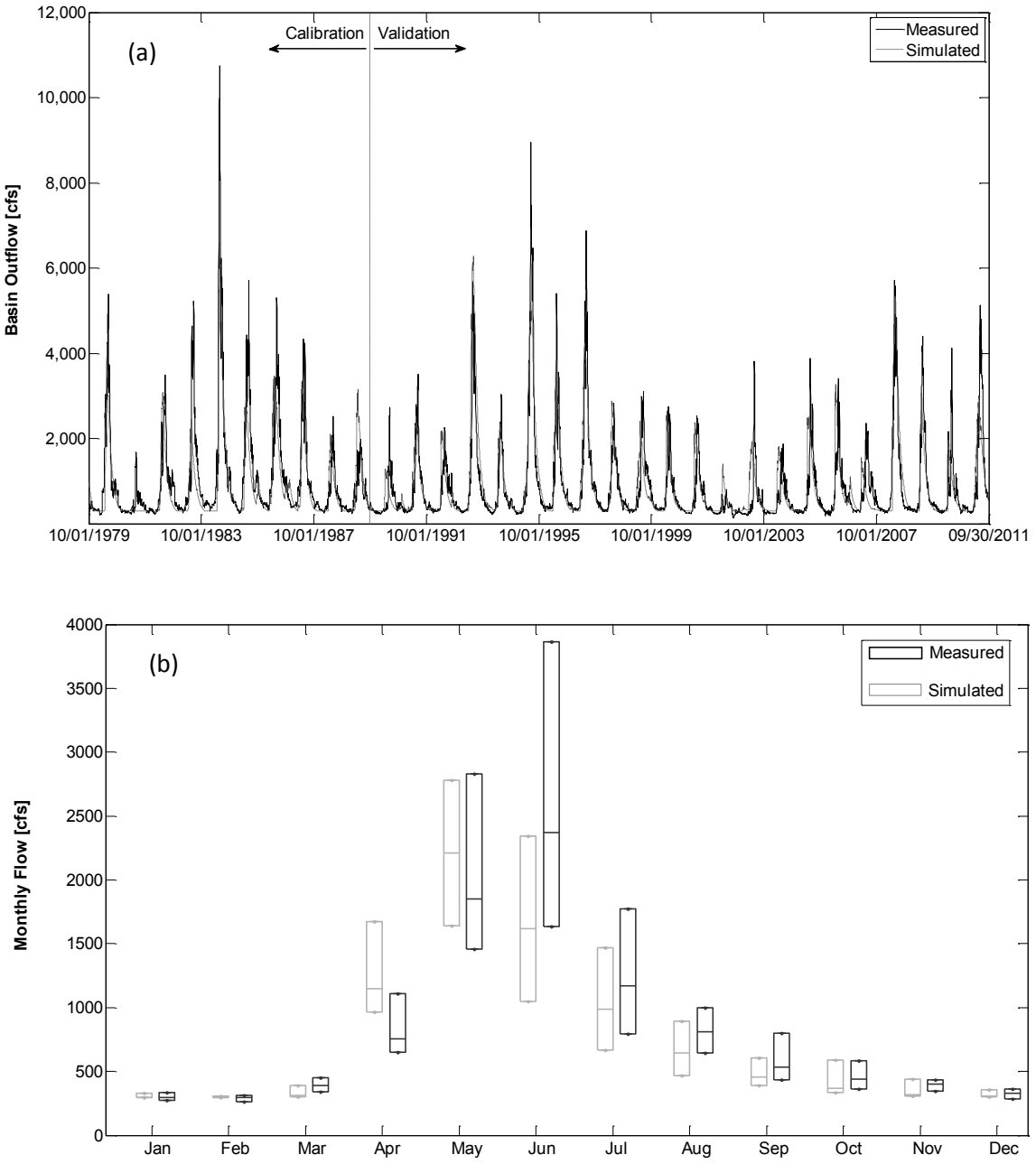

Figure 23: Comparison of the measured and simulated outflow of the GRB during 1979 to 2011 in the form of a) daily timeseries, and b) Interquartile range of monthly mean streamflow.

To implement the drought analysis, SRI (Eq. 22) is calculated for transferred, accumulated surface runoff generated at each grid cell across the basin. Surface runoff is accumulated over 6 months starting from each 12 months of a year, and the best fitted

marginal distributions are found, afterwards. Fig. 24 shows drought condition of the basin given the surface runoff at each HRU in January (on the left) and July (on the right) of 2000 thru 2005. Drought categories (D4 to Normal status) in each HRU are determined according to the SRI value. As seen, the drought of 2002 encompasses the entire basin. Generally, July runoff predictions of 2000-2005 indicate stronger droughts than their respective January runoff predictions, despite the larger monthly mean streamflow in Julies (Fig. 23b). Since drought events over a particular time window are defined relative to the average condition of that time window, droughts in high-flow seasons might have totally different characteristics than droughts in low-flow seasons. The drought maps in Fig. 24 also indicate that the SRI acquired from estimated runoff by PRMS capture the drought events during 2000-2005 which also shown in Fig. 19.

4.5 Probabilistic Drought Forecasting

Drought is an evolving extreme event that occurs over a given period of time. Drought status of a region at any time depends on the water availability (precipitation, soil moisture, runoff, etc), within the past few months or seasons. In other words, water availability in the past plays a significant role in future drought status. Since drought-related variables (e.g. runoff, streamflow, drought indices, etc.) are statistically dependent on their past status, they can be expressed within the Bayesian networks as described earlier (Eq. 19 and 20).

In the following sections, the probabilistic forecast of future droughts are studied separately for the streamflow at the GRB outlet and the runoff volume generated at each grid cell of Fig. 22. In the former case, the status of future droughts is estimated for the

entire study area upon the streamflow forecast at a given section of the river basin (the outlet); while in the latter case, the runoff forecast for each grid cell is used to estimate the spatial variation of future droughts across the basin.

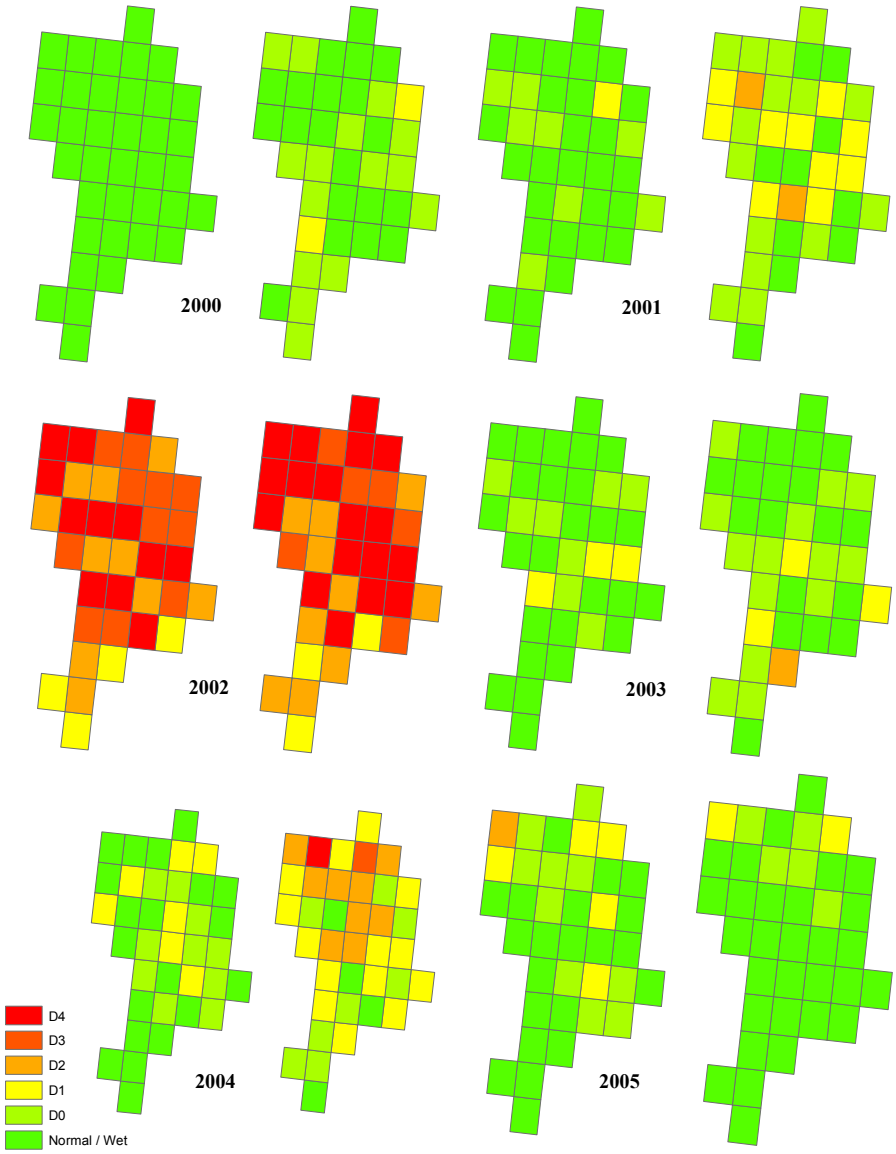

Figure 24: Droughts in GRB during the past years, a) SSI with respect to the observed streamflow at the basin outlet. The line SSI=-0.5 is the threshold to separate the dry and wet periods, b) spatial variation of drought events throughout the basin. The drought maps are shown for January (on the left) and July (on the right) for each year.

4.5.1 Basin Outflow

Basin outflow is chosen as the forecast variable for drought study in this section. The spring total flow (Apr-May-Jun) is taken as the forecast variable, and the predictor variable is determined based on the correlation and dependencies of spring flow with the prior seasonal flows. Figure 25 shows the autocorrelation between the transferred spring flow and the total flow of the prior seasons. The seasonal flows are transferred by the marginal distributions found in earlier sections (Table 6 and Fig. 18). As seen, the transformed spring flow has the highest correlation with the transformed winter flow (Jan-Feb-Mar) among the other seasons of the year. Yet, the correlation between the seasonal flow of spring and fall or even summer is not insignificant; and the analysis of spring flow should be established upon either one season (winter) or two seasons (winter and fall) earlier. Therefore, two different Bayesian networks are applied to study the conditional probabilities of spring flow. In the first network, the spring flow is assumed to be only dependent on the winter flow and hence the drought forecasting is conducted within Eq. 19. The second network adds the impact of fall status on spring drought and it considers the seasonal flow of both past winter and fall in drought forecasting of spring season (Eq. 20). However, given the greater correlation between the spring and winter flow, it is expected that the winter influences the spring flow more than the fall.

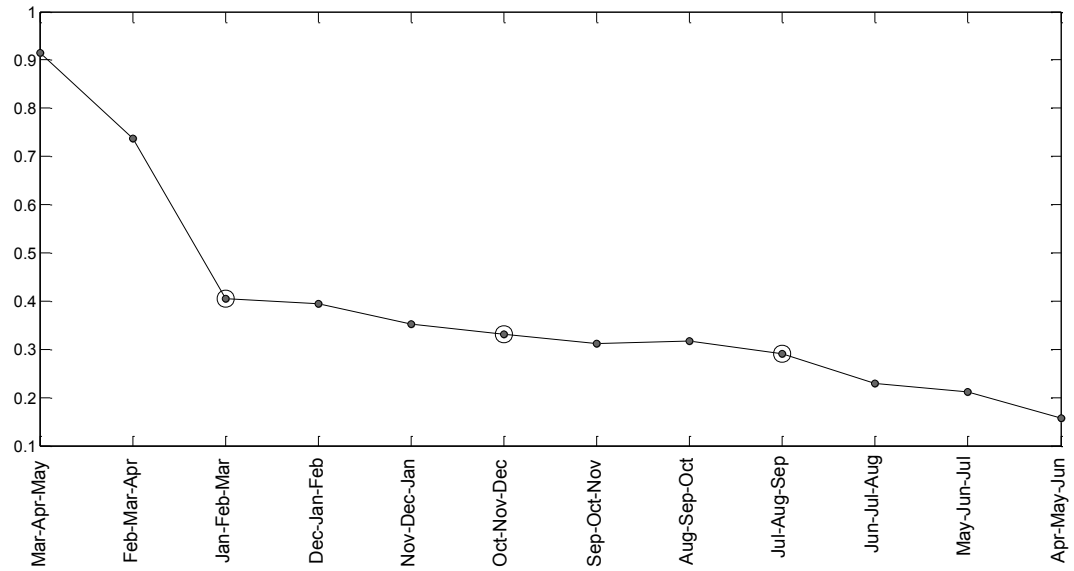

Figure 25: The autocorrelation of the transformed spring flow (Apr-May-Jun) to the prior 3-month flows. The moving window locates no further than the previous year spring season (Apr-May-Jun). The big circles are associated with the transformed seasonal flows before spring (winter, fall, and summer).

4.5.1.1 First-Order Conditional Forecast

In the first-order conditional forecast, the spring drought is assumed to depend only on its past winter flow (Madadgar and Moradkhani, 2013). Thus, Eq. 19 applies to drought forecasting where x_{t_2} and x_{t_1} represent the seasonal flow of the spring and winter, respectively, and u denotes the corresponding probabilities from associated marginal distributions. To implement the probabilistic forecast analysis, an appropriate bivariate copula function should join the marginal distributions of the spring and winter seasonal flow. The best marginal distributions fitted the observed flow of each season during the training period (1950-1990) are the same as those found earlier (see Table 6 and Fig. 18). Archimedean and Elliptical families of copula functions (Table 1) are used to join the marginal distributions. In a group of copulas, the one with the smallest S_n and the

greatest p-value (greater than the significance level as well) is selected as the best copula. In this study, the significance level is set to $\alpha = 0.05$ and the p-values are obtained by the parametric bootstrapping procedure with 1000 replications. As summarized in Table 7, the Gaussian copula with the smallest S_n and the greatest p-value is the best choice among others.

Table 7: Statistics of the GOF test to find the best copula joining the marginal variables of seasonal flows in Eq. 19 and 20 (u_{t_3}, u_{t_2}, and u_{t_1}). The u_{t_3}, u_{t_2}, and u_{t_1} refer the marginal variables of spring, winter, and fall flows, respectively. The Cramér-von Mises statistic (S_n) and the corresponding p-value are presented in each case. The results for the superior copulas are shown in bold.

Copula	S			p-value		
	u_{t_3}, u_{t_2}	u_{t_2}, u_{t_1}	u_{t_3}, u_{t_2}, u_{t_1}	u_{t_3}, u_{t_2}	u_{t_2}, u_{t_1}	u_{t_3}, u_{t_2}, u_{t_1}
Gaussian	**0.038**	**0.023**	**0.034**	**0.057**	**0.312**	**0.256**
t	0.040	0.028	0.046	0.038	0.180	0.122
Gumbel	0.044	0.030	0.059	0.028	0.132	0.043
Clayton	0.059	0.076	0.083	0.028	0.009	0.018

After picking the best-fitted copula for the data, several probabilistic analyses of drought status in spring season can be conducted using Eq. 19. In such an analysis, one might be interested in spring-flow distribution conditional upon a given winter drought status in winter. In this case, the winter drought conditions might be fixed at the very transition point of drought categories, where a drought status turns to another. Fig. 26 shows the distribution of spring flow (Apr-May-Jun) conditional on the drought status in winter (Jan-Feb-Mar) (Madadgar and Moradkhani, 2013). Each curve represents the probability distribution function (PDF) associated with a particular drought status in

winter (D0-D4). The analysis is narrowed down to the fixed drought conditions in winter. According to the drought PDFs, as the winter flow increases, which is equivalent to less intense drought in winter, the spring drought is expected to be less intense as well. For example, if a D4 drought occurred in winter, the spring drought-status is likely to be more intense than if a D0 winter-drought occurred. Moreover, when an intense drought is experienced in winter, the distribution of spring flow is rather narrow around its mode. For instance, the PDF associated with D0 winter-droughts is wider than the PDF associated with the D4 winter-drought. This leads to a larger range of spring flow given the D0 drought-status in winter, as compared to the D4 winter-drought.

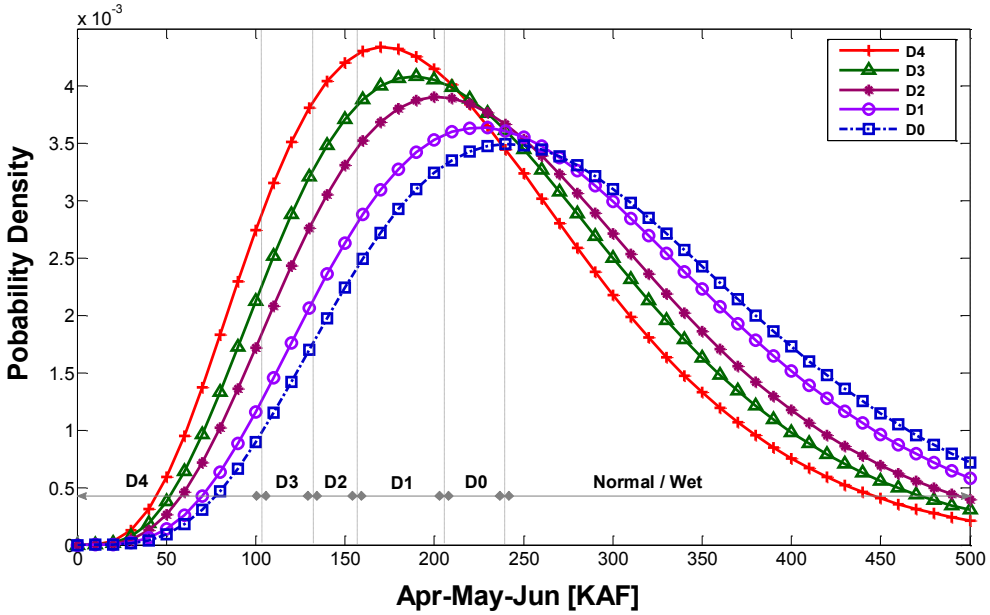

Figure 26: Distribution of seasonal flow in the spring given the drought status in winter. Each PDF is in accordance with a particular winter drought-status.

To expand the results and demonstrate the usefulness of this approach, the conditional probability of drought in spring season, given the drought condition in winter, is shown in a shaded scheme by Fig. 27 (Madadgar and Moradkhani, 2013). To show all the PDFs in

a same plot, the probability distributions are scaled between 0 and 1; where 1 (the red shade) represents the most probable spring flow (mode of the PDF), hence drought condition, given the flow magnitude (i.e., hydrologic drought condition) in winter. Similarly, the areas with more yellowish shade represent the tails of the spring-flow PDF given the winter flow. Therefore, the red shade closely surrounds the mode of the PDFs; hence, the associated range of spring flow is more likely to happen if the given winter flow is observed. The scatterplot of the spring flow against the winter flow during the entire analysis period, 1950-2011, is also shown in the x-y range of Fig. 27. The scatterplot is showing both training (1950-1990) and validation (1990-2011) periods. As seen, the red area (most likely situations given the winter flow) captures almost the entire scatterplot which approves the reliable performance of the forecast methodology in both training and validation phases. The range of seasonal flows is split by the dashed lines, for both winter and spring, to illustrate the range of seasonal flows corresponding to various drought conditions, in each season. Fig. 27 helps to find out the most likely drought status in spring, given the winter flow, by simply looking at the dark regions. Given D4 drought in winter, for instance, the spring drought-status is most likely to be D4, D3, or D2 depending on the exact value of the winter flow. As another example, if a D2 drought occurs in winter, the spring drought-status will likely be located in either D1 or D0 spans. Visual inspection of Fig. 26 also verifies that the PDF of the spring flow is narrower within the D1 and D0 spans, given the winter drought of type D2. Hence, Fig. 26 is a limited version of Fig. 27 where only a few conditional PDFs are illustrated.

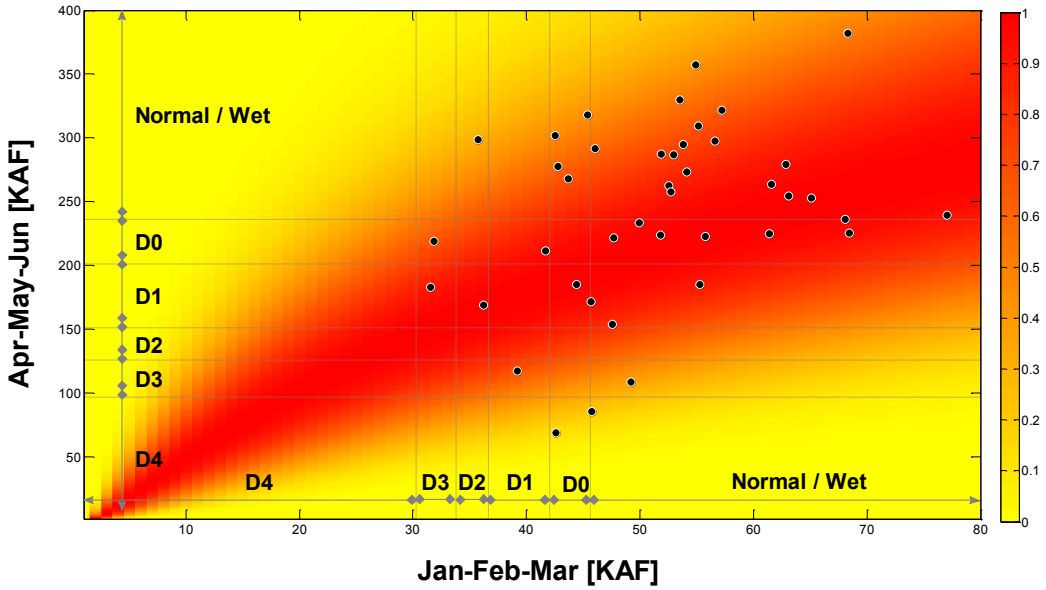

Figure 27: Conditional PDF of spring flow given the winter flow. The conditional PDFs are scaled between 0 and 1 for visualization purposes. The shade level in each pixel indicates its conditional probability density. The circles show the spring flow volume against the winter flow volume during the analysis period of 1950-2011. The dash lines identify the range of either winter or spring seasonal flow within each drought category.

While the conditional PDFs of spring flow, given the winter flow, are shown in Figs. 26-27, the probability of various droughts occurring in spring is not evaluated to this extent. In this study, the following expression is used to analyze the probability of spring droughts:

$$P(X_{t_2} \geq x_{D_i} \mid x_{t_1}) = 1 - P(X_{t_2} \leq x_{D_i} \mid x_{t_1}) \tag{24}$$

where x_{D_i} is the spring flow causing a D_i drought-status. Eq. 24 gives the probability of spring flow exceeding the thresholds defined for a particular drought status (D_i), while the winter flow is observed (x_{t_1}). Fig. 28 shows the exceedance probability of spring flow ($X_{t_2} \geq x_{D_i}$) given the winter flow (x_{t_1}) (Madadgar and Moradkhani, 2013).

For instance, if the flow magnitude of 35 KAF (a D2 drought) occurs in winter, the probability of spring drought having a D0 or wetter status would be 0.44. Likewise, this probability would be equal to 0.57, 0.77, 0.85, and 0.93 for D1, D2, D3, and D4 drought conditions. The curve for the D0 drought (the lowest one) gives the probability of spring flow leading to a D0 or wetter condition. Hence, this plot is useful in drought mitigation planning and decision making where the probability of dry-period termination is of interest. The probability of terminating the dry-periods with severities other than D0 (D4, D3, D2, or D1) can be also obtained using Fig. 28. Moreover, as either curve approaches 1, the difference between the exceedance probabilities decreases. This is in agreement with the fact that less-dry springs are anticipated when the winter flow increases, presuming that the correlation of spring flow with earlier seasonal flows dramatically decreases beyond the previous winter.

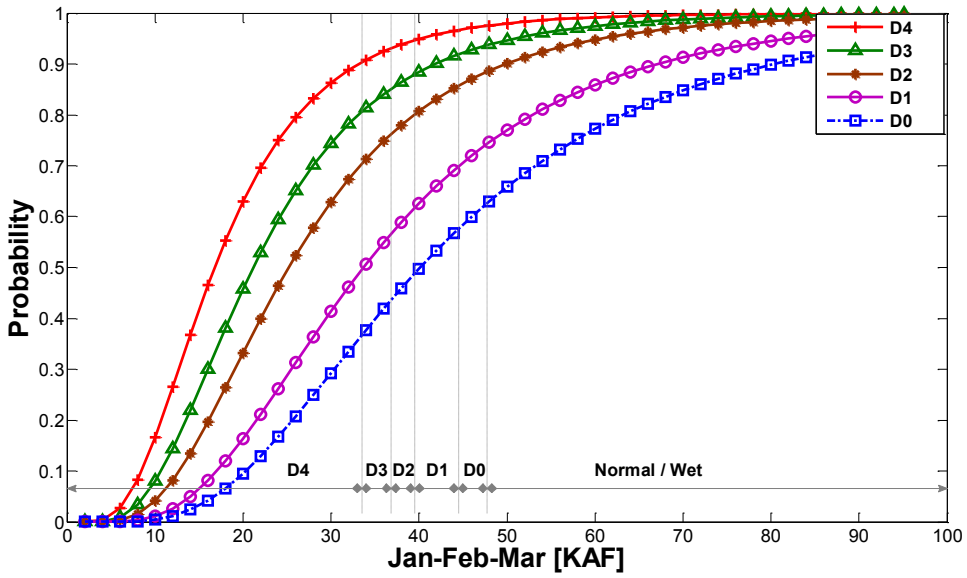

Figure 28: The conditional probability of spring flow (given the winter flow) exceeding particular threshold associated with the drought status of Di.

To provide an operational insight towards the developed forecast methodology, the presented technique is compared with ESP technique as described in previous chapter. ESP has been extensively used by various operational hydrological forecast centers including the National Weather Service (NWS). ESPs are generated to characterize the uncertainty of hydrological forecasts. They use the observed meteorology in a historical time period to reflect on the unseen future climate. To predict the seasonal flow and generate the ESPs, PRMS is driven by the historical climatology during the spinup period before the forecast date. Beginning from the forecast date, the model is forced by the resampled historical meteorology to produce an ensemble of hydrologic forecasts. Since the resampled climate data reasonably reflects the uncertainty of the unseen future meteorology, the generated ESP is assumed to properly model the uncertainty of future hydrology caused by unknown climatology. To implement the retrospective forecast of

drought events in the Gunnison River Basin, the duration of 1980-1990 is taken as the spinup period and the ESPs are generated starting from the Jan. 1st of each year during 1990 to 2011 with a lead time of 6 months. Therefore, each ESP is built for the period of Jan-Jun of each year; where, the PRMS is driven with the resampled meteorology of Jan to Jun from each year in the entire period (1980-2011) -except the year that the ESP is generated for.

To compare the forecast results of the presented method with ESP, Fig. 29 is developed showing the 90% predictive uncertainty bound of the retrospective forecasts within the validation period (1990-2011) (Madadgar and Moradkhani, 2013). As seen, there are only few spring seasons with drought conditions during 1990-2011. The uncertainty bound for the copula method is the limited representation of Fig. 27 where, given any winter flow, only the 5% and 95% bounds of the PDFs are shown. Unlike the copula-based forecast, the uncertainty bound of the ESP forecasts do not change smoothly as the winter flow increases. The uncertainty bound gradually expands in the copula-based forecasts while it does not follow a particular trend for the ESP approach. To ensure the validity of the generated ESPs, the PRMS simulations are plotted vs the observations in Fig. 30. As seen, PRMS performs quite reasonably in simulating the 3-monthly flows implying that the generated ESPs (shown in Fig. 29) are reliable to compare with copula-based forecasts. According to Fig. 29, the significance of the copula-based forecast model over the ESP approach is that the generated uncertainty bound is reasonably large to encompass the observations showing a discernible trend against the increase in winter flow. Moreover, according to the expected values of

forecasts, the performance of copula-based method is seen to be slightly better than the ESP forecasts.

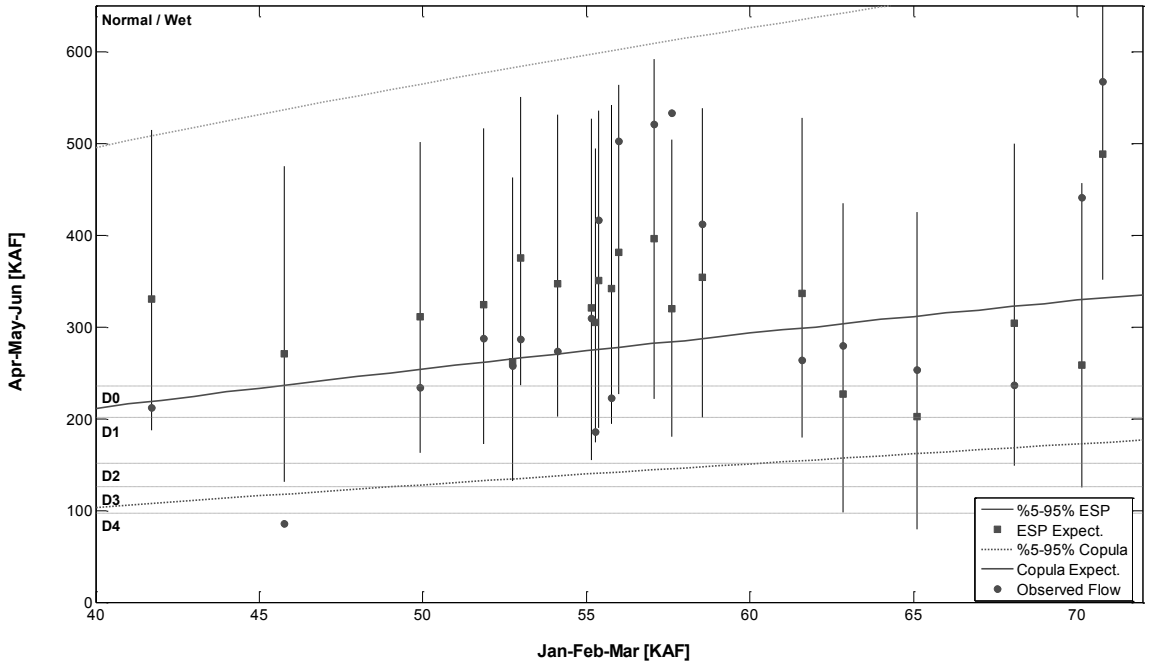

Figure 29: Seasonal flow forecast using the developed method vs the ESP forecasts generated by PRMS. Flow forecasts are corresponding to the validation period (1990-2011).

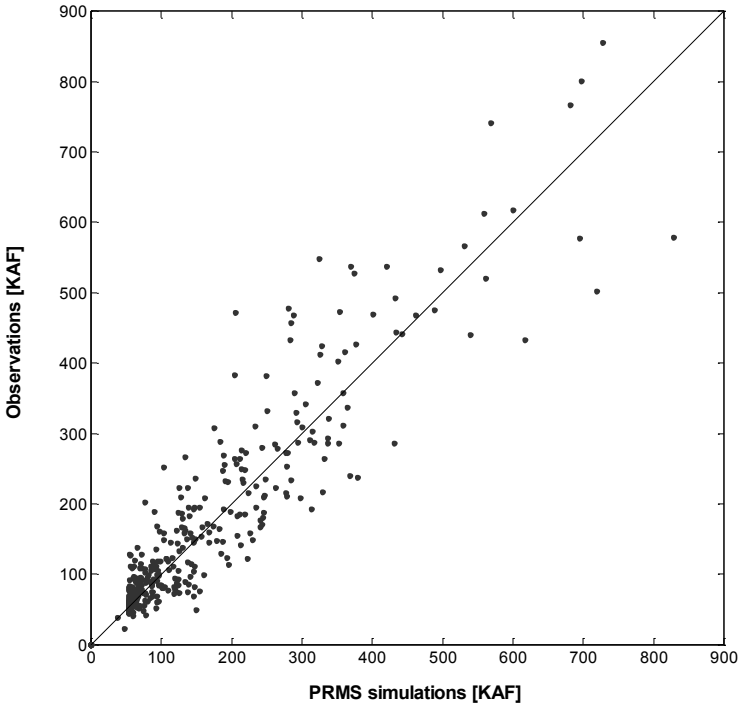

Figure 30: Observations vs PRMS simulations of 3-monthly flows beginning from each calendar month during 1980-2011.

4.5.1.2 Second-Order Conditional Forecast

Given the correlation of spring flow to the past winter and fall seasons (Fig. 25), the spring droughts might be analyzed using the second-order conditional probabilities (Eq. 20). In Eq. 20, the random variables x_{t_3}, x_{t_2}, and x_{t_1} denote the seasonal flow of spring, winter, and fall, respectively, with the corresponding probabilities of u. The best copula to join the marginal distributions (u_{t_3}, u_{t_2}, and u_{t_1}) is found among multiple candidates. According to the Cramér-von Mises statistics, the best alternative to connect all three marginal variables is the trivariate Gaussian copula (Table 7). It is also required to find a bivariate copula to join the marginal distributions of the winter and fall flows (u_{t_2} and u_{t_1}). The results of Table 7 indicate that the Gaussian copula is a suitable choice for the

bivariate copula as well. The parameters of copulas are found within the same training period as used before (1950-1990).

Eq. 20 returns the second-order conditional pdf of spring flow given the winter and fall observations. Fig. 31 shows the conditional pdfs of spring flow given various droughts in the past seasons (Madadgar and Moradkhani, 2013). In Fig. 31a, the fall drought is fixed at D4 and the winter drought varies from D0 to D4. Similar to Fig. 26, the modes of pdfs move towards smaller spring flows as the winter drought becomes more intense. The very little difference between Fig. 31a and Fig. 26 indicates that the fall status does not have noticeable impact on the spring drought. This fact is approved with Fig. 31b as well where, for a given winter drought (D4), even a big change in fall status (D0 to D4) does not make a significant change in spring status. As seen, the pdfs in Fig. 31b are clustered together and are quite similar to the pdf associated with D4 drought in Fig. 26 and Fig. 31a. This is an evidence of high influence of winter status on the spring drought. In Fig. 31a and b, all the pdfs are conditional on a particular drought (D4) fixed for either fall or winter. Fig. 31c displays the effect of any possible variation in winter and fall status on the spring drought. The pdfs are associated with two situations (D0 and D4) for either fall or winter. While the fall status is fixed at D0 (circle markers), the spring drought would change rather significantly upon the magnitude of change in winter status. In opposite, if the winter status is fixed at a particular drought, e.g. D0 (solid markers), the spring status does not considerably change with even a big change in fall status. Hence, the spring drought is found to be more sensitive to the winter status

than the fall status which approves practicing the reduced-dimension form of the forecast model (denoted as the first-order conditional forecast).

(a)

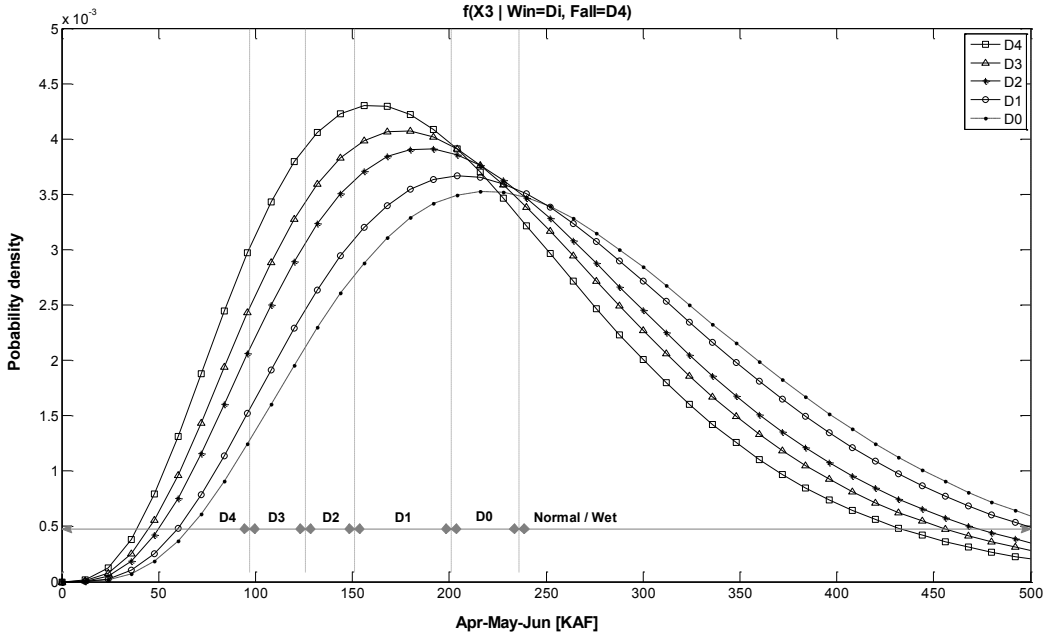

(b)

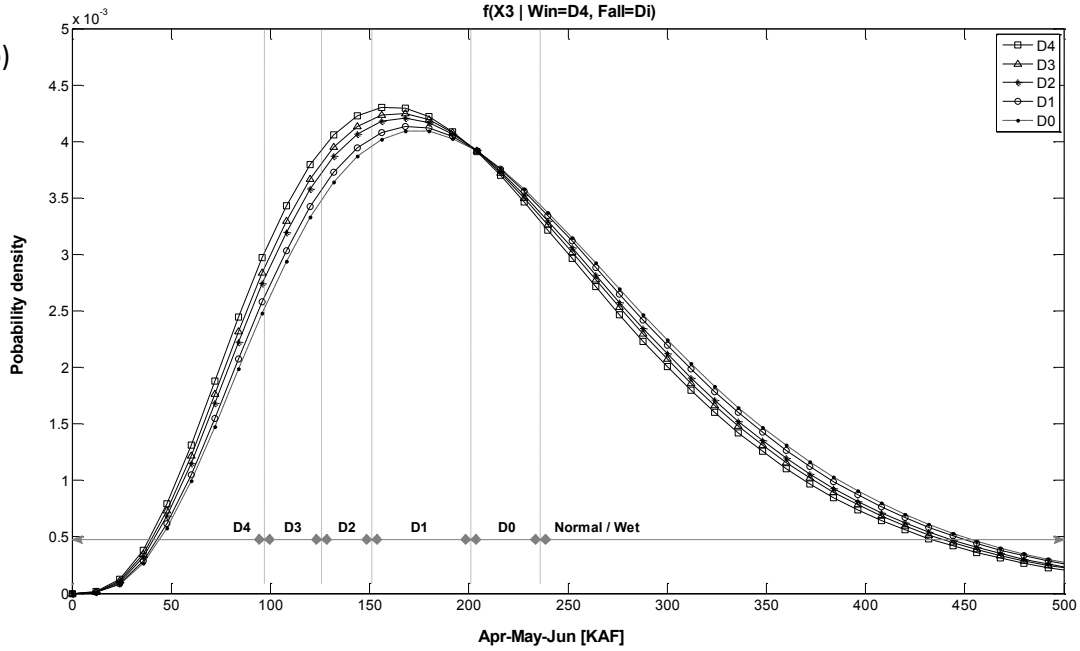

(c)

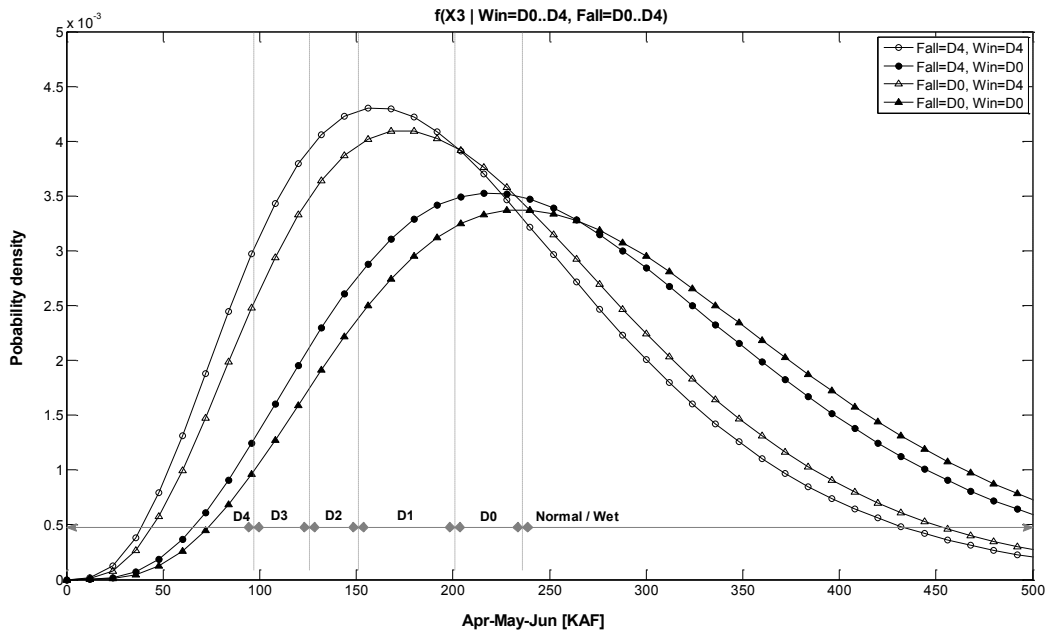

Figure 31: Distribution of spring flow given the drought status of a) Di in winter and D4 in fall, b) D4 in winter and Di in fall, c) D0 to D4 in winter and/or in fall.

Another outlook to the spring drought would be the exceedance probability of spring flow given the winter and fall observations. This is equivalent to the probabilities developed in Fig. 28 with the exception that both fall and winter flows are used and therefore the two dimensional plot of Fig. 28 turns to a 3D plot (Fig. 32). Given the seasonal flow of winter and fall, Fig. 32 illustrates the conditional probability of spring drought being equal or wetter than Di. For example, the probability layer associated with D0 (the lowest one) gives the probability of spring flow exceeding the threshold for D0 drought. Similar to Fig. 28, as the winter or fall flow increases, the probability layers approach 1 and get close together. This is a valid observation since the high-flow winters and falls are usually followed by wet rather than dry springs. Furthermore, for a particular drought status, the probabilities change more quickly by winter-flow variations than fall-flow variations. Given a particular winter flow and variable fall flow, the probabilities do

not change as significant as if the fall flow was fixed and the winter flow varied. This is consistent with the outcomes of Fig. 31 where the winter flow was found to have stronger impact on the spring status than the fall flow.

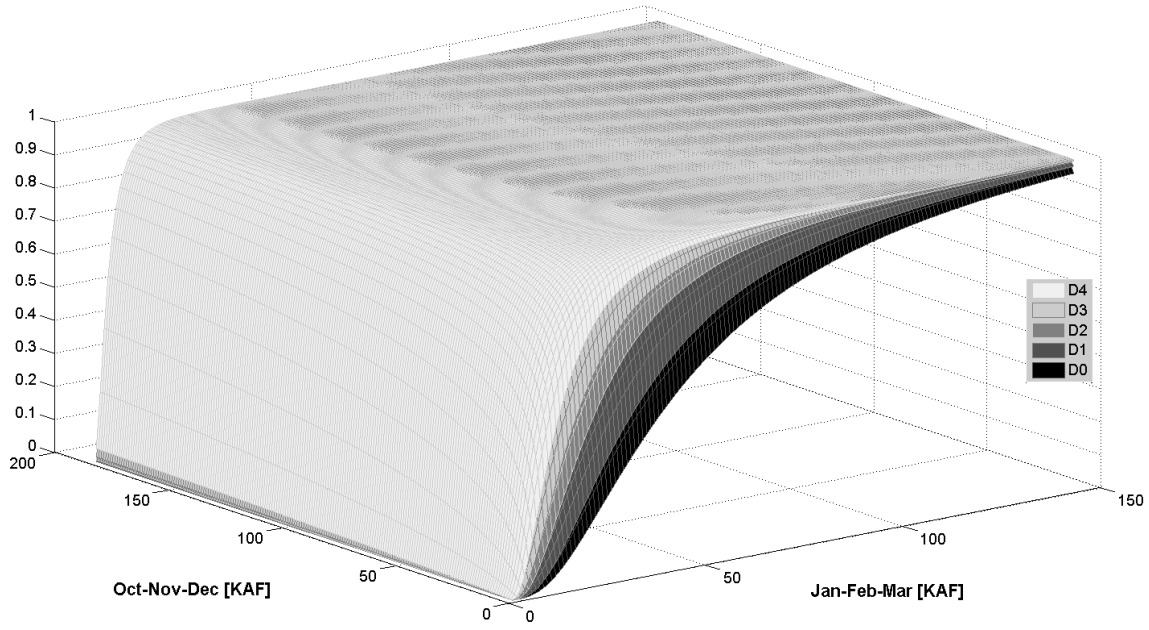

Figure 32: The conditional probability of spring flow (given the winter and fall flow) exceeding particular threshold associated with the drought status of Di. Each layer represents the exceeding probability of a particular drought in spring.

The seasonal flow hindcast during the validation period (1990-2011) is shown in Fig. 33 (Madadgar and Moradkhani, 2013). This plot is the 3D version of Fig. 29 where the conditional forecast of spring flow is upon the past winter and fall seasonal flows. The mesh grids show the uncertainty bound of spring flow generated by copula model. Similar to Fig. 29, the uncertainty bound associated with copula model gradually expands as the winter and/or fall flow increase and it also captures the observed spring flows during the validation period. Furthermore, the variation of uncertainty bound is more

dependent on the variation of winter flow than the fall flow as earlier approved by Fig. 31 and Fig. 32. This is the reason that the hindcasts of Fig. 29 and Fig. 33 are very similar.

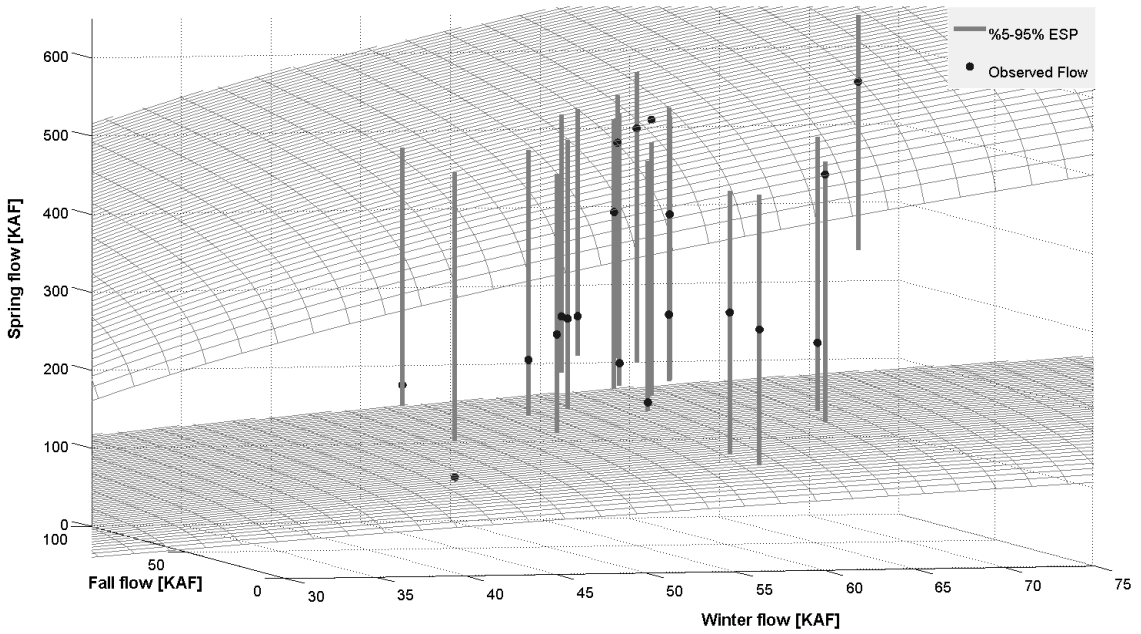

Figure 33: Performance of the copula model vs the ESP approach in spring flow hindcast given the observed flow of past winter and fall. The mesh grids show the 5-95% uncertainty bound of spring flow generated by copula model. The observations are corresponding to the validation period (1990-2011).

4.5.2 Runoff across the Basin

Surface runoff generated across the basin is considered as drought variable in this section. As described earlier, the PRMS watershed model is used to estimate the runoff volume at each grid cell throughout the basin (Fig. 22). The drought index, SRI (Eq. 22), is used to forecast the drought status upon the estimated surface runoff at each grid cell. SRI with k=6 is utilized for drought analysis, where the runoff volume at each grid cell should be accumulated over 6 months. To develop the conditional probabilities, the drought status of a forecast season is assumed to be dependent on the status of the last

adjacent season. This assumption is in agreement with the results of the last section too. Therefore, Eq. 19 is used for drought forecasting where x_{t_1} and x_{t_2} are defined as the runoff volume accumulated over 6 months, beginning from the predictor month t_1 and the forecast month t_2, respectively. As explained later, the predictor month is set to January and the forecast month is set to July, with a 6-month accumulation window (i.e. Jan-Jun, and Jul-Dec, respectively). A lapse of 6 months is fit between the predictor and forecast months to avoid an overlap of the accumulation periods.

4.5.2.1 Correlation Analysis and Copula Fitting

Basically, a conditional forecast model performs better with highly- rather than lowly-correlated forecast and predictor variables. To find the predictor and forecast months with reasonable dependency in associated accumulated runoffs, a correlation analysis is examined is this section. Surface runoff of each grid cell (HRU) across the basin is accumulated over six months, beginning from different months (Jan-Dec) during 32 years from 1979 to 2011. Table 8 shows the correlation results for possible pairs of forecast and predictor periods. For each HRU, the accumulated runoff over six months are transformed to the unit interval [0, 1] by the associated marginal distributions, and then the Pearson correlation coefficient is obtained for any possible pair of transformed variable:

$$\rho_{X,Y} = \frac{Cov(X,Y)}{\sigma_X \ \sigma_Y} \tag{25}$$

where, X and Y are the transformed accumulated runoff over six months beginning from months m_1 and m_2. The transformed variables, X and Y, are identical to $u^s_{.,m_1,k}$ and $u^s_{.,m_2,k}$ in Eq. 22 for the spatial unit s. A correlation matrix is then obtained for each spatial unit (HRU). Table 8 summarizes the 10, 50, and 90 percentiles of correlation coefficients over all HRUs. For instance, the correlation coefficient of 0.44 in row Jan and column Jun in 10% matrix means that the correlation coefficient of 10% of the HRUs is less than 0.44 for the transformed accumulated runoff beginning from months Jan and Jun. The correlation coefficient for the same months increase to 0.9 and 0.95 for 50 and 90 percent of the HRUs, respectively, which indicates a rather high correlation for these particular months. According to the window size of six months for accumulated runoff, the forecast month should be located later than six months from the predictor month. Otherwise, the accumulation period beginning from the forecast month would have some overlap with the accumulation period beginning from the predictor month. For predictor months of Jan to Jun, the forecast month with 6-month lag is issued at some time in the same year (upper triangle of Table 8). However, for the predictor months of Jul to Dec, the forecast month locates in the next coming year (lower triangle). As seen, the correlation matrix of Table 8 is not symmetric; e.g. correlation coefficients of Jan/Jul and Jul/Jan are not equal. In the Jan/Jul case, Jan is the predictor month and the correlation coefficient with Jul would be 0.87 in the 50% table. Otherwise, if Jul is chosen as the predictor month (Jul/Jan case), the correlation coefficient significantly decreases to 0.04. In general, the numbers in lower triangle of Table 8 are smaller than those in upper triangle. The reason should be explored in the coherence of monthly runoff for

consecutive months. As shown in Fig. 23b, the outflow of the basin is much larger during April-July than the rest of the year. Therefore, if some high-flow months fit in a 6-month accumulation period, the aggregated runoff would suddenly increase, and the corresponding marginal probability would move towards the tail of the distribution. According to the influence of high-flows in increasing the accumulated runoff, a high correlation is guaranteed if the high flows in the accumulation window for predictor month are followed by the high flows in accumulation window for the forecast month. In other words, the high flows should occur in consecutive months when the predictor and forecast windows are connected adjacently. Looking at Fig. 23b, the predictor month of Jan, which includes Apr-May-Jun in its accumulation window, is followed by the high flows of July and Aug (of the same year) for the accumulation window, beginning from July as the forecast month. Hence, the high flows should be from consecutive months to expect a high correlation. This is the reason that the upper triangle of the correlation matrix has greater values than the lower triangle (Table 8). In Jul/Jan case, the high flows in predictor period (Jul and Aug) are not followed by the high flows in the forecast period (Apr, May, Jun of the next year) and a low correlation is thus expected for that case. Summaries of 10, 50, and 90 percent of correlation coefficients over all HRUs indicate that the most correlated predictor and forecast months are Jan and Jul, respectively. The correlation coefficient decays for later predictor months, and in general, the winter months (Jan, Feb, Mar) show high correlation with the summer months (Jul, Aug, Sep). Thus, Jan is selected as the predictor month and Jul is set to be the forecast month to evaluate our forecast technique in the remainder of this paper.

The primary assignment to develop the conditional probabilities as defined in Eq. 19 is to find a copula function to appropriately join the marginal distributions of correlated and dependent variables. The marginal distributions are chosen from the set of alternatives as: Gamma, Generalized Extreme Value, Lognormal, Gaussian, Weibull, Gumbel, and Exponential distributions. The K-S test and AIC test statistics (Eq. 7-8) are used to find the best fitted distribution to accumulated runoff volumes. For each HRU, a separate copula is required to join the marginal distributions of the accumulated runoff during the predictor and forecast periods (Jan-Jun and Jul-Dec). Thus, each HRU is assigned a particular copula function, set as the best fit from those listed in Table 1. The Cramér-von Mises (Eq. 4) statistic is applied in choosing the best copula from the set of Elliptical and Archimedean copulas.

4.5.2.2 Drought Forecasting Products

One advantage of the forecast model defined by Eq. 19 is the ability to estimate the forecast uncertainty via the conditional pdfs. Using the conditional pdf obtained from Eq. 19, the uncertainty of runoff at each grid cell can be estimated for the forecast period. Surface runoff at each grid cell can be shown by a particular uncertainty bound around the pdf mean (median), rather than a single deterministic value. Fig. 34 shows forecast uncertainty for the runoff produced in a few HRUs across the basin during the hind-cast period from 1980 to 2010. Note that the forecast variable is called as the hindcast variable during a historical time period. The predictor month is Jan followed by the forecast month, Jul. Observed runoff (solid black dots) during the hindcast period is estimated by the deterministic PRMS and the forecast runoff is shown within the 5-95% uncertainty

bound around the pdf median (dash line). As seen, the uncertainty bound fairly encompasses the observed runoff of associated HRUs and the median of forecast pdf (dash line) generally passes through the observations. The uncertainty bound is found to be rather large (small) for high flows (low flows), which is quite reasonable due to the heteroscedastic nature of streamflow.

Table 8: Summary of 10, 50, and 90 percentiles of correlation coefficients over all HRUs. In each HRU, the Pearson's correlation coefficient is estimated for each pair of accumulated runoff (with a particular starting month) having been transformed to the unit interval [0, 1]. The grey cells are associated with the forecast months being six months later than each predictor month in the first column on the left.

Forecast month of the same year

10%	Jan	Feb	Mar	Apr	May	Jun	Jul	Aug	Sep	Oct	Nov	Dec
Jan	1	0.90	0.75	0.73	0.64	0.44	0.43	0.29	0.00	-0.02	-0.13	-0.29
Feb	-0.24	1	0.93	0.85	0.79	0.77	0.58	0.30	0.00	-0.03	-0.11	-0.28
Mar	-0.26	-0.25	1	0.97	0.91	0.84	0.71	0.46	0.17	0.08	-0.13	-0.29
Apr	-0.26	-0.25	-0.21	1	0.90	0.89	0.73	0.50	0.17	0.09	-0.12	-0.29
May	-0.21	-0.22	-0.21	-0.20	1	0.94	0.82	0.59	0.24	0.08	-0.12	-0.25
Jun	-0.18	-0.18	-0.17	-0.15	-0.17	1	0.92	0.68	0.28	0.14	-0.07	-0.21
Jul	-0.18	-0.17	-0.17	-0.16	-0.18	-0.17	1	0.81	0.39	0.09	-0.08	-0.20
Aug	-0.10	-0.11	-0.10	-0.11	-0.12	-0.12	-0.13	1	0.45	0.17	-0.02	-0.12
Sep	-0.07	-0.07	-0.10	-0.08	-0.08	-0.08	-0.09	-0.11	1	0.50	-0.01	-0.06
Oct	-0.12	-0.12	-0.13	-0.15	-0.15	-0.12	-0.20	-0.27	-0.26	1	0.06	-0.07
Nov	-0.21	-0.33	-0.39	-0.42	-0.52	-0.50	-0.41	-0.34	-0.30	-0.31	1	0.32
Dec	0.41	0.14	-0.02	-0.04	-0.13	-0.24	-0.15	-0.08	-0.17	-0.13	-0.12	1

Predictor month

50%												
Jan	1	1.00	0.98	0.97	0.91	0.90	0.87	0.80	0.62	0.39	0.11	-0.04
Feb	0.00	1	1.00	0.99	0.95	0.93	0.91	0.85	0.67	0.45	0.10	-0.05
Mar	0.02	0.00	1	1.00	0.97	0.94	0.92	0.87	0.68	0.45	0.09	-0.03
Apr	0.05	0.04	-0.02	1	0.97	0.95	0.93	0.86	0.68	0.43	0.10	-0.02
May	0.03	0.04	0.04	0.01	1	0.98	0.94	0.87	0.69	0.44	0.10	-0.02
Jun	0.04	0.04	0.05	0.05	0.08	1	0.97	0.89	0.74	0.40	0.14	0.00
Jul	0.04	0.02	0.04	0.03	0.04	0.05	1	0.93	0.69	0.46	0.13	0.01
Aug	0.05	0.03	0.05	0.05	0.07	0.09	0.11	1	0.79	0.50	0.15	0.03
Sep	0.12	0.09	0.05	0.05	0.05	0.08	0.07	0.08	1	0.73	0.20	0.12
Oct	0.08	0.04	0.02	0.01	0.05	-0.01	-0.02	-0.02	0.01	1	0.32	0.09
Nov	0.44	0.40	0.37	0.36	0.27	0.37	0.29	0.15	-0.03	-0.02	1	0.55
Dec	0.95	0.94	0.89	0.87	0.82	0.80	0.64	0.54	0.33	0.24	0.11	1

Predictor month

90%												
Jan	1	1.00	1.00	1.00	0.96	0.95	0.94	0.90	0.82	0.67	0.37	0.27
Feb	0.25	1	1.00	1.00	0.97	0.96	0.95	0.92	0.85	0.76	0.41	0.27
Mar	0.24	0.23	1	1.00	0.98	0.97	0.96	0.92	0.87	0.78	0.41	0.24
Apr	0.25	0.23	0.20	1	0.99	0.98	0.96	0.94	0.87	0.79	0.42	0.24
May	0.17	0.18	0.16	0.15	1	0.99	0.98	0.96	0.91	0.82	0.42	0.24
Jun	0.20	0.19	0.20	0.18	0.21	1	0.99	0.97	0.92	0.83	0.41	0.18
Jul	0.20	0.19	0.19	0.20	0.21	0.25	1	0.99	0.95	0.88	0.46	0.21
Aug	0.21	0.20	0.21	0.19	0.23	0.25	0.25	1	0.98	0.94	0.51	0.25
Sep	0.30	0.27	0.23	0.24	0.26	0.26	0.27	0.21	1	0.98	0.53	0.35
Oct	0.48	0.36	0.32	0.30	0.24	0.26	0.19	0.15	0.20	1	0.70	0.43
Nov	0.98	0.96	0.87	0.88	0.83	0.82	0.73	0.54	0.25	0.19	1	0.92
Dec	1.00	1.00	0.99	0.99	0.94	0.93	0.92	0.88	0.73	0.45	0.27	1

Forecast month of the next year

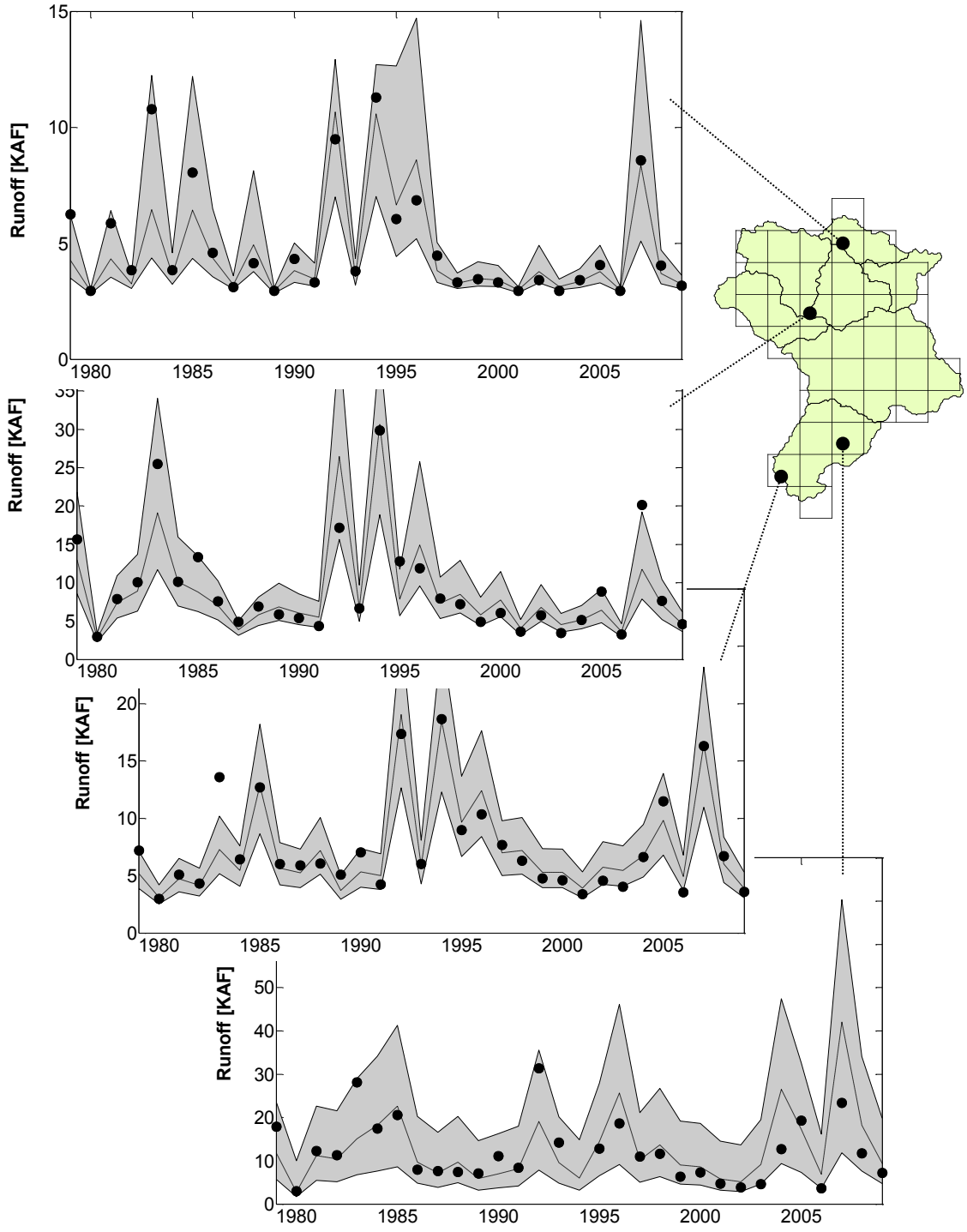

Figure 34: Runoff volume accumulated over Jul-Dec estimated by the forecast model for a few HRUs across GRB in the hindcast period (1980-2010). The hindcast is shown within the 5-95% uncertainty bound along with the corresponding observations (black dots); the dash line is showing the median of the conditional pdf.

In the probabilistic predictions, the probability of a particular future drought can be estimated conditional on the past drought status. In other words, the question is to find the probability of a specific drought at time $t+1$, given the status of time t. Another feature of probabilistic prediction is the identification of the future drought state associated with a particular probability. This alternative asks for the future drought at time $t+1$ associated with a specific probability. In earlier sections, the conditional pdf and cdf of future droughts (Fig. 26-28 and Fig. 31-32) are developed based on the basin outflow. Fig. 35 shows the two possible cases described above; where X_2 and X_1 are the drought-related variables in the future and in the past, respectively. The probability of future drought given a particular drought in an earlier time ($X_1 = x_1$) is equal to the area under the conditional pdf, $f(X_2 \mid X_1 = x_1)$. Given X_1, the former case (explained earlier) asks for the probability $P(X_2 < x_2 \mid X_1 = x_1)$ of a particular x_2, while the latter asks for the X_2 associated with a particular $P(X_2 \mid X_1 = x_1)$. Thus, a probability map of future droughts at each HRU, across the basin, using the runoff variable at each cell (Fig. 36) can be produces, as well as the runoff map with particular chance of occurrence in the forecast period (Fig. 37).

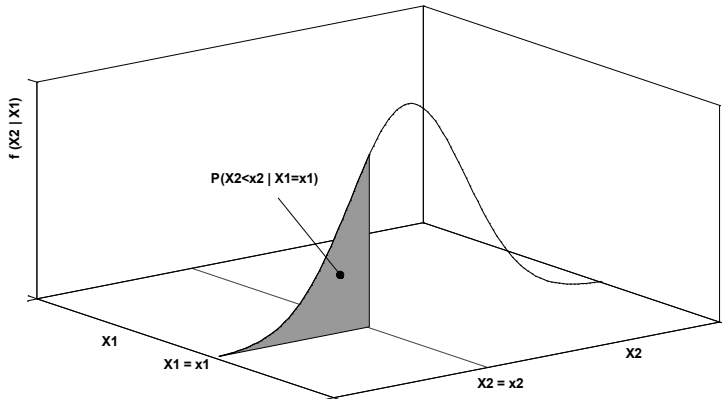

Figure 35: Schematic of the conditional probability of variable X_2 given X_1. In this paper, either the probability of a particular drought or the drought status associated with a particular probability for a future time is analyzed.

Fig. 36 displays the matrix of probability maps in the forecast month. It shows the probability of drought status being equally wet or wetter than a particular drought status in the forecast month (July), given the drought status in the predictor month (Jan). These probability maps are identical to the first case explained earlier, where the conditional probability is estimated for a particular future drought, given the condition in the past. The estimated probability at each HRU is equal to the area under the associated curve of conditional pdf as illustrated in Fig. 35. In Fig. 36, all possible pairs of drought status for the predictor and forecast months are evaluated. The label of each row (column) is associated with the drought status in the predictor (forecast) month. As the status in Jan gets drier (moves towards D4), the probability of rather intense dry conditions in next Jul increases. In other words, the probability of drought condition in Jul being equally wet or wetter than a particular dry status decreases as the Jan drought becomes more severe. For example, the drought state of D2 or any wetter states (D1, D0, Normal) in Jul is more likely if the past Jan experienced normal/wet condition rather than D4 (compare the maps in [row=1, col=4] and [row=6, col=4]). Such probabilistic maps are useful to

approximate the chance associated with each drought status in the future upon the observation of the past drought status. They are also helpful in estimating the chance of drought recovery (normal/wet condition) in the forecast period.

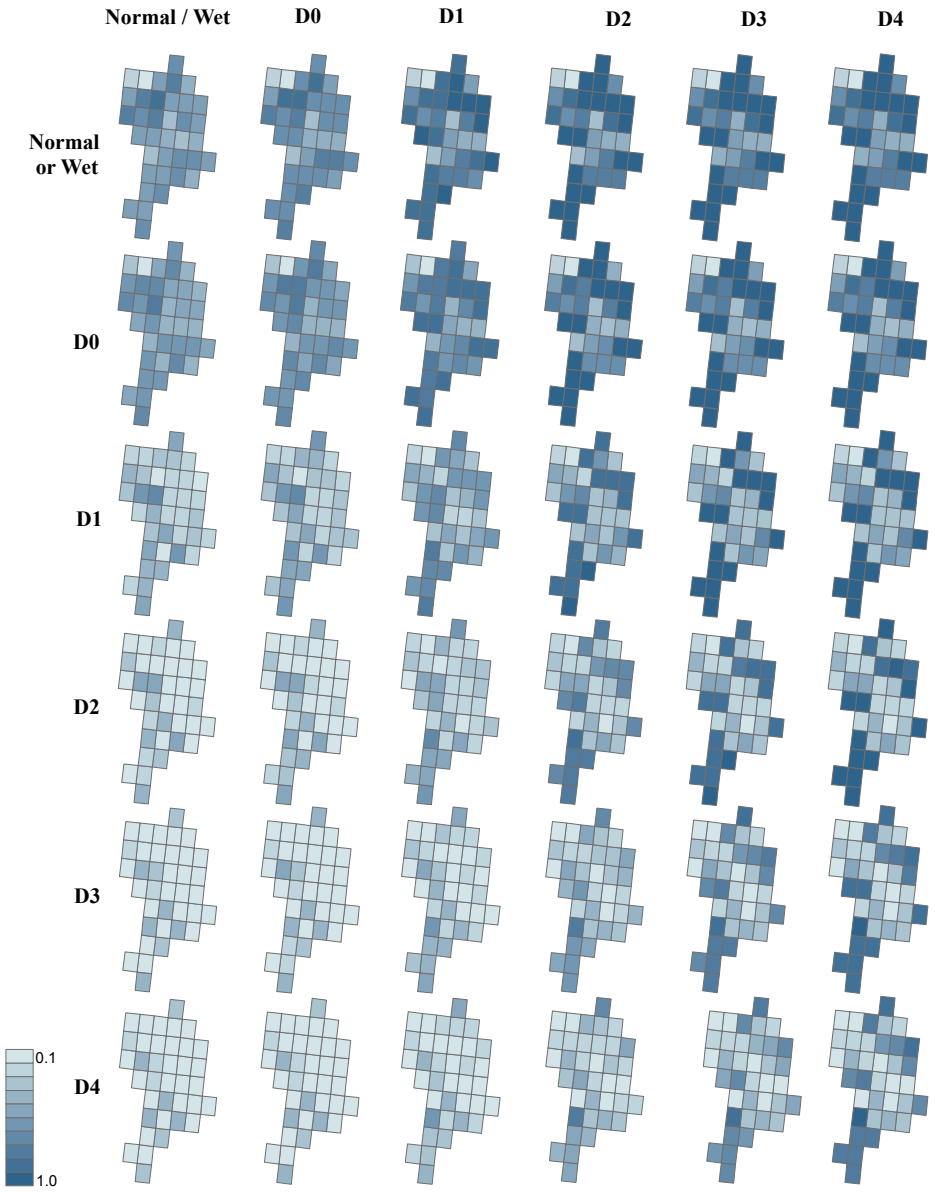

Figure 36: Probability maps that are estimated for drought status in the forecast month (Jul) being equally wet or wetter than a particular condition, where the status of the predicting month (Jan) is given. The label of each row (column) is associated with the drought status of the predicting (forecast) month.

The next alternative, as discussed earlier, is to estimate the runoff volume at each HRU with a specific probability of occurrence. This is similar to find X_2 associated with a particular probability $P(X_2 \mid X_1 = x_1)$ in Fig. 35. Given the drought status of predictor month (Jan), the variation of runoff across the basin with particular probabilities (0.25, 0.5, and 0.75) in the forecast month (July) is shown in Fig. 37. Row labels show the drought status of Jan. As seen, for a particular drought status in Jan, the non-exceedance probability is higher for larger runoff volumes in July. For example, the runoff volume in July increases as the non-exceedance probability increases from 0.5 to 0.75. Furthermore, for a same non-exceedance probability, a larger volume of runoff is expected in July, as the intensity of drought status in the predictor month (Jan) reduces. For clarification purposes, it should be noted again that the runoff in July refers to the accumulated runoff over six months, beginning from July. Analysis similar to what presented in Fig. 37 helps water managers to find out what runoff volumes are expected across the basin with a specific chance of occurrence; and therefore they can regulate their policies upon the runoff volumes associated with the particular probabilities they apply in their planning.

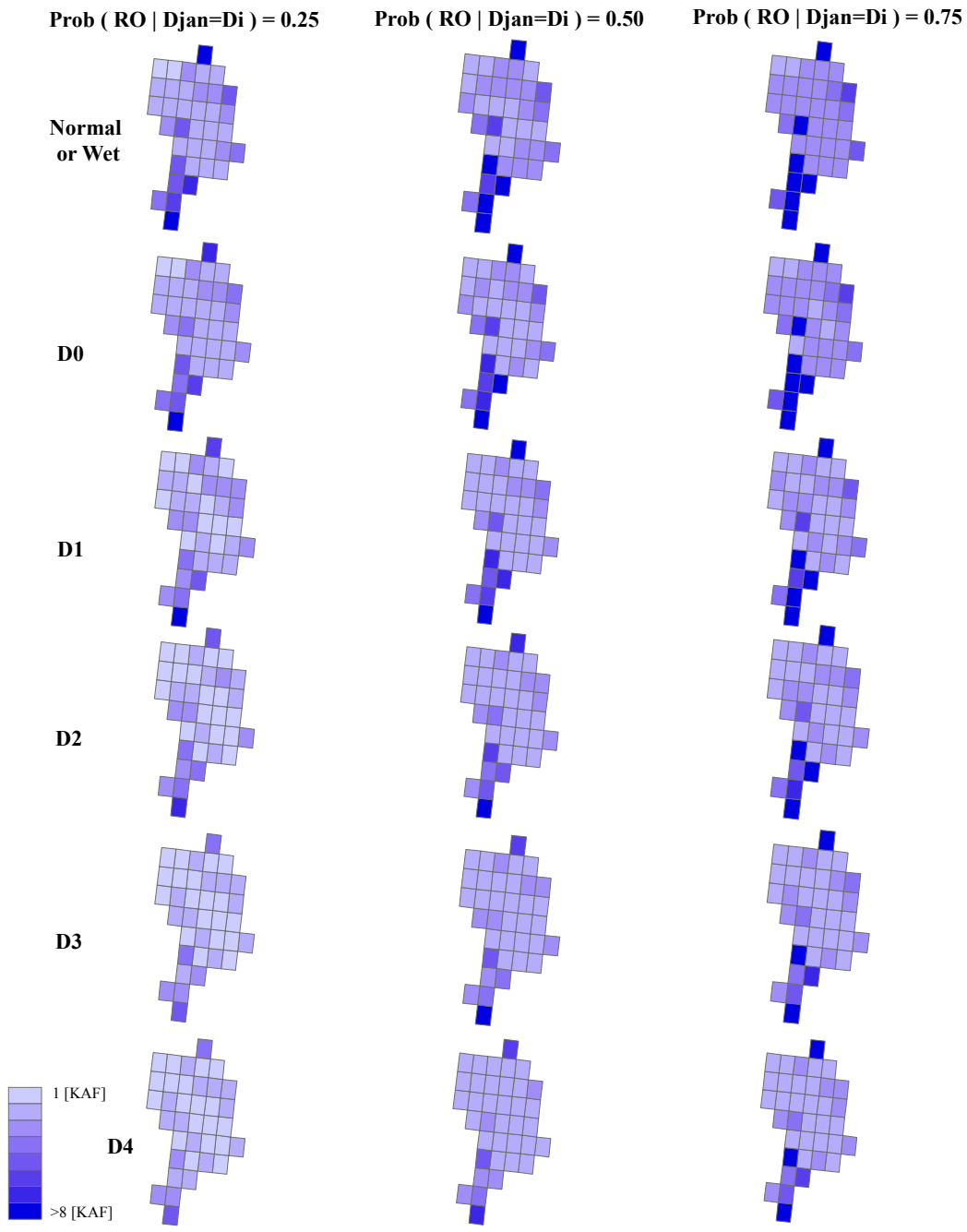

Figure 37: Maps of runoff volume in the forecast month (Jul) associated with different non-exceedance probabilities. Row labels show the drought status of the predicting month (Jan).

5. Summary and Conclusion

Improving the hydrologic forecasts with more reliability and less uncertainty has been the main focus of this study. Appropriate policies to allocate the available water resources among the different users need reliable forecast of the future status of available water. Climatology, the structure and parameters of hydrologic models, initial conditions at the forecast date are the main sources of uncertainties in hydrologic forecasts. A variety of techniques have been examined during the past several years to incorporate the different sources of uncertainty into the hydrologic forecasts. Depending on the source(s) of uncertainty to be addressed, the single value forecasts of the hydrologic models are usually combined and an ensemble of forecasts is generated. Regardless the employed technique, the forecast ensemble represents the uncertainty of forecasts raised from the associated source(s). However, if the raw forecast of the hydrologic model is highly biased or unreliable, addressing the uncertainty sources would not be appealing in improving the forecasts; and the raw forecasts might be even degraded under some circumstances.

5.1 Post-processing of Hydrologic Forecasts

The first theme of this study was involved in the post-processing of streamflow forecasts. In spite of the significant efforts on the calibration of hydrologic models during the past decades, they are still subject to errors and systematic biases that affect the forecast quality in small to large extents. Hence, the post-processing of model forecasts is necessary to ensure that forecasts are unbiased and fairly reliable and have the proper dispersion. Mathematically, post-processing is to approximate the most likely observation

given the forecast which is identical to find the mode of the conditional probability distribution of the observed variable given the forecast.

A potential post-processing technique should preserve the correlations and joint behavior between the observed and forecast variables. Since the conditional probabilities of these correlated variables can be defined with Bayesian networks, a group of multivariate distribution functions called copula were applied to the post-processing of forecasts. Unlike the most of multivariate functions, copulas do not make any restriction on the type of marginal distributions. Using copula functions make it possible to estimate the conditional probability of the observed variable at any particular forecast value. Using the marginal distribution of the variables, the original forecasts should be first transferred into their particular probability space and then copulas are applied to establish the joint distribution of transferred variables. Hence, the unknown connections between the hydrologic variables arisen from the complicated relationships in hydrological processes cannot limit developing the multivariate joint distribution function.

In 2500 hypothetical case studies, the proposed multivariate copula-based post-processor generally outperformed the traditional Quantile Mapping technique. Since QM is frequently used in different hydrologic applications, the shortcomings of this statistical technique were explained in detail and an auxiliary index, the so called failure index (γ), was introduced to predict the overall performance of QM or any other post-processing methods from an analysis period before the forecast period. The failure index is a measure of consistency between the post-processed forecasts and corresponding observations; it varies between 0 and 1, with $\gamma = 0$ for perfect post-processing. The

forecast skill of QM shows that this statistical technique is not always successful in improving initial forecast trajectories. Testing 2500 hypothetical case studies indicates that the performance of the QM technique constantly degrades as γ increases. Post-processing of a real case study was also tested. Using a distributed parameter hydrologic model, PRMS, several ensembles of monthly streamflow forecasts of the Sprague River basin in southern Oregon were generated with a forecast horizon of 6 months. Unlike the QM, the forecast skill of the post-processed ensembles was effectively improved when the multivariate post-processor was applied. The performance metrics indicated that QM was the dominated technique; however, weak performance of the QM technique was predictable from the failure ratio of the analysis period ($\gamma = 0.3$). Superiority of a multivariate copula-based method in considering the joint behavior of forecast and observed variables was evidently demonstrated in the post-processing results. Further improvement of postprocessing may be achieved by combining the strengths of Bayesian multimodeling (Duan et al., 2007; Parrish et al., 2012) and copula function.

5.2 Probabilistic Drought Forecasting

After improving the hydrologic forecast by means of post-processing, drought forecasting was exclusively examined in this study. Since frequent droughts have recently affected the southwestern U.S. with different water issues, reliable forecast of future droughts are essential for this region of the United States. The historical records across the Colorado River Basin denote the water year 2012 as the 4^{th} driest year of the region in the past century (since 1904), with consequences like insufficient water supply, poor pasture and crop conditions, and region-wide wildfires. Whereas the recent droughts of

CRB might be referred to the worldwide impacts of global warming on extreme events, accurate estimation of ongoing droughts across the region is crucial for future planning and managements of water resources in the area. The spatio-temporal variation of future droughts across the Gunnison River Basin, one of the headwater sub-basins of the Upper Colorado River Basin, was examined within a new drought forecasting methodology.

The proposed forecast model develops the probabilistic characteristics of future droughts using copula functions applied to the Bayesian networks. Similar to the forecast and observed variables in the post-processing of model forecasts, drought status of consecutive seasons forms a Bayesian network of variables; where their connections can be explained by copula functions. The outstanding feature of the proposed model is that it pictures the future drought status of a region (D4, D3, …, D1, Normal) given the drought status of the predictor season(s). Without any need to an initial guess of the forecast variable by hydrologic models, the forecast model predicts the future droughts via the copula functions. Drought forecasting was implemented for the river flow at a particular section of the river basin (the outlet) and also for the runoff volume generated at grid cells across the basin. The Standardized Streamflow Index (SSI) and Standardized Runoff Index (SRI) were used to analyze and forecast the hydrologic droughts related to the streamflow and runoff, respectively.

The main advantage of the proposed forecast methodology is its probabilistic features. It can develop the conditional probability density function (PDF) and cumulative distribution function (CDF) of future droughts given the drought status of past season(s). The most and least probable droughts during the forecast season as well as the

uncertainty of future droughts around the likely status can be acquired from the conditional PDFs. Unlike the conventional methods, the new technique is able to estimate the uncertainties of future droughts without incorporating the uncertainties of meteorological forcing and hydrologic models in the forecast model. The width of estimated uncertainty bound was larger for the high flows, which would reflect the greater uncertainty in high flows than the low flows. The results of the proposed forecast model are in agreement with the real-time observations of the hindcast period for the Gunnison River Basin. As a product of the conditional CDFs, the chance of a particular drought in the forecast period is approximated given the drought status of the earlier period(s). According to the results, the more intense droughts are expected in the forecast season as the previous season gets drier. In other words, the probability of dry status in the forecast period increases as the predictor period undergoes intensive dry conditions. The probabilistic maps are also useful to approximate the chance of drought recovery (normal/wet condition) in the forecast period, given the drought status observed in the predictor period. Another outcome of the conditional CDFs produced by the forecast model was the estimation of drought variable with a particular chance of occurrence. These products along with similar analyses within this forecast methodology would help the water managers and decision makers to regulate their policies according to the uncertainties in the future droughts.

The proposed technique only requires the knowledge about the predictor and forecast variables to establish the forecast model communicating between them. Although it is a purely statistical forecast model, the parameter estimation of copula function and

marginal distributions is totally based on the joint behavior of the predictor and forecast variables in the past. Given the basics of copula modeling, correlation and dependency are the essential components of the conditional forecast methodologies; whereas without dependent variables, the conditional forecast would not be meaningful.

The forecast methodology developed in this study shows promises in generating various products using its probabilistic features. With the application of copula functions, the proposed methodology can generate useful products in estimating the spatial variation of future droughts. Further enhancement of probabilistic forecasts by accounting for hydrologic initial condition at the time of forecast is possible. In light of advances in the area of ensemble data assimilation (Moradkhani et al., 2005a&b; Moradkhani and Sorooshian, 2008) the uncertainty in hydrologic initial condition can be characterized (DeChant and Moradkhani, 2011a) and these information may be used as another correlated variable in statistical drought forecasting using Copula functions. Recent advances in data assimilation by means of particle filter Markov Chain Monte Carlo (MCMC) as elaborated by Moradkhani et al., (2012) allows for more reliable quantification of uncertainty and characterization of initial condition. Soil moisture and snow as the main state variables representing the initial condition have successfully been estimated using data assimilation (Moradkhani, 2008; DeChant and Moradkhani, 2011b; Leisenring and Moradkhani, 2012). The proposed probabilistic approach helps the decision makers to develop drought mitigation plans and policies with an appropriate insight towards the future drought status.

References

Ajami, N. K., Q. Duan, and S. Sorooshian (2007), An integrated hydrologic Bayesian multimodel combination framework: Confronting input, parameter, and model structural uncertainty in hydrologic prediction, Water Resour. Res., 43, W01403, doi:10.1029/2005WR004745.

Akaike, H. (1974), A new look at the statistical model identification, IEEE Transactions on Automatic Control, 19 (6), 716–723.

Barros, A. P., and G. J. Bowden (2008), Toward long-lead operational forecasts of drought: An experimental study in the Murray-Darling River Basin, J. Hydrol., 357, 349–367.

Bates JM, and C. W. J. Granger (1969), The combination of forecasts. Oper Res Q 20:451–468.

Berg, D. (2009), Copula goodness-of-fit testing: An overview and power comparison, European Journal of Finance, vol. 15, 675-701.

Biagorria G. A., Jones, J. W., Shin, D. W., Mishra, A., and J. J. O'Brien (2007), Assessing uncertainties in crop model simulations using daily bias-corrected Regional Circulation Model outputs. Climate Research, vol. 34, 211-222.

Brown, J. D., and D. J. Seo (2010), A Nonparametric Postprocessor for Bias Correction of Hydrometeorological and Hydrologic Ensemble Forecasts, Journal of Hydrometeorology, vol. 11, 642–665. doi: http://dx.doi.org/10.1175/2009JHM1188.1

Buckland ST, Burnham KP, and N. H. Augustin (1997), Model selection: an integral part of inference. Biometrics 53:603–618

Burnham KP, and D. R. Anderson (2002), Model Selection and Multimodel Inference: a practical information-theoretic approach, 2nd edn. Springer, New York.

Cancelliere, A., Mauro, G. D., Bonaccorso, B., and G. Rossi (2007), Drought forecasting using the Standardized Precipitation Index, Water Resour. Manag., 21, 801–819.

Candille, G., Beauregard, S., and N. Gagnon (2010), Bias Correction and Multiensemble in the NAEFS Context or How to Get a "Free Calibration" through a Multiensemble Approach, Monthly Weather Review, vol.138, 4268–4281.

Carbone, G. J., and K. Dow (2005), Water Resource Management and Drought Forecasts in South Carolina, J. Am. Water Resour. As. (JAWRA), 41 (1), 145-155.

Cherubini, U., Luciano, E., and W. Vecchiato (2004), Copula methods in finance, Wiley, Chichester, U.K.

Clark, M.P., and L.E. Hay (2004), Use of medium-range numerical weather prediction model output to produce forecasts of streamflow, J. Hydrometeorology, 5(1): 15-32.

Cui, B., Z. Toth, Y. Zhu, and D. Hou (2008), Statistical downscaling approach and its application, Preprints, 19th Conf. on Probability and Statistics, New Orleans, LA, American Meteorological Society, 11.2.

Dai, A. (2011), Drought under global warming: a review. WIREs Clim Change, 2: 45–65. doi: 10.1002/wcc.81

Day, G.N. (1985), Extended streamflow forecasting using NWSRFS, Journal of Water Resources Planning and Management, 111(2), 157–170.

DeChant, C., and H. Moradkhani (2011a), Improving the characterization of initial condition for ensemble streamflow prediction using data assimilation, Hydrol. Earth Syst. Sci., 15, 3399-3410, doi:10.5194/hess-15-3399.

DeChant, C.M, and H. Moradkhani (2011b), Radiance Data Assimilation for Operational Snow and Streamflow Forecasting using the Particle Filter, Advances in Water Resources, 34 (3), 351-364.

Diks, C., Panchenko, V., and D. van Dijk (2010), Out-of-sample comparison of copula specifications in multivariate density forecasts, Journal of Economic Dynamics and Control, vol. 34, 1596–1609.

Diks, C. G. H., and J. A. Vrugt (2010), Comparison of point forecast accuracy of model averaging methods in hydrologic applications, Stoch. Environ. Res. Risk Assess., 24, 809–820, doi:10.1007/s00477-010-0378-z.

Dingman, S. L. (1994), Physical hydrology, Prentice Hall Upper Saddle River, NJ.

Djalalova, I., Wilczak, J., McKeen, S., Grell, G., Peckham, S., Pagowski, M., DelleMonache, L., McQueen, J., Tang, Y., Lee, P., McHenry, J., Gong, W., Bouchet , V., and R. Mathur (2010), Ensemble and bias-correction techniques for air quality model forecasts of surface O3 and PM2.5 during the TEXAQS-II experiment of 2006, Atmospheric Environment, 44(4): 455e467.

Duan, Q., Sorooshian, S., and V.K. Gupta (1994), Optimal use of the SCE-UA global optimization method for calibrating watershed models, Journal of Hydrology, v. 158, p. 265-284.

Duan, Q., N. K. Ajami., X. Gao, and S. Sorooshian (2007), Multi-model ensemble hydrologic prediction using Bayesian model averaging, Adv. Water Resour., 30(5), 1371–1386.

Dupuis, D. J. (2007), Using Copulas in Hydrology: Benefits, Cautions, and Issues, J. Hydrologic Engineering, 12(4), 381-393.

Embrechts, P., Lindskog, F., and A. J. McNeil (2003), Modelling dependence with copulas and applications to risk management, Handbook of heavy tailed distributions in finance, S. T. Rachev, ed., Elsevier Science, Amsterdam, Netherlands.

Federal Emergency Management Agency (1995), National Mitigation Strategy: Partnerships for Building Safer Communities, Report, 40 pp., Washington, D. C.

Fleig, A. K., Tallaksen, L. M., Hisdal, H., and D. M. Hannah (2010), Regional hydrological drought in north-western Europe: linking a new Regional Drought Area Index with weather types, Hydrological Processes. DOI: 10.1002/hyp.7644.

Genest, C., Ghoudi, K., and L. P. Rivest (1995), A semiparametric estimation procedure of dependence parameters in multivariate families of distributions, Biometrika, 82(3), 543–552.

Genest, C., Quessy, J.F., and B. Rémillard (2006), Goodness-of-fit procedures for copula models based on the probability integral transform, Scandinavian Journal of Statistics, vol. 33, 337-366.

Genest, C., and B. Rémillard (2008), Validity of the parametric bootstrap for goodness-of-fit testing in semiparametric models, Annales de l'Institut Henri-Poincaré, 44(6): 1096-1127.

Genest, C., Rémillard, B., and Beaudoin, D. (2009), Goodness-of-fit tests for copulas: A review and a power study, Insurance: Mathematics and Economics, vol. 44, 199-213.

Granger CWJ, and R. Ramanathan (1984), Improved methods of combining forecasts. J Forecast 3:197–204

Halmstad, A., Najafi, M.R., and H. Moradkhani (2012), Analysis of Precipitation Extremes with the Assessment of Regional Climate Models over the Willamette River Basin-U.S., Hydrol. Process., DOI: 10.1002/hyp.9376.

Hansen, B. E. (2008), Least-squares forecast averaging. J Econom 146:342–350.

Hashino, T., Bradley, A. A., and S. S. Schwartz (2006), Evaluation of bias-correction methods for ensemble streamflow volume forecasts. Hydrol. Earth Syst. Sci. Discuss., 3, 561–594.

Hay, L.E., and M. Umemoto (2006), Multiple-objective stepwise calibration using Luca, U.S. Geological Survey Open-File Report, 2006-1323, 25p.

Hoeting, J. A., Madigan, D., Raftery, A. E., and C. T. Volinsky (1999), Bayesian model averaging: a tutorial. Stat Sci 14:382–417.

Hollinger, S. E., Isard, S. A., and M. R. Welford (1993), A new soil moisture drought index for predicting crop yields, Preprints, Eighth Conf. on Applied Climatology, Anaheim.

Hwang, Y., and G. J. Carbone (2009), Ensemble forecasts of drought indices using a conditional residual resampling technique, J. Appl. Meteor. Climatol., 48, 1289-1301.

Ines A.V.M., and J. W. Hansen (2006), Bias correction of daily GCM rainfall for crop simulation studies, Agricultural and Forest Meteorology, 138:44–53.

Isaaks, E. H., and R. M. Srivastava (1989), An Introduction to Applied Geostatistics, Oxford University Press, New York, 561 pp.

Joe, H. (1997), Multivariate Models and Dependence Concepts, Chapman & Hall, London.

Johnson, C. R. (1970), Positive Definite Matrices, Amer. Math. Monthly 77, 259-264.

Jung, I., Moradkhani, H., and H. Chang (2012), Uncertainty Assessment of Climate Change Impact for Hydrologically Distinct River Basins, J. Hydrol., 466-467, p73-87, http://dx.doi.org/10.1016/j.jhydrol.2012.08.002.

Kalman, R. E. (1960), A new approach to linear filtering and prediction problems. J Basic Engineering 82 (1), 35–45.

Kao, S, and R. S. Govindaraju (2008), Trivariate statistical analysis of extreme rainfall events via Plackett family of copulas, Water Resources Research, 44, W02415, doi:10.1029/2007WR006261.

Kao, S, and R. S. Govindaraju (2010), A copula-based joint deficit index for droughts, J. Hydrology, 380, 121–134.

Karl, T., Quinlan, F., and D. S. Ezell (1987), Drought termination and amelioration: its climatological probability, J. Clim. Appl. Meteor., 26(9),1198-1209.

Kendall, J. R., and D. A. Dracup (1992), On the generation of drought events using an alternating renewal-reward model, Stochastic Hydrology and Hydraulics, 6, 55–68.

Klamath Basin Ecosystem Foundation (2007), Upper Sprague Watershed Assessment. Klamath Falls, OR.

Kolmogorov, A. N. (1933), Sulla Determinazione Empirca di una Legge di Distribuzione, Giornale dell' Istituto Italiano degli Attuari, 4, pp.83-91.

Laio, F., and S. Tamea (2007), Verification tools for probabilistic forecasts of continuous hydrological variables, Hydrology and Earth System Sciences, vol. 11, 1267-1277, doi:10.5194/hess-11-1267-2007.

Leavesley, G. H., Lichty, R. W., Troutman, B. M., and L.G. Saindon (1983), Precipitation-Runoff Modeling System: User's Manual, U.S. Geological Survey Water-Resources Investigations 83-4238, 207 p.

Leisenring, M., and H. Moradkhani, (2012), Analyzing the Uncertainty of Suspended Sediment Load Prediction Using Sequential Data Assimilation, Journal of Hydrology, vol. 468–469, p268–282.

Li, H., Luo, L., Wood, E.F., and J. Schaake (2009), The role of initial conditions and forcing uncertainties in seasonal hydrologic forecasting, Journal of Geophysical Research, 114(D4): D04114.

Liu, W. T., and F. N. Kogan (1996), Monitoring regional drought using the vegetation condition index, International Journal of Remote Sensing, 17, 2761−2782.

Loaiciga, H. A., and R. B. Leipnik (1996), Stochastic renewal model of low-flow streamflow sequences, Stochastic Hydrology and Hydraulics, 10, 65–85.

Lohani V. K., and G. V. Loganathan (1997), An early warning system for drought management using the palmer drought index, J. Am. Water Resour. As., 33(6), 1375-1386

Lott, N., and T. Ross (2000), NCDC Technical Report 2000-02, A Climatology of Recent Extreme Weather and Climate Events. [Asheville, N.C.]: National Climatic Data Center.

Lott, N., and T. Ross (2006), Tracking and evaluating U.S. billion dollar weather disasters, 1980–2005. Extended Abstracts, AMS Forum: Environmental Risk and Impacts on Society: Successes and Challenges, Atlanta, GA, Amer. Meteor. Soc., 1.2.

Madadgar, S. and H. Moradkhani (2011), Improving the Ensemble Streamflow Prediction by Adjusting Hydrologic Ensemble Traces, In the proceedings of ASCE World Environmental and Water Resources Congress 2011, Palm Spring, CA.

Madadgar, S., Moradkhani, H., and D. Garen (2012), Towards Improved Post-processing of Hydrologic Forecast Ensembles, J. Hydrol. Process., doi: 10.1002/hyp.9562.

Madadgar, S., and H. Moradkhani (2013), Drought Analysis under Climate Change Using Copula, J. Hydrol. Eng., 18(7), 746–759.

Madadgar, S., and H. Moradkhani (2013), A Bayesian Framework for Probabilistic Seasonal Drought Forecasting, J. Hydrometeorology, doi:10.1175/JHM-D-13-010.1, in press.

Massey, F. J. (1951), The Kolmogorov-Smirnov Test for Goodness of Fit, Amer. Statist. Assoc., 46(253), 68–78.

McEnery, J., Ingram, J., Duan, Q. Y., Adams, T., and L. Anderson (2005), NOAA's advanced hydrologic prediction service, Building pathways for better science in water forecasting, Bulletin of American Meteorological Society, 86, 375–385.

McKee, T. B., Doesken, N. J., and J. Kleist (1993), The relationship of drought frequency and duration to time scales, Paper presented at 8th Conference on Applied Climatology, American Meteorological Society, Anaheim, Calif.

McKee, T. B., Doesken, N. J., and J. Kleist (1995), Drought monitoring with multiple time scales, Paper presented at 9th Conference on Applied Climatology, American Meteorological Society, Dallas, Texas.

Mishra, A. K., and V. R. Desai (2005), Drought forecasting using stochastic models, Stoch. Env. Res. Risk A., 19(5), 326–339

Mishra, A. K., and V. R. Desai (2006), Drought forecasting using feed-forward recursive neural network, Ecol. Modell., 198, 127–138.

Mishra, A. K., and V. P. Singh (2010), A Review of Drought Concepts, J. Hydrology, 391, 202-216.

Moradkhani H., C.M. DeChant and S. Sorooshian (2012), Evolution of Ensemble Data Assimilation for Uncertainty Quantification using the Particle Filter-Markov Chain Monte Carlo Method, Water Resources Research, VOL. 48, W12520, 14 PP., doi:10.1029/2012WR012144.

Moradkhani, H., M. Meier, (2010), Long-Lead Water Supply Forecast using Large-scale Climate Predictors and Independent Component Analysis, J. of Hydrologic Engineering, 15(10), 744-762.

Moradkhani, H. (2008), Hydrologic Remote Sensing and Land Surface Data Assimilation", Sensors, 8, 2986-3004, DOI: 10.3390/s8052986.

Moradkhani, H. and S. Sorooshian (2008), General Review of Rainfall-Runoff Modeling: Model Calibration, Data Assimilation, and Uncertainty Analysis, in

Hydrological Modeling and Water Cycle, Coupling of the Atmospheric and Hydrological Models, Springer, Water Science and Technology Library, Volume 63, pp 1-23.

Moradkhani H., Baird, R.G., and S. Wherry (2010), Impact of Climate Change on Floodplain Mapping and Hydrologic Ecotones, Journal of Hydrology, 395, 264–278, DOI: 10.1016/j.jhydrol.2010.10.038.

Moradkhani H., C.M. DeChant and S. Sorooshian (2012), Evolution of Ensemble Data Assimilation for Uncertainty Quantification using the Particle Filter-Markov Chain Monte Carlo Method, Water Resources Research, VOL. 48, W12520, 14 PP., doi:10.1029/2012WR012144.

Moradkhani, H., K. Hsu, H.V. Gupta, and S. Sorooshian (2005a), Uncertainty Assessment of Hydrologic Model States and Parameters: Sequential Data Assimilation Using Particle Filter, Water Resources Research, 41, W05012, doi:10.1029/2004WR003604.

Moradkhani, H., S. Sorooshian, H.V. Gupta, and P. Houser (2005b), Dual State-Parameter Estimation of Hydrological Models using Ensemble Kalman Filter, Advances in Water Resources, 28, 2,135-147.

Najafi, M., H. Moradkhani, and I. Jung (2011), Assessing the uncertainties of hydrologic model selection in climate change impact studies, Hydrol. Processes, 25(18), 2814–2826.

Najafi, M.R., Moradkhani, H., and T. Piechota (2012), Ensemble Streamflow Prediction: Climate Signal Weighting vs. Climate Forecast System Reanalysis, J. Hydrology, 442–443 (p105–116), http://dx.doi.org/10.1016/j.jhydrol.2012.04.003.

Nalbantis, I. (2008), Evaluation of a Hydrological Drought Index, European Water, 23/24, 67-77.

Nash, J.E., J. V. Sutcliffe (1970), River flow forecasting through conceptual models part I- a discussion of principles, J. Hydrology, 10(3):282–290.

National Climate Data Cechantenter (2003), Climate of 2002, Annual review U. S. drought, http://www.ncdc.noaa.gov/oa/climate/research/2002/ann/drought-summary.html, Asheville, N. C.

National Drought Mitigation Center, What is drought? Understanding and Defining Drought, http://www.drought.unl.edu/whatis/concept.htm

Nelsen, R. B. (1999), An Introduction to Copulas, Springer, New York.

Olsson, J., and G. Lindström (2008), Evaluation and calibration of operational hydrological ensemble forecasts in Sweden. J. Hydrology, 350, 14–24.

Özger, M., Mishra, A. K., and V. P. Singh (2012), Long Lead Time Drought Forecasting Using a Wavelet and Fuzzy Logic Combination Model: A Case Study in Texas, J. Hydrometeor, 13, 284–297.

Palmer, W. C. (1965), Meteorologic Drought, U.S. Department of Commerce, Weather Bureau, Research Paper No. 45, 58 pp.

Palmer, W. C. (1968), Keeping track of crop moisture conditions, nationwide: The new crop moisture index, Weatherwise, 21, 156–161.

Parrish, M. A., H. Moradkhani, and C. M. DeChant (2012), Toward reduction of model uncertainty: Integration of Bayesian model averaging and data assimilation, Water Resour. Res., 48, W03519, doi:10.1029/2011WR011116.

Peterson, T. C., Stott, P. A., and S. Herring (2012), Explaining Extreme Events of 2011 from a Climate Perspective. Bull. Amer. Meteor. Soc., 93, 1041–1067.

Piani, C., Haerter, J. O., and E. Coppola (2010), Statistical bias correction for daily precipitation in regional climate models over Europe, Theoretical and Applied Climatology, 99:187–192.

Raftery, A. E., Gneiting, T., Balabdaoui, F., and M. Polakowski (2005), Using Bayesian model averaging to calibrate forecast ensembles. Mon Weather Rev 133:1155–1174.

Renard, B., Kavetski, D., Kuczera, G., Thyer, M., and S. W. Franks (2010), Understanding predictive uncertainty in hydrologic modeling: The challenge of identifying input and structural errors, Water Resources Research, 46, W05521.

Risley, J., Moradkhani, H., Hay, L., and S. Markstrom (2011), Statistical Comparisons of Watershed-Scale Response to Climate Change in Selected Basins across the United States, Earth Interact., 15, 1–26. doi: 10.1175/2010EI364.1.

Rojas, R., L. Feyen, and A. Dassargues (2008), Conceptual model uncertainty in groundwater modeling: Combining generalized likelihood uncertainty estimation and Bayesian model averaging, Water Resour. Res., 44, W12418, doi:10.1029/2008WR006908.

Rosenblatt, M. (1952), Remarks on a multivariate transformation. The Annals of Mathematical Statistics, vol. 23, 470-472.

Roulin, E. and S. Vannitsem (2005), Skill of medium-range hydrological ensemble predictions, J. Hydrometeorology, 6(5): 729–744.

Russell, S. J., and N. Peter (2009), Artificial Intelligence: A Modern Approach (3rd ed.), Prentice Hall, New Jersey.

Savu, C. and M. Trede (2008), Goodness-of-fit tests for parametric families of Archimedean copulas, Quantitative Finance, vol. 8, 109-116.

Schaake, J.C., Demargne, J., Hartman, R., Mullusky, M., Welles, E., Wu, L., Herr, H., Fan, X., and D. J. Seo (2007), Precipitation and temperature ensemble forecasts from single-value forecasts, Hydrology and Earth System Sciences Discussions 4, 655–717.

Serinaldi, F., and S. Grimaldi (2007), Fully nested 3-copula: Procedure and application on hydrological data." Journal of Hydrologic Engineering, 12(4), 420-430.

Shafer, B. A., and L. E. Dezman (1982), Development of a Surface Water Supply Index (SWSI) to assess the severity of drought conditions in snowpack runoff areas." Preprints, Western SnowConf., Reno, NV, Colorado State University, 164–175.

Sheffield, J., and E. F. Wood (2008), Projected changes in drought occurrence under future global warming from multi-model, multi-scenario, IPCC AR4 simulations, Clim. Dynam., 31(1), 79-105.

Showstack, R. (2012), Drought research and monitoring program is focus of congressional hearing, Eos Trans. AGU, 93(32), 310, doi:10.1029/2012EO320002.

Shukla S., and A. W. Wood (2008), Use of a standardized runoff index 1368 for characterizing hydrologic drought, Geophysical Research Letters, 35, L02405, doi:10.1029/2007GL032487.

Smith, J. A., Day, G. N., and M. D. Kane (1992), Nonparametric framework for long-range streamflow forecasting, J Water Resources Planning and Management, 118, 82–91.

Steinemann, A. (2003), Drought indicators and triggers: a stochastic approach to evaluation, J. Am. Water Resour. As., 39(5), 1217-1233

Steinemann, A. (2006), Using climate forecasts for drought management, J. Appl. Meteor. Climatol., 45, 1353–1361.

Thirel, G., Rousset-Regimbeau, F., Martin, E., and F. Habets (2008), On the impact of short-range meteorological forecasts for ensemble streamflow predictions, Journal of Hydrometeorology, 9(6): 1301-1317.

Thulasiraman, K., and M. N. S. Swamy (1992), Graphs: Theory and Algorithms, John Wiley and Son.

Thyer, M., Renard, B., Kavetski, D., Kuczera, G., Franks, S. W., and S. Srikanthan (2009), Critical evaluation of parameter consistency and predictive uncertainty in hydrological modeling: A case study using Bayesian total error analysis, Water Resources Research, 45, W00B14, doi:10.1029/2008WR006825.

Todini, E. (2008), A model conditional processor to assess predictive uncertainty in flood forecasting, International Journal of River Basin Management, 6(2), 123–137.

Trenberth, K. E. (2011), Framing the way to relate climate extremes to climate change, Climat Change, 115(2), 283-290.

Twedt, T. M., Schaake, J. C., and E. L. Peck (1977), National Weather Service extended streamflow prediction, In: Proc. 45th Western Snow Conference, Albuquerque, pp. 52–57.

Vrugt, J. A., and B. A. Robinson (2007, Treatment of uncertainty using ensemble methods: comparison of sequential data assimilation and Bayesian model averaging, Water Resour Res 43:1–15.

Weghorst, K. M. (1996), The reclamation drought index: Guidelines and practical applications, Bureau of Reclamation, Denver, CO, 6 pp. [Available from Bureau of Reclamation, D-8530, Box 25007, Lakewood, CO 80226].

Weiß, G.N.F. (2011), Are Copula-GoF-tests of any practical use? Empirical evidence for stocks, commodities and FX futures, The Quarterly Review of Economics and Finance, vol. 51, 173–188.

Wilks, D. S. (1995), Statistical Methods in the Atmospheric Sciences, International Geophysics Series, Vol. 59, Academic Press, 467 pp.

Wong, G., Lambert, M. F., Leonard, M., and A. V. Metcalfe (2010), Drought Analysis Using Trivariate Copulas Conditional on Climatic States, J. Hydrologic Engineering, 15(2), 129-141.

Wood, A.W., and D.P. Lettenmaier (2006), A test bed for new seasonal hydrologic forecasting approaches in the western United States, Bulletin of the American Meteorological Society, 87(12): 1699-1712.

Wood, A. W., and D. P. Lettenmaier (2008), An ensemble approach for attribution of hydrologic prediction uncertainty, Geophysical Research Letters, vol. 35, L14401, doi:10.1029/2008GL034648.

WWA and NIDIS (2012), The 2012 Drought in Colorado, Utah and Wyoming: A July 2012 update from the Western Water Assessment and the National Integrated Drought Information System.

Zhang, L., and V. P. Singh (2007), Gumbel–Hougaard Copula for Trivariate Rainfall Frequency Analysis, J. Hydrologic Engineering, 12(4), 409-419.

Zhao, L., Duan, Q., Schaake, J., Ye, A., and J. Xia (2011), A hydrologic post-processor for ensemble streamflow predictions, Advances in Geosciences, vol. 29, 51-59.